A PROBLEM DRIVEN APPROACH TO THE MINIATURIZATION AND AUTOMATION OF ENZYME-BASED ASSAYS AND AN INVESTIGATION OF THE DISSIPATION OF CYANAZINE AND BROMIDE IN WETLAND MESOCOSMS

by

Yolanda Fintschenko

B.S. Trinity University, 1992

Submitted to the Department of Chemistry and the Faculty of the Graduate School of the University of Kansas in partial fulfillment of the requirements for the degree of Doctor of Philosophy

Date Submitted: 10/15/97

To my family with all my love.

ACKNOWLEDGEMENTS

I deeply appreciate the guidance I have received from my advisor, Prof. George S. Wilson. Additionally, I wish to thank Dr. E. Michael Thurman and Dr. Don Huggins for allowing me to work in their laboratories and for their helpful advice. I am grateful to Prof. Peter Hesketh and the Micro Actuators Lab of The University of Illinois at Chicago for allowing me to use their microfabrication facilities. Finally, I would like thank the members of the Wilson, Thurman, and Hesketh research groups for their invaluable help, support and discussions.

TABLE OF CONTENTS

TABLE OF FIGURES AND TABLES

1. General Introduction

Analytical chemistry, as a discipline, has something of an identity crisis. Its role in the development of instrumental methods frequently relegates it into the category of a technology, while the curiosity-driven fundamental studies of the technology drive it into the category of a science. Fortunately, it is possible to do both science and technology simultaneously. Fundamental studies and innovation in technology lead to the same result, better analyses. For this reason, regardless of the strategy of the study, analytical chemistry at its best is problem driven research. This work reflects the approach that it is of paramount importance to answer fundamental and technological questions in the context of real world problems.

Biological recognition elements have enjoyed popularity recently in analytical chemistry. Receptors such as antibodies have been demonstrated to achieve low limits of detection in diverse complex matrices from serum to ground water. Enzymes are an integral part of such bioassays, providing increased sensitivity as a result of the time dependence of their product production. The power of enzyme based immunoassays has been demonstrated since their introduction in 1971. However, enzymes alone have been shown to be valuable bioanalytical tools as exemplified by the plethora of research in the area of implantable amperometric glucose oxidase (GOx) based biosensors for glucose.

Biosensors or biologically based analytical methods must continue to evolve to prove useful in the changing landscape. Recent trends in new drug development have made different demands on the analytical chemist. No longer are simply good limits of detection, sensitivities, or high theoretical plates satisfactory for pharmaceutical companies. As thousands of combinatorial libraries queue up for analysis, speed and sample throughput have become increasingly important. Joining drug companies are hundreds of superfund sites, with millions of complex, toxic

samples to be analyzed in a limited time frame. New demands brought about by the political climate in hospitals are forcing clinical labs to consider innovations to improve the speed and cost effectiveness of routine screening. Other considerations, such as minimizing contact with biological fluids brought about by concerns over hepatitis and HIV, renew interest in fundamental research in sample handling and preparation.

This work reflects the approach that it is of paramount importance to answer fundamental and technological questions in the context of real world problems. In Part One two related problems are described. Chapter One demonstrates that the enzyme linked immunosorbent assay (ELISA) may be used to assess the immunogenicity of the immobilized GOx on an implantable glucose sensor. Chapter Two addresses the problem of how enzyme based analytical methods such as those used in Chapter One are automated and miniaturized.

Part Two presents in Chapter Three the results of the environmental analysis of pond water drawn from wetland mesocosms treated with a herbicide and a volume tracer. The significance of this work is two-fold. First, inherent in a field study of this scope is the analytical challenges associated with sampling, sample handling, and analysis specifically with respect to throughput. Explicitly, and more importantly, are the valuable discoveries related to the non-conservative behavior of both compounds applied.

2. Chapter 1: A Study of the Immunological Effect of Implantable Glucose Sensors in Rats

2.1. Introduction

Insulin dependent *diabetes mellitus*, a disease which results in abnormally high levels of glucose in the body, can be controlled by a combination of careful monitoring of blood glucose levels and subsequent injections of insulin. The monitoring of blood glucose requires that the diabetic draw a small amount of blood several times a day. The development of glucose sensors for long term implantation could remove this daily inconvenience.

Implantable glucose sensors developed by G.S. Wilson *et al.*. have been undergoing human trials in France *(1)*. These sensors are intended for implantation over a period of several days to a week. Once removed, new sensors are to be implanted. Thus, it becomes necessary to evaluate the immunogenicity of the sensor, specifically, the response of the immune system to the glucose oxidase immobilized on the sensor.

In order to establish safety for human use, the implantable sensors have been evaluated for biocompatibility *(2)*. The modern definition of biocompatibility does not require that an implant be inert, but rather that the effect of implantation does not impair the function of the device implanted nor impair the function of the organism or area into which it is implanted *(3)*. Two types of defense mechanisms respond to implantation: specific and non-specific. The non-specific response does not require receptor recognition of the foreign body, but rather invasion alone. Protein adsorption is the initial, immediate response. This can be minimized by the careful design of the foreign body surface structure and chemical composition *(2)*. Inflammation begins, indicating the vasodilatation of capillaries and the exudation of multinuclear and phagocytic cells from plasma to the foreign body (Figure 1.1). These cells begin digestion of the surface of the foreign body. Some of these cells also serve as antigen presenting cells and will trigger a humoral and cell-mediated

response *(4)*. After about a week, an avascular, collageneous tissue encapsulates the site. Removing anchoring points on the surface of the sensor minimizes encapsulation *(5)*. Several studies describe optimized sensor surfaces and shapes *(2,5)*.

The specific foreign body response requires the recognition of all or parts of a foreign body by a biological receptor. The specific immune response requires a large molecule (>5000 Daltons) that is foreign at an appropriate dosage. The recognition elements associated with the humoral immune response, immunoglobulins or antibodies, will be found in large quantities once the subject has been challenged by a foreign body (Fig. 1.2 and Fig. 1.3) *(4,6)*. Already, it has been demonstrated that certain metals will cause an immune response *(6)*. In the case of the implantable biosensors, metal is not accessible because it is coated with polymers. Tenenbaum has published evidence that antibodies are produced in humans to cross-linked silicone in breast implants *(7)*. Ziegler *et al.* published results in 1994 while our study was on-going indicating that antibodies against a polymer component of the glucose sensor, cellulose acetate, were found, but not antibodies against the immobilized glucose oxidase *(8)*. Thus far, no one has demonstrated that GOx in the implantable glucose sensor is accessible to the body, and that it is present in a sufficient dose to induce a specific immune response.

Glucose oxidase isolated from *Aspergillus niger* is an enzyme with a molecular weight of 160,000 Daltons comprised of approximately 16% carbohydrate *(9)*. It consists of two subunits with one mole of prosthetic group, flavin adenine dinucleotide, distributed in each mole of subunit *(9,10)*.

The large size and complicated structure of this glycoprotein make glucose oxidase (GOx) an excellent immunogen. While it has been demonstrated that GOx is immunogenic, it has also been shown to be highly toxic in mice *(11,12)*. However, the removal of the prosthetic groups, flavin adenine dinucleotide (FAD), from the holoenzyme by acid treatment results in the apoenzyme, which is not toxic or active,

but shares epitopes with the holoenzyme *(12,13)*. It has been shown that an animal immunized against the apoenzyme will produce antibodies that will cross react well with the holoenzyme *(12)*. Since rats have been used to characterize the performance of the implantable glucose sensors in the past, rats were chosen as the system in which to characterize the immunological effects of the implantable sensors *(1,8,14)*.

Our hypotheses were as follows:

1. Sensors with an outer membrane implanted in rats would not produce an immune response
2. Sensors with no outer membrane would result in an increased immune response compared to the case where there is an outer membrane
3. Rats injected with the soluble apoenzyme would produce antibodies with a high cross-reactivity to the native enzyme.

Three populations of six rats each were studied. Because of the toxicity of the native GOx in mice, the positive control rats were immunized against apoGOx (abbreviated POS). The second population of rats was immunized against two glucose sensors with no outer membrane separating the immobilized active GOx from the body, and the third group was immunized against two glucose sensors with an outer membrane (abbreviated SNM and SWM, respectively). The sera from seven rats unexposed to sensors or soluble apoenzyme was used as the negative control.

The immunological effect of the three antigens introduced was evaluated using ELISA, enzyme-linked immunosorbent assay, and UV detection to determine the titer of the sera. The break in the titer is defined as the dilution of the serum where the optical density is at half the maximum optical density. If the concentration of the IgG in the serum is known, the binding constant of each antibody binding site can be determined. However, for screening purposes, it is sufficient to know at what dilution the titer break occurs. This number can be compared within a population and with other populations.

What follows is a discussion of the theory behind immunity to provide background for the conclusions that will be presented later. Also in the discussion of theory will be a detailed explanation of the ELISA and titer determinations to give clarity to the methods outlined in the Experimental section. The Results and Discussion section focuses on if and how the results support our hypotheses, new questions raised, and a discussion of a new hypothetical model for the behavior observed. Also in this section is a discussion of the statistical methods employed. A summary of the results and hypotheses is found in the conclusion.

2.2. Background and Theory

2.2.1. Immunity

As discussed above, immunity to invasion in mammals is conferred via two routes, non-specific or innate and specific or acquired. Non-specific immunity provides four types of barriers to foreign body invasion: mechanical, chemical, cellular, and inflammatory. Figure 1.1 provides a good visual aid in understanding the complex processes involved in innate immunity described below.

The skin and mucous membranes mechanically prevent penetration. Ciliated endothelial cells, saliva, tears and mucous sweep away invaders. In addition, the above anatomic defenses use chemical weapons such as pH, antibacterial, and antiviral proteins that inhibit the proliferation of bacteria and viruses.

Cells play a crucial role by actually ingesting extracellular macromolecules by endocytosis or phagocytosis. Endocytosis can be non-specific, as in pinocytosis, or specific, as in receptor-mediated endocytosis. In the latter case, the macromolecule must first bind to a receptor on the cell surface, while in the former, no surface recognition is required. Once ingested, the endocytic vesicles fuse to each other and deliver their contents to a cellular garbage dump, endosomes, where they are digested. Phagocytosis ingests a particulate material, including whole pathogenic

microorganisms. No receptor recognition is required, but only specialized cells are capable of phagocytosis, while virtually all cells use endocytosis. Blood monocytes, neutrophils, and tissue macrophages, cells important in the specific immune response, are capable of phagocytosis.

Figure 1.1

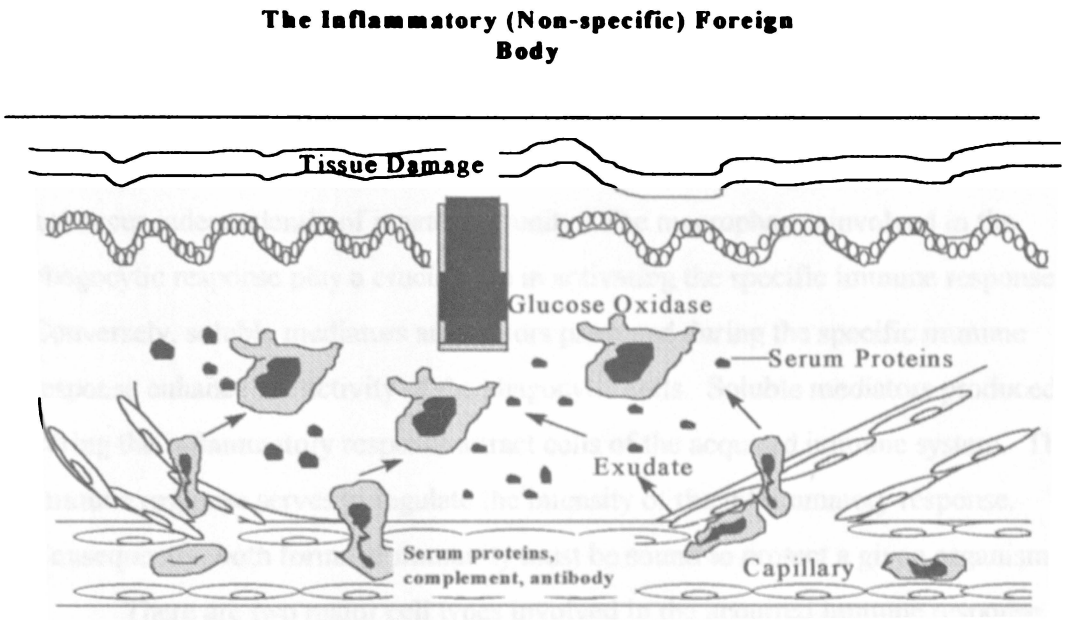

Figure 1. 1. Illustration of the non-specific immune response to invasion by a sensor.

Any tissue damage, whether caused by a wound or a microorganism, induces a complex series of events known as the inflammatory response. The cardinal signs of inflammation, redness, swelling, heat, pain, and loss of function correspond to the three major events of the inflammatory response: (1) increased blood flow, (2) increased capillary permeability and (3) influx of phagocytic cells. As the blood vessels from the affected area constrict, the blood flow increases, engorging capillaries and causing redness and heat. Increased capillary permeability facilitates an influx of fluid and cells from the engorged capillary to the surrounding tissue.

This fluid accumulates (called exudate) has a much higher protein content than normal vascular fluid and contributes to tissue swelling. Severe swelling eventually leads to pain and loss of function.

The migration of phagocytic white blood cells to the area is also facilitated by the increase in capillary permeability. The phagocytes first adhere to the endothelial wall of the capillary, then move through the wall into the tissue, then finally move through the tissue to the wound or infection. These phagocytic cells, as will be explained in more detail later, are critical to the specific immune response.

Acquired or specific immunity, unlike innate immunity, displays specificity, diversity, memory, and self/nonself recognition. However, acquired immunity does not occur independently of innate immunity. The macrophages involved in the phagocytic response play a crucial role in activating the specific immune response. Conversely, soluble mediators and factors produced during the specific immune response enhance the activity of the phagocytic cells. Soluble mediators produced during the inflammatory response attract cells of the acquired immune system. The immune response serves to regulate the intensity of the inflammatory response. Consequently, both forms of immunity must be sound to protect a given organism.

There are two major cell types involved in the acquired immune response, the B- and T-lymphocytes. Figure 1.2 shows a simplified list of the interactions of the two cell types. B-cells, the critical players in the humoral immune response, mature within the bone (B) marrow, expressing a unique antigen binding receptor called an antibody molecule.

Figure 1.2

The Immune (Specific) Foreign Body Response

The Acquired Immune Response Displays: Specificity Diversity Memory Self/Nonself Recognition	
Humoral Response	**Cell-Mediated Response**
B - cells activated	T_H - cells activated
T_H autostimulates T_H - cell clonal expansion T_H - cells secrete lymphokines	
Clonal selection Memory and plasma cell proliferation	T_C becomes CTL

Figure 1. 2. Sequence of events for the immune response.

The basic structure of the antibody, or immunoglobulin G (IgG), is shown in Figure 1.3

Figure 1.3

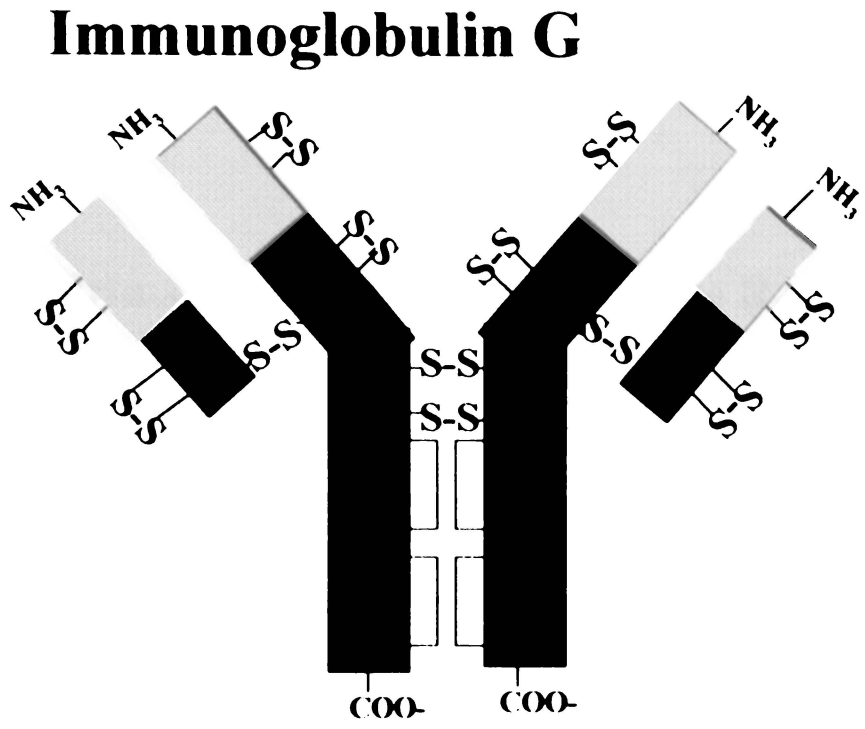

Figure 1. 3. The general structure of immunoglobulin G.

Immunoglobulin G (IgG) consists of two heavy polypeptide chains and two identical light polypeptide chains linked together by a several disulfide bonds. The amino-termini of each heavy and light chain pair form the cleft for antigen binding. Once a B cell encounters the antigen for which it is IgG specific, the cell begins to divide rapidly producing memory B cells that have antibody cells on the surface and secretory cells called plasma cells. This process, known as clonal expansion, is the basis of the seemingly lifetime immunity observed in animals surviving exposure to disease. Memory B cells have a long life span and only express membrane bound

IgG with identical specificity to the parent cells. The plasma cells secrete soluble antibody. The plasma cells live only a few days, but each cell is capable of producing more than 2000 molecules of antibody per second. The soluble antibody plays a crucial role in the secondary immune response, and also has been harnessed by analytical chemists in search of specific receptors for a variety of molecules. The results of clonal expansion can be observed by examining the difference between the primary and the secondary immune response diagrammed in Figure 1.4.

Figure 1.4

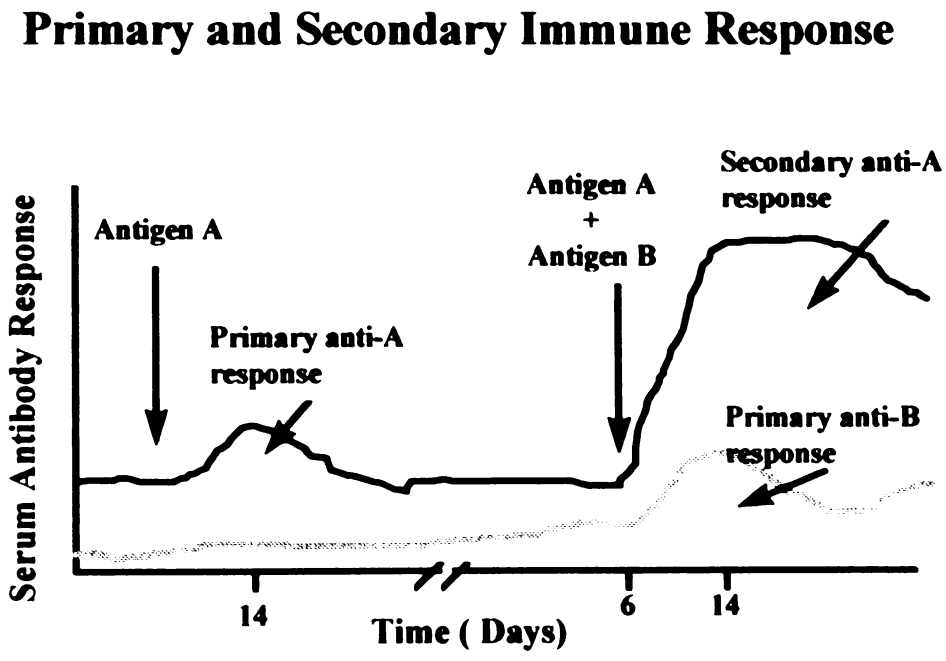

Figure 1. 4. Illustration of the serum antibody response to multiple immunizations.

T cells, involved in the cell-mediated immune response, arise from the same bone marrow stem cells as B cells, but they mature in the thymus (T). Like B-cells,

maturation results in the expression of a membrane receptor specific for an antigen. The T-cell receptor, unlike antibodies on the B cell, cannot recognize soluble antigen alone, but rather only in a complex with a major histocompatibility complex (MHC) molecule. However, like the B-cell, once a T cell receptor associates with an antigen-MHC complex, the T cell clonally expands into memory T cells and effector T cells.

Two sub-populations of T cells are T helper cells (T_H) and T cytotoxic cells (T_C). In response to antigen /MHC binding, the T_H cell secretes lymphokines that activate B cells, T_C cells, and phagocytic cells. T_C cells that recognize antigen/MHC binding in the presence of TH lymphokines proliferate and differentiate into cytotoxic T lymphocytes (CTL) which eliminate any body cells that display antigen, such as virus-infected cells, tumor cells, and foreign tissue cells.

While two distinct cell types operate, clearly they operate in concert. Lymphokines secreted from T_H cells stimulate the transformation of T_C cells to CTL and the clonal expansion and differentiation of B cells. However, due to the nature of IgG secreted by plasma B cells, it is the humoral response that can easily be measured simply by analyzing the blood. One method for this determination, the ELISA, is discussed below.

2.2.2. Enzyme Linked Immunosorbent Assay (ELISA)

The ELISA, introduced independently and simultaneously by two groups, Engvall and Perlmann, and Van Weemen and Schuurs in 1971, revolutionized the analytical use of the immunoassay *(15,16)*. The principle of the ELISA depends upon using an enzyme label, rather than a radioisotope. Figure 1.5 is a diagram showing the sequence of an sandwich ELISA. As seen in the figure, the antigen is immobilized on the surface by adsorption, then the serum containing antibody is introduced. The unbound antibody is removed by washing. In order to detect the amount of bound antibody, an enzyme labeled reporter antibody specific for an

epitope on the antibody bound to the antigen is added in excess. This binds to the antigen bound antibody. Detection is effected by adding the enzyme substrate. Conversion to product by the enzyme causes a measurable physical or chemical change, in most cases a color change in induced. The power of the enzyme label lies in the fact that the signal magnitude depends on how long the enzymatic reaction is allowed to proceed. This makes possible assays with sensitivities in the nM to pM range without the hazards associated with radiolabeling *(15,16)*.

Figure 1.5

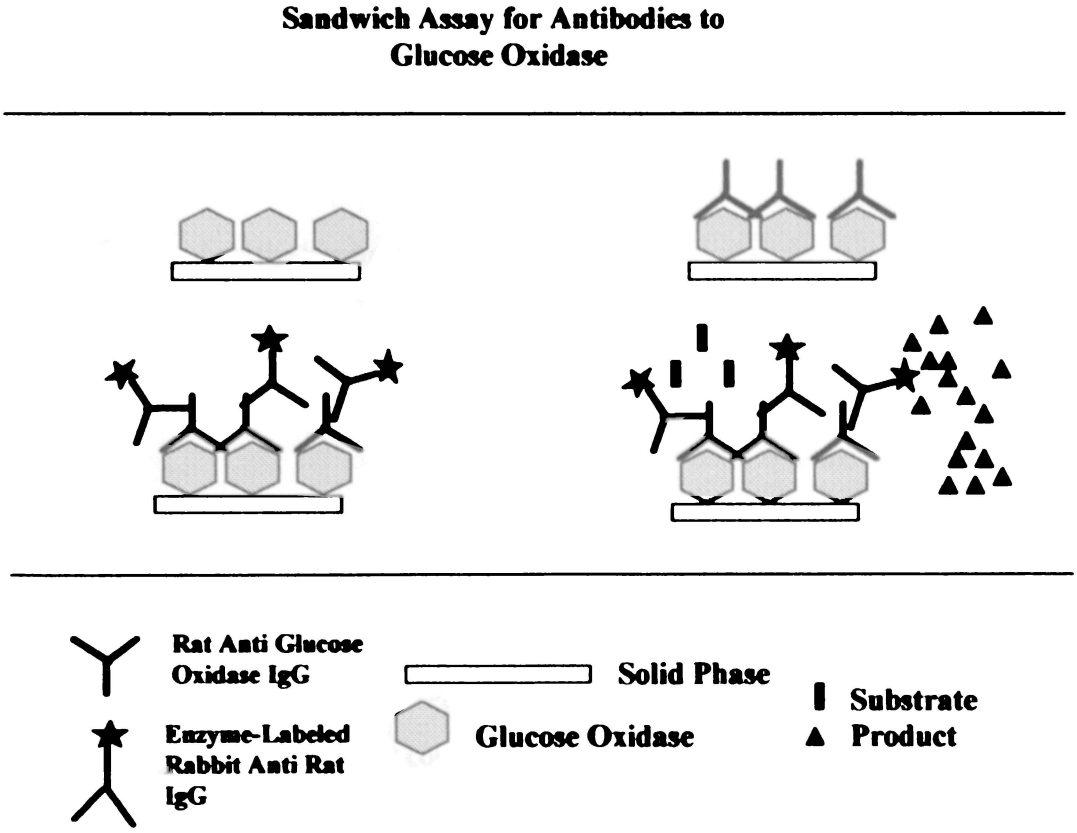

Figure 1. 5. Schematic of the sandwich ELISA for screening rat antisera to glucose oxidase.

2.2.3. Antibody Titer

Enzyme immunoassays can be used for the determination of antibody titer. Consider the titration of the binding sites of the antibody by an antigen where the antigen is immobilized and the concentration of the antibody is varied. The equilibrium equation can be written as follows:

$$[Ab] + [Ag] \underset{k_b}{\overset{k_f}{\rightleftharpoons}} [AbAg] \qquad (1.1)$$

where k_f and k_b are the association and dissociation rate constants, respectively. The equilibrium affinity constant, K, is a measure of the affinity of the binding sites for the antigen and can be determined as shown below.

$$K = k_f/k_b = [AbAg]/[Ab][Ag] \qquad (1.2)$$

If at $OD_{1/2max}$ half the binding sites are filled then

$$[AbAg] = [Ag] \qquad (1.3)$$

Then

$$K = 1/[Ab] \qquad (1.4)$$

In the case of polyclonal antibodies, where there are antibodies with a variety of affinities for the antigen, this procedure determines the average or apparent affinity constant only. Where the exact concentration of antibodies cannot be determined, the dilution factor corresponding to $OD_{1/2max}$ can be used. The dilution volume becomes larger as the affinity increases. The dilution factor, $1/2^x$, can be compared between a positive and negative control to determine if the positive control has a specific response *(4)*.

2.2.4. Immunogenicity

The amount of antibody found specific for a particular epitope is directly related to the immunogenicity of the molecule used for immunization. Immunogenicity is the measure of how well a particular molecule induces the specific immune response. Generally speaking, proteins are the best immunogens followed by polysaccharides. Nucleic acids and lipids are typically not immunogenic unless complexed to either proteins or carbohydrates. However, immunogenicity is less an intrinsic property of the macromolecule than the result of a combination of factors. Immunogenicity is largely determined by the size, foreignness, chemical complexity and composition, ease of degradation, dose, and route of administration.

Two closely related factors must be met for an organism to mount an immune response. First, the molecule must be large enough to be "seen" by the body, with molecules on the order of 100,000 Dalton (Da) being the best immunogens, and substances less than 5 to 10 KDa being poor immunogens. Glucose oxidase, the enzyme whose immunogenicity is being investigated, is a 160 KDa protein, and therefore meets this requirement. The second factor required is foreignness. The molecule must be recognized as nonself for an immune response to occur. Any molecule not presented during the critical phase of fetal development when the immature lymphocytes are exposed to self components will be recognized as foreign. Generally speaking, proteins from phylogenetically distant species are recognized as foreign. As glucose oxidase is isolated from the one-celled organism, *Aspergillus niger*, it is expected that all mammals will find it foreign.

However, even with a molecule such as glucose oxidase that is large and foreign, the chemical composition and heterogeneity still play a role in immunogenicity. For example, synthetic homopolymers (polymers that consist of a single amino acid or sugar) lack immunogenicity regardless of size. The addition of aromatic amino acids increase the immunogenicity of these synthetic polymers. Finally, topological organization, from the primary level to quaternary level in

proteins, affect the structural complexity and the resulting immunogenicity. Glucose oxidase contains many aromatic amino acids, and has topological complexity as well. No matter how large, foreign, and complex an antigen, it must be degradable so it can be presented in association with the MHC. If it is resistant to degradation by proteolytic enzymes, this cannot occur, and the T_H cells will not stimulate the B cells and T_C cells. For example, mammalian enzymes recognize only L-amino acids. A large polymer of D-amino acids will not be immunogenic. Glucose oxidase is composed of L-amino acids, and has no special protection against proteolysis. Therefore, it should be immunogenic.

The biological system of the animal to be immunized plays a heavy role. Species differences as well as animal to animal variations play a role. For example, it has previously been shown that the holoenzyme, glucose oxidase with its flavin adenine dinucleotide prosthetic group, is toxic in mice. However, the removal of that group makes it an excellent immunogen. Similarly, the dose is crucial. Another way to immunize with the native glucose oxidase is to use a low dose with slow release. The route of administration affects which part of the body is involved in the response. Intravenous injection carries the immunogen first to the spleen, while subcutaneous injection goes to the local lymph nodes. Differences in the lymphoid cell populations in different areas determine the difference in the intensity of the subsequent immune response. Additionally, the addition of adjuvants, materials which enhance the immunogenicity of the molecule used for immunization, improves the immune response. The mechanism for this increased immunogenicity is unclear, but mechanisms that seem to play a role are increasing persistence, creating an antigen precipitate, and activating macrophages directly.

2.3. Experimental

2.3.1. Protocol for Sensor Preparation and Implantation

2.3.1.1. Materials

All solutions used were mixed w/v except where otherwise indicated. Cellulose acetate (CA) (39.8 acetyl content) and Nafion (5% solution (wt/wt)) in low aliphatic alcohols) were purchased from Aldrich. Polyurethane (PU) (SG 85A) was from Thermedics Inc. (Woburn, MA).

All *in vitro* measurements were conducted in 0.1 M pH 7.4 phosphate buffer containing 0.15 M NaCl and 0.1 g/L NaN_3 prepared from deionized distilled water. 5% CA solution (wt/wt) was prepared by dissolving CA in 1.2 : 1 acetone:ethanol. 5% PU (wt/wt) was made in 98% tetrahydrofuran (THF) and 2% dimethylformamide (DMF) stirring over 15 hours at room temperature. Glucose sensors were prepared from a Teflon coated Pt-Ir wire obtained from Medwire Corp. (Mount Vernon, NY) with a wire diameter of 0.17 mm and overall diameter of 0.25 mm. Silver wire of 0.05 mm (o.d.) from Aldrich was used to form coil Ag/AgCl reference electrode. The reference electrode was coated with an external polyurethane membrane.

2.3.1.2. Procedure

A Teflon coated Pt/Ir wire was cut into 8 mm in length to which a sensing cavity was created at one end by making a circular cut and then moving the Teflon tubing toward the tip. A cavity of 3 mm in length was thus created. The extra 3 mm Teflon tubing at the tip was then cut and discarded.

The sensor cavity was dip-coated in a 5 % CA solution followed by a loop-coating of Nafion. The same process was repeated one more time and the sensor was air dried.

Enzyme was immobilized by delivering 0.4 µl freshly prepared enzyme solution with a microsyringe to the cavity. The solution contained 4 % glucose

oxidase, 0.1 % glutaraldehyde and 1 % bovine serum albumin, respectively. Two drops of the enzyme solution were needed to fill the entire cavity. The enzyme loading was approximately 3 U in each sensor (assuming that activity was preserved after the cross-linking). A total of 0.016 μg of glucose oxidase was deposited on the electrode.

The outer membrane of the sensor was coated on the entire sensor with a loop and immediately soaked in phosphate buffer to acquire desired membrane permeability. The sensors were kept in buffer for one week and washed in pure water before drying for sterilization. Sensors without the outer membranes were also fabricated similarly except that the step for outer membrane coating was eliminated. The sensors were sterilized in ethylene oxide gas for over ten hours at 1 atm pressure and thoroughly degassed before implantation.

2.3.2. Protocol for Immunization and Screening

2.3.2.1. Materials

Glucose oxidase from *aspergillus niger* (I.U.B. 1.1.3.4; 250,000 U/g) used in both the native or apoenzyme form was obtained as the native enzyme from Biozyme Laboratories International, Ltd. (San Diego, CA.; Lot 218 A). Both Freund's complete and incomplete adjuvant were purchased from GIBCO Laboratories (Grand Island, NY). The antibody-enzyme conjugate, Fc - specific horseradish peroxidase - labeled goat anti rat IgG(GTxRT -Fc specific -HRP), was purchased from Pierce (Rockland, IL; Lot #920521004). HRP substrate consisting of a one to one solution of 3,3',5,5' - tetramethylbenzidine (TMB) and hydrogen peroxide was purchased in combination from Kirkegaard and Perry Laboratories, Inc. (Gaithersburg, MD). The wash buffer and diluent was prepared using reagents from Fisher Scientific (St. Louis, MO). Bovine serum albumin and Tween 20 was obtained from Sigma Chemicals (St.Louis, MO). All buffers were made using 18 MΩ filtered water from a Barnstead NanoPure system.

The rats used for the immunization experiment were male Sprague-Dawley rats approximately 350 g in weight purchased from Sasco, Inc. (Omaha, NE).

2.3.2.2. Equipment

All ELISAs were performed using Corning nonsterile 96 well polystyrene flat bottom plates from Corning Glass Works (Corning, NY). Plates were read using a Molecular Devices Kinetic Microplate plate reader and accompanying software (Menlo Park, CA). Apoglucose oxidase was centrifuged in a Beckman J-21B centrifuge at low temperature.

2.3.2.3. Procedures

2.3.2.3.1. Preparation of the Apoenzyme

Apoglucose oxidase was prepared according to the method of Swoboda with some modifications from the method used by Wimalasena *(12,13)*. The apoenzyme was prepared by adding a 20 mg/mL solution of glucose oxidase (20 mg/mL in 0.1M PBS pH 7.4) to 20 mL of a saturated solution of ammonium sulfate, pH 1.4, at -3 °C with stirring. It was then centrifuged at 20,000 rpm (48384 x g) for 15 min at -5 to +10°C (for Batch II apoGOx 20000 x g was used). The yellow supernatant fluid was discarded and the white solid pellet was resuspended in a 0°C 2.5 M sodium acetate solution. The resuspended pellet was treated with the acidified ammonium sulfate solution, centrifuged, and neutralized as described above. A total of three acidification cycles were completed. After the last acidification cycle was completed the pellet was resuspended in a 90% saturated solution of ammonium sulfate and centrifuged as above. The resulting solid was dissolved in 2 mL 0.1 M PBS, pH 7.4, and dialyzed against the same for two days replacing the buffer with fresh solution three times during this period. The removal of the FAD was determined by observing no absorbance at 450 nm, the absorbance maximum for FAD *(13)*. The dialyzed solution was then concentrated under vacuum about 5 hours to a final volume of

approximately 4 to 6 mL. Protein concentration was determined by the BCA(bicinchoninic acid) protein assay which is based on the biuret reaction (Pierce; Rockland, IL). Batch I apoGOx was identical to Batch II apoGOx except that Batch I was passed through a 0.2 micron Corning nylon membrane filter, greatly reducing its concentration (Corning Glass Works, Corning, NY). Consequently, the filtering step was omitted for Batch II.

2.3.2.3.2. The Immunization Protocol

The six rats serving as the positive control were initially injected in 10 to 14 sites subcutaneously with 71 micrograms Batch I apoGOx per site in a solution of 1:3 apoGOx to Freund's complete adjuvant (1.4 mL total volume injected). The rats were boosted 14 days later with a 1:3 solution of Batch II apoGOx in Freund's incomplete adjuvant. A total of one hundred micrograms per rat of Batch II apoGOx was injected subcutaneously divided equally among four sites. The rats were reboosted 28 days from the first injection with all conditions identical to the boost injections. The 18 rats were reboosted as above 120 days after the first injection. The rats were anesthetized with halothane throughout all the injections. All injections were performed using a sterile 22 gauge needle.

Similarly, the 12 rats implanted with sensors were anesthetized with halothane while two sensors were completely embedded subcutaneously through a 21 gauge needle requiring no stitches. The same procedure was repeated for all subsequent implantations, or boosts, which followed the same schedule as the positive control rats. The sensors were not removed once they were implanted. Therefore, there were eight sensors in each rat after the completion of the immunization schedule. The rat immunization schedule is shown in tabular form (Table 1.1). Seven randomly selected rats were untreated with either soluble apoenzyme or sensors. These rats were used as negative controls and were designated NEG.

2.3.2.3.3. The Bleeding Protocol

One rat from each group was bled 41 days after the first injection and then again 64 days from the first injection. All eighteen rats were bled 76 days (1/25/94) from the first injection and again 98 days (2/19/94) from the first injection. The 18 rats were then bled again 119 days (3/9/94) from the first injection and implantation. They were reboosted with either Batch II apoGOx or with the appropriate sensor on day 120. They were then bled nine days later at 128 days (3/19/94) from the first injection.

Blood was taken from the tail of an anesthetized rat. Approximately 0.500 mL of blood per rat was obtained in this fashion. The blood was then coagulated and spun down. The serum remaining was screened by ELISA.

Table 1. 1

Designation	Treatment	Number	Boosts (Days from Initial Immunization)	Bleeds (Days from Initial Immunization)
NEG	no treatment	7	N/A	N/A
POS	apoGOx	6	14, 28, 120	76, 98, 119, 128
SWM	Sensors with an outer membrane	6	14, 28, 120	76, 98, 119, 128
SNM	Sensors with no outer membrane	6	14, 28, 120	76, 98, 119, 128

2.3.2.3.4. The ELISA Protocol

All solutions of antigen for coating microtiter plates were 10 microgram/mL in 0.1 M carbonate buffer, pH 9.5. The wash buffer was 0.01 M PBS, pH 7.4, 0.05% Tween 20. The block buffer was identical to the wash buffer except that it also contained 1% bovine serum albumin. Between each coating the plates were washed with wash buffer 4 times then patted dry unless otherwise indicated. Prior to addition to the plate, all sera were diluted 1:50 in 0.1 M PBS, pH 7.4. Each plate was coated with apoGOx on the first half (rows A-E) and native GOx on the second half (rows F-H). Two rats were assigned per plate and were screened against both the apo- and holoenzyme with a repetition of two wells per rat. Each plate for the positive control rats used column 11 as the negative control with 100 µL of serum from a negative control rat in each well. Each plate for the sensor rats had column 10 as the positive control and column 12 as the negative control. Both controls were prepared 1:50 in 0.1 M PBS, pH 7.4. A schematic of the plate and the corresponding contents and dilution factors is shown in Fig. 1.6.

Nine microtiter plates were coated with both Batch II apoGOx and native GOx (Lot#218) with 48 wells per antigen per plate and 100 µL antigen per well. The plates were incubated at 37°C for 90 minutes. All wells were blocked with 200 µL of block buffer and incubated for 1 hour at 37°C . To each well, 100 µL of block buffer was added. A serial dilution of the rat serum across the plate was achieved by adding 100 µL of diluted serum to the first wells. The results dilutions of this procedure is shown in Figure 1.6. The solution was then mixed in the pipette and 100 µL from the first well was delivered to the second well. The mixing and delivering steps were repeated across the plate leaving the last column (column 12) as a blank. The plates were incubated for 60 minutes at 37°C . The horseradish peroxidase antibody-enzyme conjugate, GtxRt-Fc specific-HRP, was diluted 1:35,000 in block buffer, and 100 µL was added to each well and incubated as previously. Finally, 100 µL of a 1:1 TMB and hydrogen peroxide solution was added to each well and

incubated for 15 minutes at room temperature. The reaction was stopped by the addition of 50 µL of 1M HCl to each well. The plates were read at 450 nm.

Because the titers for all negative controls were about 2^2 and the negative control well on the plate at the highest concentration gave an optical density of essentially zero, a negative control titer experiment was not run with or subtracted from any screening of the three groups.

Figure 1.6

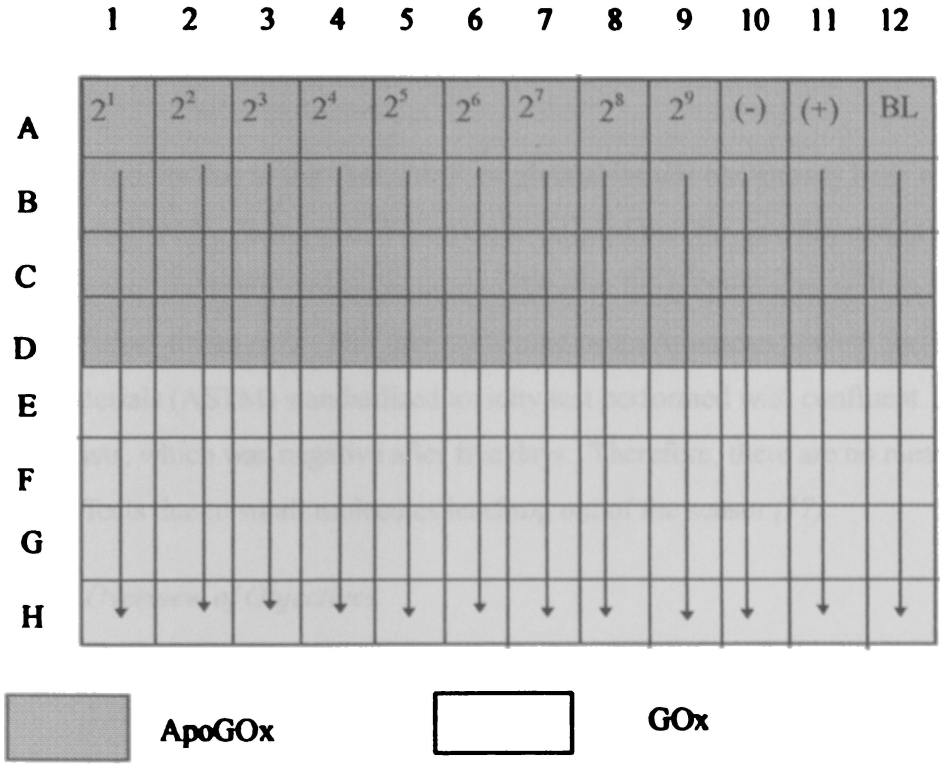

Figure 1. 6. Schematic of microtiter plate. Shaded area was coated first with apoGOx, the remainder with GOx. Dilution factors for the serial dilution of the 1:50 sera:PBS solution used for the titer is shown. Placement of the controls and blanks is also indicated.

2.4. Results

All three populations of rats were screened against apoGOx and the holoenzyme, but the highest affinity for all three populations was for the holoenzyme. Only these results are considered here.

The optical density for each dilution was averaged and plotted versus the dilution factor ($1/2^x$) for each rat. Plots for each bleed were consolidated onto one plot for each population and can be seen in the Appendix. From measuring the dilution corresponding to the optical density at half the maximum the dilution factor which corresponded to a titer break was determined for each rat. The titer is said to be higher representing a higher concentration of antibodies as the dilution factor decreases.

Toxicity due to the THF, DMF, or glutaraldehyde has already been eliminated. Studies in 1991 by Zhang and Wilson demonstrated that the five day conditioning step removes the small molecules used to dissolve the polymers, as well as the enzyme cross-linker *(17)*. This was confirmed by an American Society for Testing and Materials (ASTM) standardized toxicity test performed with confluent fibroblasts, which was negative after five days. Therefore, there are no measurable toxic effects due to small molecules leaching out of the sensor *(17)*.

2.4.1. Overview of Objectives

The objectives were to answer the following questions:

1. Does the sensor stimulate an immune response?
2. Do different immunization routes produce a difference in the immune response?
3. Does the outer membrane have an effect on the immune response?
4. Does sensitization occur with repetitive injection/implantation?

There are three methods of evaluating the results: 1. Descriptive; 2. Graphical; and 3. Statistical. The above questions will be answered using all three of

these methods where necessary. Since the questions we are asking require asking whether a particular treatment results in a measurable difference, statistics will be used only to give confidence at a specified confidence level that the differences are most likely a result of the treatment and not to chance alone.

2.4.2. Does the sensor stimulate an immune response to glucose oxidase?

The titers of the negative control rats shown in Table 1.2, are uniformly low, at 2^2. The titers of the treatment groups, POS, SNM, and SWM, are given below (Table 1.3). The mean titers for the positive control were high (about 2^7) compared to that of the negative control sera (less than 2^2). The two groups immunized against the sensors also produced titers that were significantly higher than the negative controls (2^5 to 2^8) except for two rats that had titers around 2^3.

Table 1. 2

Titers of Negative Control Rats (X 10^{-4})

Rat Identity	Titer given as dilution factor
NA	40
NB	30
N319	40 (2^2)
N320	70 (2^2)
N321	40 (2^2)
N324	30 (2^2)
N325	30 (2^2)

Table 1. 3

Titer Breaks Given as (Dilution Factors)$^{-1}$

Rat	POS 1/25/94	POS 2/16/94	POS 3/9/94	POS 3/16/94	Rat	SNM 1/25/94	SNM 2/16/94	SNM 3/9/94	SNM 3/16/94	Rat	SWM 1/25/94	SWM 2/16/94	SWM 3/9/94	SWM 3/16/94
1	2^{8}	2^{7}	2^{7-8}	2^{8}	7	2^{3}	2^{6}	2^{6}	2^{5-6}	13	2^{3}	2^{3}	2^{6}	2^{7-8}
2	2^{9}	2^{7}	2^{6}	2^{6-7}	8	2^{6}	2^{6}	2^{7}	2^{5}	14	2^{7}	2^{6}	2^{4}	2^{4}
3	2^{7}	2^{7}	2^{6}	2^{7}	9	2^{5}	2^{7}	2^{5}	2^{5-6}	15	2^{6}	2^{4}	2^{6}	2^{6-7}
4	2^{7}	2^{9}	2^{6}		10	2^{5}	2^{7}	2^{6}	2^{4}	16	2^{5}	2^{8}	2^{7-8}	2^{8-9}
4	2^{8}	2^{6-7}	2^{6}	2^{7}	11	2^{6}	2^{5}	2^{5}	2^{5-6}	17	2^{4}	2^{7}	2^{3}	2^{3}
6	2^{8}	2^{8}	2^{6}	2^{6}	12	$2^{5.5}$	2^{5}	2^{6}	2^{3}	18	2^{6}	2^{7}	2^{7}	2^{6-7}

Simply by inspecting the data and comparing the titers of the negative controls to the rats immunized by various methods, it is obvious that an immune response occurred in the POS, SWM, and SNM rats. The POS group gave slightly higher titers than the SNM group and both groups gave less variable results within the group as compared to the SWM group which has rats with both very high and very low concentrations of anti-GOx antibodies as indicated by their titers.

A graphical representation of the data also shows that all the treatment groups give an immune response compared to the negative control. Figure 1.7 shows a representative plot. It is a graphical comparison of SWM,SNM,POS, and NEG rat populations screened against holoGOx. The average titers with error bars are shown. Not only do the negative controls (NEG) give a low response, but the response does not display any concentration dependence. In contrast, as the dilution increases, the SWM, POS, and SNM rats all show a titer plateau, followed by a decrease. This is characteristic of the presence of specific antibodies to the screen antigen, glucose oxidase. The titers from each bleed plotted by treatment can be viewed in Figures 1.8 to 1.19 in Appendix 1.1.

Figure 1.7

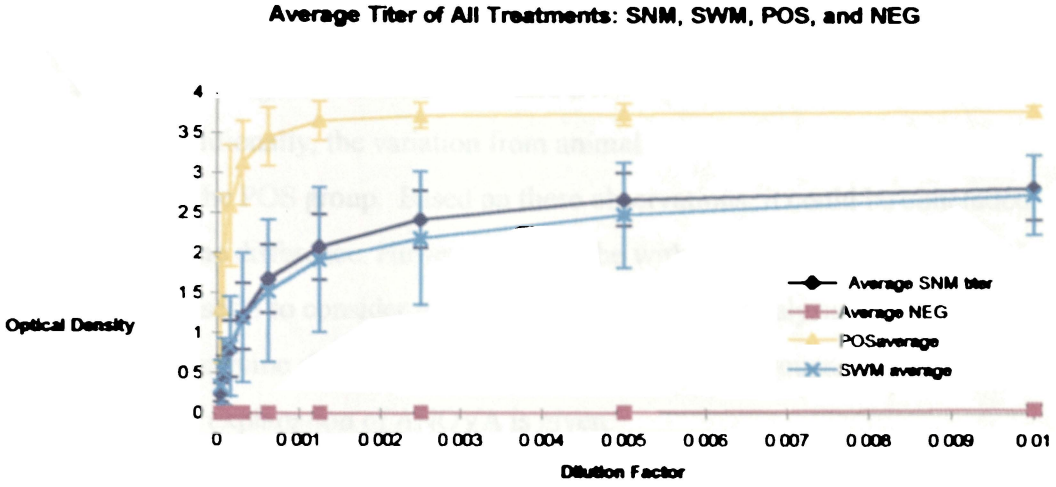

Figure 1. 7. Average rat serum titer of SNM, SWM, and POS rats compared to the negative control serum titer. The sera from the bleed on 1/25/94 were screened against the holo glucose oxidase.

While statistical analysis is not required to conclude that all glucose oxidase treatments produced an immune response, an analysis of variance (ANOVA) was used to verify the above observations. The one way ANOVA at the 95% confidence level comparing all four groups showed that there was a significant difference. However, this test does not establish where the difference lies. A series of follow-up two way ANOVA tests comparing each treatment group to the negative control group proved that there was a significant difference between each group and the negative control. The ANOVA tables are found in the Appendix. The next question deals with differences in the degree of immune response.

2.4.3. *Are there differences in the immune response as a result of immunization route?*

A visual inspection of the data in Table 1.2 shows that the titer of the POS does appear to be higher than both SNM and SWM by one to two orders of magnitude. Additionally, the variation from animal to animal appears to be less pronounced in the POS group. Based on these observations, it could be concluded that there is some difference. However, due to the within group variation from animal to animal it is useful to consider using a statistical method, analysis of variance, or ANOVA, to determine if there are true differences between groups. In the Appendix a more detailed explanation of ANOVA is given.

The null hypothesis that was tested can then be stated as the following: There is no significant difference between the mean titer produced by rats immunized using apo-GOx, sensors with no outer membrane, and sensors with the outer membrane. This hypothesis was tested using ANOVA. The result was then compared to what is expected from simply looking at the data.

The results of the overall ANOVA comparing the mean titers of three populations, SWM, SNM, and POS, gave an F ratio = 1.30 which was less than the critical F number, 3.28, at the 95% confidence level. Thus, the null hypothesis is not rejected, suggesting that the differences observed between treatments are due to chance alone. The observation that the mean titers in the SWM and SNM group are lower than the POS group suggests that this may not be true. Also, since the variance in the SWM group was so different, the validity of the test was questioned. The source of the variation could be explained in two ways: the variation in the animal immune response or the variation in the sensors themselves.

2.4.4. *Does the outer membrane have an effect on the immune response?*

Since the rats with the lowest titers in the SWM group consistently display a low titer throughout the study (Table 1.3), it seems reasonable that part of the source

of variation is due to the differences in the animals themselves These variations in the randomly assigned rats could not be corrected for by experimental design. Although the rats were all of the same breed, sex, approximate weight range, and housed in the same room there were several variables that could not be controlled that could have affected the immune response of the animals. Among these were the somatic mutations in the antibody hypervariable region and the concentrations of interleukins *(8)*.

However, unpublished data from our lab indicate that while the sensor inner membrane is reproducible from sensor to sensor, the outer membrane, presented only to the SWM rats, is highly variable. It is possible that there is an effect of the membrane that could depress or enhance the immune response. For this reason, it is not justified to label low titer rats as outliers and exclude them from the study.

To get more detailed statistical information and to correct for experimental bias, such as the biological factors that will make each rat's immune system vary, the analysis of covariance can be applied (ANCOVA). In certain ANOVA situations there is a need to remove potential bias due to the fact that categories differ in their values of a covariate X *(18)*. In the case of this experiment, the covariate is the physiological condition of each animal. The measure of this was the titer value before the boost on 3/19/94. The means prior to the boost are adjusted based on the assumption that the titers should not be different if differences in individual animal's physiology is taken into account. If the null hypothesis is rejected, than it is more likely the variation is due to the sensors themselves or some other factor, since the ANCOVA adjusts the means to account for differences in titer.

The adjusted means are listed in Table 1.4. They were calculated using standard methods *(18)*. Note that for the POS, SWM, and SNM groups the adjusted means are very close, while the observed means were not. For ease in manipulation all titers were multiplied by 10^4 and then the statistical test was applied.

Table 1. 4

Adjusted Means for the Dependent Variable (Titer Post Intervention)

Factor	Code	Observed Mean	Adjusted Mean
Group	POS	2.474	5.891
Group	SWM	7.542	5.228
Group	SNM	9.083	7.980

The results of the ANCOVA of all three treatments, SWM, SNM, and POS, are listed in Table 1.5. The ANCOVA of the adjusted means rejected the null hypothesis at the 95% confidence level. This overall ANCOVA only shows that the null hypothesis is rejected, it does not give enough information to determine for which pair or pairs of data this occurs.

Table 1. 5

Results From ANCOVA

of All Three Groups(POS, SEN, SNM—17 subjects)

α=0.05, average squared correlations for both pre-and post-intervention variables are 1.00000

source of variation	sum of squares	degrees freedom	mean square	F	Sig. of F
Pre	695.764	1	695.764	215.78	0.000
Group	24.487	2	12.244	3.797	0.050 (sig.)
explained	720.251	3	240.084	74.457	0.000
residual	41.918	13	3.224	-	-
total	762.169	16	47.636	-	-

A follow-up series of two-way ANCOVA tests of the same hypothesis comparing only two groups simultaneously is seen in Table 1.6. In Table 1.6, the significance of F, expressed as a probability, rather than the F ratio is used to accept or reject the null hypothesis. If the significance of F is less that the α value (0.05), the null hypothesis is rejected. This is only true in the comparison between the mean adjusted titers of SWM and SNM (Significance of F = 0.02). Therefore, the pre-boost results, are adjusted for the covariate (animal bias as measured by the titer), these two groups still differ significantly in their response to the last boost at the 95% confidence level. This supports the hypotheses that the titer is influenced by the presence or absence of the outer membrane.

Table 1. 6

ANCOVA Between Two Groups

α =0.05

(uses same raw data and adjusted means as above)

Source of Variation	Sum of Squares	Degrees Freedom	Mean square	F	p
Within Cells	41.92	13	3.22	-	-
Regression	592.81	1	592.81	183.85	0.000
Btw. POS & SWM	1.04	1	1.04	.32	0.579
Btw. POS & SNM	10.87	1	10.87	3.37	0.089
Btw. SWM & SNM	22.54	1	22.54	6.99	0.020

2.4.5. *Does sensitization occur with repetitive injection/implantation?*

The t-test for paired data tests data that involves multiple or repeated measurements on the same subject, for example before and after the injection of the apoenzyme. The t-test tests the null hypothesis, H_0, that there is no difference between the pairs (before and after injection). Simply put, H_0: $\mu = 0$, where μ is the mean of the difference in titer before and after treatment. This test is useful in determining if immunization boosts affect the titer.

In order to determine if the boost was affecting the titers within the three groups, the hypothesis that the difference between the titer at Time 1 and Time 2 within each group equals zero was tested by the t-test. The results are given in Table 1.7. The null hypothesis was only rejected for the SWM group suggesting that the addition of more sensors changed the titer while in the other groups the boost had no effect. This is consistent with the titers observed for days 3/9 and 3/16 (Table 1.2). It is seen that the titers for all rats in the SNM group and 3/5 of the rats in the POS group have decreased or stay the same. In the SWM group only two animals had titers that remained the same.

Table 1. 7

Dependent t-Tests Within Groups Comparing the Means at 3/9/94 and 3/18/94

Group	Date	# of cases	Mean	Mean Difference	t value	Degrees Freedom	2-tail Prob.
POS	3/9/94	5	3.0800± 1.363	.6060	1.41	4	0.230
POS	3/18/94	5	2.4740± 1.187				
SWM	3/9/94	6	9.9500± 12.510	2.4083	2.87	5	.035
SWM	3/18/94	6	7.5417± 10.724				
SNM	3/9/94	6	8.500± 3.523	0.5833	0.50	5	.637
SNM	3/18/94	6	9.0833± 3.288				

2.4.6. Comparison of Screening Antigens

Both native GOx and apoGOx were used as screen antigens for the ELISAs of all rat sera. These results are shown in the Appendix, Figures 1.8 to 1.19. The native enzyme in every case gave a much higher maximum optical density and higher titers. A similar experiment using mouse monoclonal antibodies produced by injecting apoGOx into the spleen reported by Wimalasena *(12)* showed different results. In every case, the native and apoenzyme gave the same results. This may reflect differences in mouse and rat anatomy, as well as the difference in immunization route. Subcutaneous injection of GOx would result in lymphocyte response from local lymph nodes, while the direct injection into the spleen results in lymph activity from the spleen. These differences had no adverse effects on the experiment, but are worth noting here for future workers.

2.5. Discussion

The presentation of the antigen, glucose oxidase, on the surface of a sensor protected by an outer membrane and on the surface of a sensor with no outer membrane effectively generated an immune response. In some cases, the presentation of the antigen on the sensor with the outer membrane generated a better response than the presentation of the apoenzyme in solution. In one-third of the animals of the SWM group there is essentially no immune response. In the case where there is no outer membrane, the immune response is lower than the positive control but with less within group variation than the SWM group. Finally, the SWM group still showed effects of the third boost, while the other groups appeared to be sensitized by this time.

The presumed effect of the outer membrane has multiple explanations. According to Ziegler's work, cellulose acetate alone, not polyurethane or glucose oxidase, produced an immune response *(8)*. Perhaps the observation that the SNM

group had less within group variation reflects that the outer membrane protected the GOx layer from exposure to the body somewhat, but variations in the outer membrane conferred different levels of protection. Conversely, one might propose that some outer membrane - GOx conjugate produced increased immunogenicity to the GOx in some animals. However, Ziegler's experiments do not indicate that the polyurethane (12 % w/v in DMF) is immunogenic *(8)*. Recall that the outer membrane used on the sensors SWM is a 5 % polyurethane membrane.

Comparisons to Ziegler's study should be made with caution. The first reason is that this study used male Sprague-Dawley rats, while his study used female Lewis rats. The second reason is that he did not report the titer of the animals, rather only the optical density at one concentration. This could be significant, because without evidence that the titer of the positive controls is high, it is possible that the dilutions that Ziegler used were inappropriate *(8)*. The high dose hook effect sometimes observed in sandwich assays can contribute to the suppression of apparent antibody response at high doses *(20)*. Since the titer was not determined, there is no evidence that they were working at optimized dilutions to prevent this kind of phenomenon.

There are several possible explanations for the fact that antibodies to glucose oxidase immobilized on the sensors were observed. The apoenzyme was presented with Freund's adjuvant facilitating the immune response by both irritation and slow release of the antigen, but it was eventually cleared. The sensors, on the other hand, were not implanted with an adjuvant but hydrogen peroxide is produced at both types of sensors and the sensors were not excised. Consequences of this are the stimulation of macrophage migration to the site as a result of irritation by hydrogen peroxide and the continued availability of antigen. In addition, in the case of both types of sensors, the degradation of the inner or outer membrane could serve as an irritant and a slow delivery system.

Sensitization can be explained as well. Self proteins could adsorb to the outer membrane, denaturing them and causing an immune response against altered

self proteins, thus decreasing the immune response to the glucose oxidase. The continual slow release of glucose oxidase did not lead to tolerance in both sensor groups, as was expected. This could be related to the heterogeneity of the outer membrane from sensor to sensor.

The absence of the outer membrane in the SNM group may enhance the effects of denaturing of self protein, thus the results would have less variability from animal to animal as observed in the SNM group. It is reasonable that the SWM sensors, because of the variable outer membrane, would produce slightly different self-membranes with every implantation, while the more homogeneous SNM sensors will lead to the sensitization faster. POS, of course, has little variation from immunization from immunization, but is dosed much higher than either sensor group. Both dose and availability can contribute to sensitization.

2.6. Conclusion

Clearly the immobilization of glucose oxidase on an electrode covered by an outer polyurethane/silicone membrane was an effective method of generating antibodies to glucose oxidase. Moreover, there was a significant difference in the immune response tied to the presence or absence of the outer membrane. Therefore, it can be concluded that the presentation of the holoenzyme on the glucose sensors was as effective in some animals as the injection of the apoenzyme in generating an immune response to the holoenzyme and the presence of the polyurethane/silicone membrane was critical to this response.

2.7. Future Work

The role of the outer membrane is unclear at this point. Further work to characterize the immune response to the membrane materials themselves must be done to fully assess the role of the outer membrane and permanent implantation in the immunogenicity of this method of antigen delivery. This would include implanting whole sensors and implanting the membranes alone. The membranes

currently used for human trials are a mixture of polysiloxane and polyurethane. This polymer mixture and the sensors with this mixed polymer as the outer layer should be tested in a parallel experiment. Another approach would be to try and make a soluble glucose oxidase-polymer conjugate, and determine if this combination is immunogenic. This would be useful in determining if the polymer must be presented as a membrane, or if the polymer building blocks themselves can enhance immunogenicity.

Additionally, improvements could be made in carrying out the animal study. It would be advantageous to screen each rat prior to the immunization. This would provide another negative control measure, and could be used to determine any immune response bias prior to immunization. Moreover, it would be of interest to use the holoenzyme as the positive control and compare these results to that obtained using the apoenzyme. This would be useful in further characterizing the rat as a model animal for immune response tests to this sensor system.

It is clear that there is much work yet to be done. Nevertheless, the impact of this study is the suggestion that the evaluation of the biocompatibility of biosensors in the future should include the determination of the specific immune response to all the biosensor materials.

2.8. References

1. Bindra, D.S.; Zhang, Y.; Wilson, G.S.; Sternberg, R.; Thevenot, D.R.; Moatti, D.; Reach, G. *Analytical Chemistry* **63**, 169 (1991).
2. Reichert, W.M.; Saavedra, S.S., "Materials Considerations in the Selection, Performance and Adhesion of Polymeric Encapsulants for Implantable Sensors", in Materials Science and Technology - A Comprehensive Treatment, Vol. 14 - Medical and Dental Materials, D.F. Williams, Ed. VCH, Weinheim, FRG, 1991; pp. 303 - 343.
3. Reach, g.; Feijen, J.; Alcock, S. *Biosensors and Bioelectronics* **1994**, *9*, R21-R28.
4. Kuby, Janis *Immunology* W. H. Freeman & Company, USA: 1992.
5. Woodward, S.C. *Diabetes Care* **1982**, *5*, 278-281.
6. Black, J. *Biological Performance of Materials. Fundamentals of Biocompatibility*, Marcel Dekker, NY:1992, pp. 125-147, 188 - 192.
7. Tenenbaum, S.A.; Cuellar, M.L.; Citera, G.H.; Silveira, L.AH.; Garry, R.F.; Espinoza, L.R. *Arthritis and Rheumatology* **1993**, *S118*, A123 *(abstr).*
8. Ziegler, M; Schlosser, M.; Abel, P.; Ziegler B. *Biomaterials* **1994**, *15*, 859-864.
9. Tsuge, H; Natsuaki, O.; Ohashi, K.; *Journal of Biochemistry.* **1975**, *78*, 835.
10. O'Malley, J.J. and Weaver, J.L. *Biochemistry* **1972**, *11*, 3572.
11. Steinmeitz, H.T. and Pfreundschuh, M.G. *Journal of Immunological Methods.* **1987**, *101*, 251.
12. Wimalasena, R.L. *Preparation and Characterization of Immunochemical Reagents for Bioanalytical Applications*, Ph.D. Dissertation, The University of Kansas, 1991.
13. Swoboda, B.E.P. *Biochimica Biophysica. Acta* **1969**, *175*,365.
14. Wilson, G.S. and Zhang, Y. *Analytica Chimica Acta* **1993**, *281*, 513 .
15. Engvall,E.; Perlman, P. *Immunochemistry* **1971**, *8*, 871.
16. Van Weemen, B.K.; Schuurs, A.H.W.M. *FEBS Letters* **1974**,*15*,232.

17. Zhang, Y.; Bindra, D.S.; Barrau, M.B.; Wilson, G.S. *Biosensors & Bioelectronics* **1991**, *6*, 653-661.

18. Sincich, T. *Business Statistics by Example*, Dellen Publishing Company, San Francisco, CA: 1989, pp. 516-525.

19. Huitema, B.E., *The Analysis of Covariance and Alternatives*, John Wiley & Sons, NY:1980, p. 17.

20. Rodbard, D; Feldman, Y.; Jaffe, M.L.; Miles, L.E.M. *Immunochemistry*, **1978**, *15*, 77-82.

3. Chapter 2: A Fabrication Template for the Mass Production of a Micro Flow Cell for Flow Injection Analysis Immunoassay (FIA-IA)

3.1. Introduction

The miniaturization of analytical instrumentation for separations such as liquid chromatography and capillary electrophoresis has been driven by a desire for increased throughput, decreased separation times, and increased theoretical plates and resolution. Considerations such as portability, decreased reagent consumption, and decreased waste production are secondary benefits. Finally, by using silicon processing technology the entire package can be mass produced as a functional chip similar to integrated circuits.

For techniques such as flow injection analysis (FIA) miniaturization offers the option of making channel arrays to increase throughput. As described in Chapter 1, enzyme based assays such as the sandwich ELISA are powerful tools for screening. However, when faced with multiple samples, it is tedious, time consuming, and error prone.

Flow injection analysis automates the reagent and sample introduction steps, as well as reagent separation steps effectively, but only one sample at a time. Moreover, the binding kinetics of the immobilized molecular recognition element (MRE) is limited by the diffusion distance. Therefore, the development of a microfabricated, miniaturized flow cell array for the automation of enzyme based assays was of primary interest.

The challenges in constructing such a device stem primarily from the decreased dimensions. Mixing becomes diffusion controlled, the surface area of the channel limits the amount of MRE that can be immobilized, and specialized detectors must be employed.

At dimensions of about 100 μm the flow through these miniaturized channels is exclusively laminar with Reynold's numbers on the order of 1 or less. This means that mixing does not occur readily. Workers such as Brody and Yager *(1)*, and

Ruzicka *(2)* have exploited this ability to segregate flowing streams. Brody's and Yager's device uses a low-Reynolds-number flow to extract molecules and particles by their diffusion coefficient differences *(1)*. Ruzicka *et al.* use flow restriction to sort cells *(2)*. However, the ability to induce mixing is a requirement for any useful chemical interaction such as immunocomplex formation, enzyme-ligand, and phase partitioning. Yager and Brody have proposed channel designs to solve this problem *(3)*.

Along with the scaling effects on the flow rate and flow profile, miniaturization introduces another complication by decreasing the surface area. Typically, in a flow cell reactants are immobilized on the surface of the channel *(4)*. When the length of a tubular channel is decreased by a factor of 2, the surface area is decreased by the same factor. But when the diameter is decreased by a factor of 2, the surface area is decreased by the square root. Several workers have compensated for this loss in surface area by increasing the channel length *(4,5)*; however, this then requires either a longer analysis time or much faster flow rates. Another strategy is to actually change the surface to a porous structure. Laurell *et al. (6)* have demonstrated that a glucose oxidase based bioreactor that uses a porous silicon surface has a 100-fold increase in activity. However, it is limited in that the flow rate is not sufficiently fast to replenish oxygen at the enzyme layer surface. Additionally, the length has to square not merely double. Moreover, regeneration of the biomolecule is still an issue.

A more attractive solution is to actually manipulate particles in a flowing stream. On these particles, protein or other reagents may be immobilized. Egodage has already demonstrated a ten-fold increase in surface area by using a magnetic particle based immunoassay compared to a routine microtiter plate surface *(7)*. A new surface is provided for each assay, so regeneration is not a problem. Additionally, Pollema and Ruzicka have described a bead based flow injection assay using both optical and electrochemical detection using their patented ring jet cell

(8,9).

The concept of flow injection renewable surface immunoassay (FIRSI) for mouse IgG was introduced in 1994 by Pollema and Ruzicka *(8,9)*. An optimized volume of beads is held by a ring jet cell in the path of a microscope focused fluorescence detector and functions as a renewable fluidized bed reaction zone for each analysis. Because the beads can be easily expelled, on-line regeneration between samples is eliminated. The analyte and conjugate are introduced and react with the beads allowing the detection of the total amount of label present. The free label is then washed off and the corresponding signal is that resulting from the bound label only. The flow is reversed and the layer of beads is flushed to waste for off-line regeneration. The flow is stopped for 25 sec. for the incubation of the analyte and conjugate with the beads. A new aliquot of beads is injected for the next sample. The linear range of this assay is limited, 1-5 μg/ml (6.3 nM to 31 nM). However, real time antibody binding kinetics have been measured using this technique *(9)*. The total assay time is two minutes, a time advantage offered by the elimination of on-line regeneration. One limitation of the method is the need to keep the beads suspended *(8)*.

A possible second strategy would be to use a flow cell configuration similar to Liu *et al.*. They used a replaceable membrane with high surface area to covalently attach protein *(10)*. The channel was formed by using a spacer membrane out of which a 0.15 cm wide, 0.01 cm thick, and 2.5 cm channel is cut. This was sandwiched against the immunomembrane between two clear Plexiglas ™ pieces. However, while this was demonstrated using a Plexiglas ™ flow cell for chemiluminescent detection, it had not been demonstrated with either electrochemical detection nor with a microfabricated silicon structure.

The manipulation of particles, introduction of a membrane, modification of the channel surface, and potential applications of a bioreactor flow cell with microdialysis as a sampling method makes mechanical pumping necessary.

Electrophoretic pumping has been very popular for miniaturized systems because it requires no moving parts *(11)*. However, any disruption of the zeta potential of the channel wall changes the electroosmotic flow. Several miniaturized mechanical pumps have been described in the literature (*12*), and one recently developed at the University of Illinois - Chicago has been demonstrated with the bioreactor described here.

Electrochemical detection offers a simple, sensitive detection method. Thin film metal deposition is a technology long used in the integrated circuit industry, and it has been applied to electrochemical research (*13,14,15*). Current research utilizes optical detection which can require expensive coherent light source due to the window dimensions. As a result, optical detectors are relatively large and expensive, often the most expensive component of the miniaturized system.

This chapter describes the design, fabrication, and characterization of a flow cell made for flow injection enzyme-based assays like immunoassays. Proposed here is a generalized fabrication method for the high yield production of a novel microfabricated flow cell for FIA-IA with on-channel electrochemical detection. The proposal is general enough to sustain major changes in channel design and geometry, and also electrode material choice. The flow cell represents one module of the generalized FIA-IA system shown in Figure 2.1. Also demonstrated is the miniaturized flow cell with miniaturized versions of the remaining components of the generalized FIA-IA scheme (Figure 2.1). This is a significant contribution to the drive toward a micro total analysis system or μTAS.

Figure 2.1

Flow Injection Analysis Components

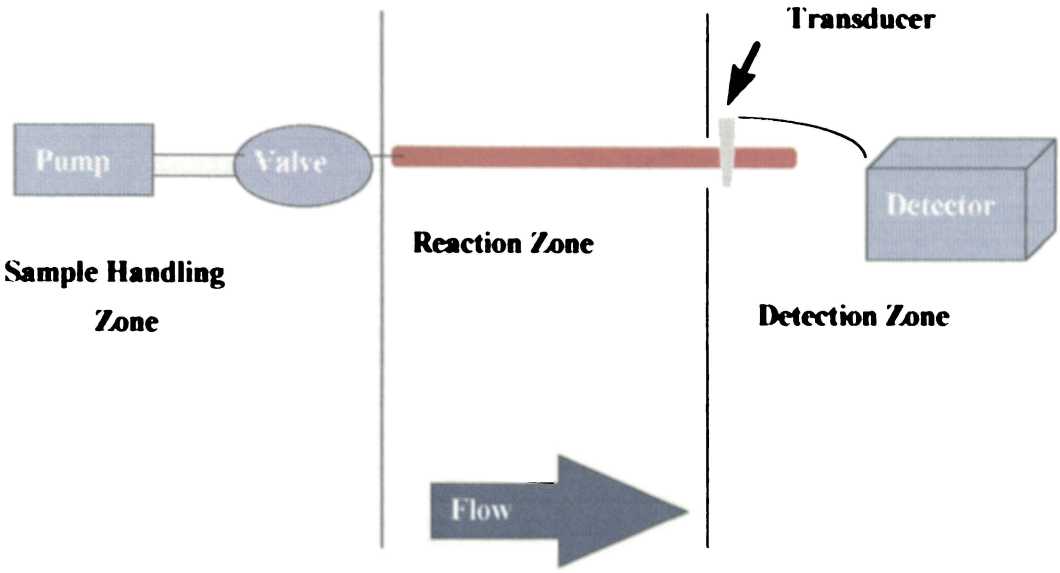

Figure 2. 1. Schematic of a generalized flow injection analysis set-up.

The strategy employed was to first construct a Plexiglas™ model of a microfabricated flow cell to determine the feasibility of using a replaceable immunomembrane. Figure 2.2 shows the dimensions of the channels carved into the Plexiglas™ plate. Figure 2.3 shows the model flow cell in two configurations. The details of these figures will be discussed in later sections.

Figure 2.2

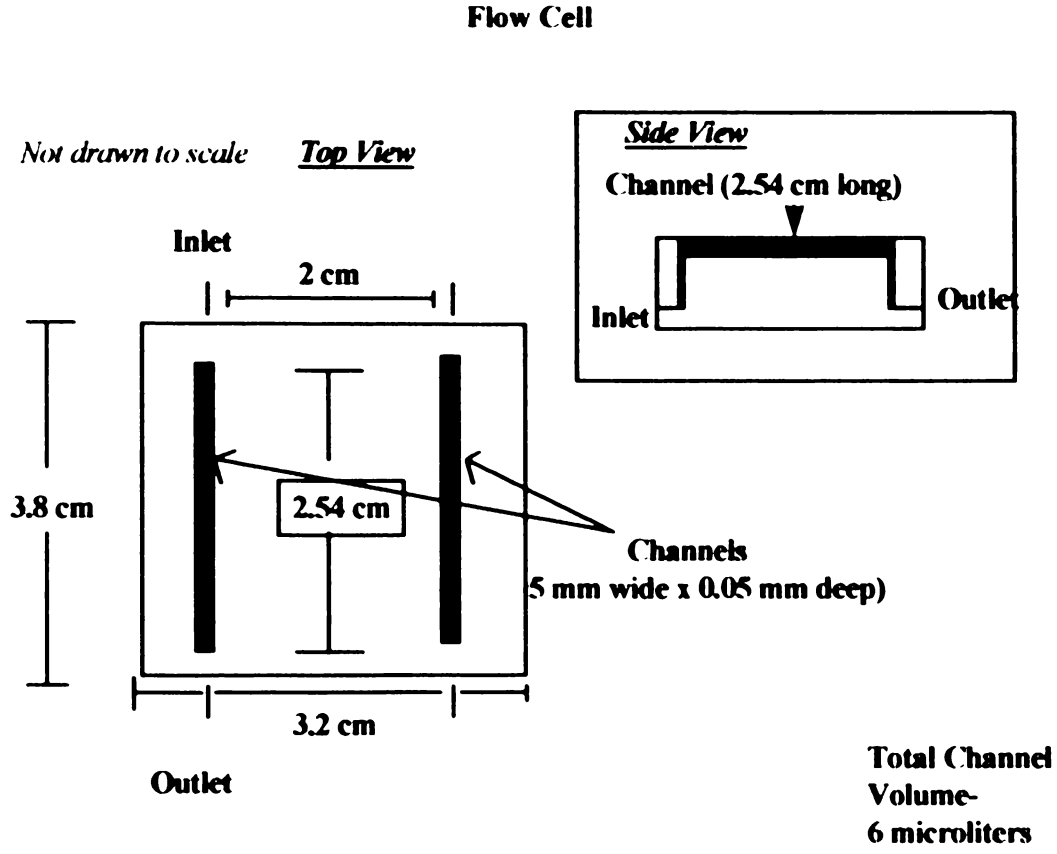

Figure 2. 2. Illustration and dimension of Plexiglas™ model.

Figure 2.3

a.

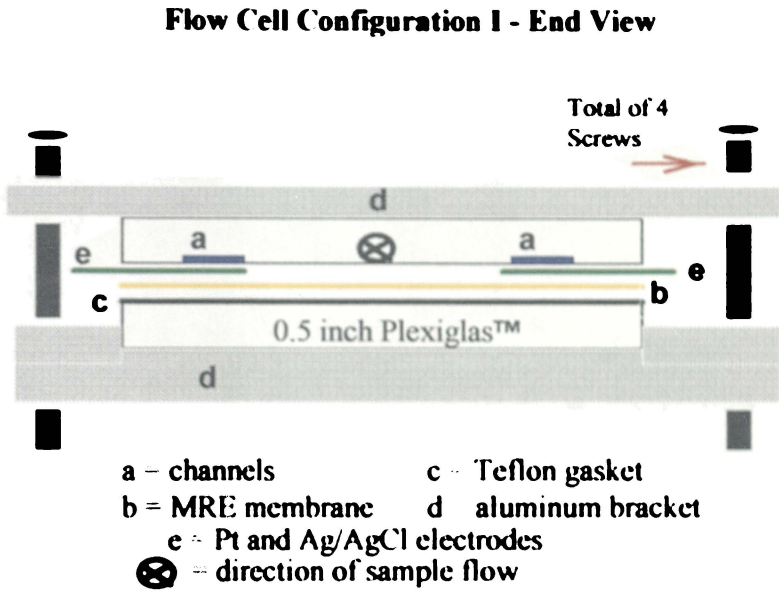

b.

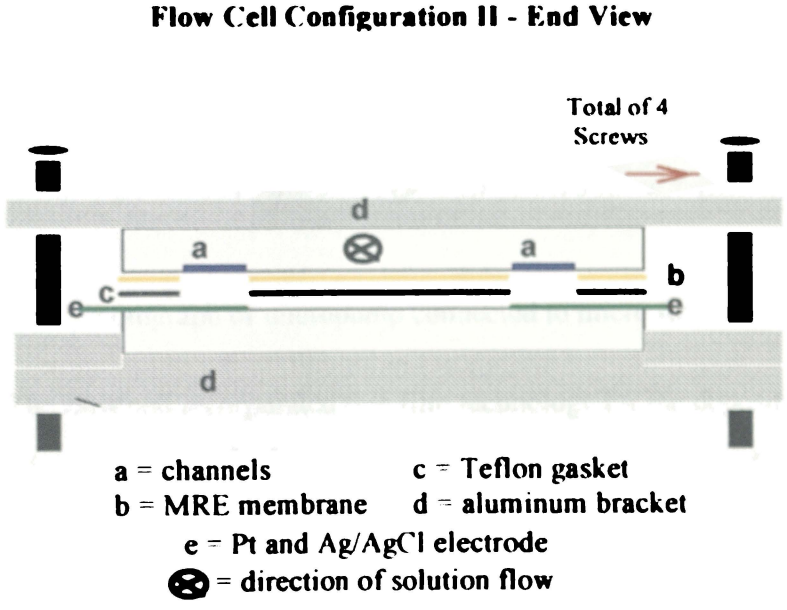

Figure 2. 3. Schematic of a. Configuration I and b. Configuration II.

Based on this evaluation, a miniaturized sandwich flow cell was constructed from three inch diameter silicon and glass wafers. A picture of the operating flow cell is shown in Figure 2.4.

Figure 2.4

Micro Flow Cell Connected to Micropump

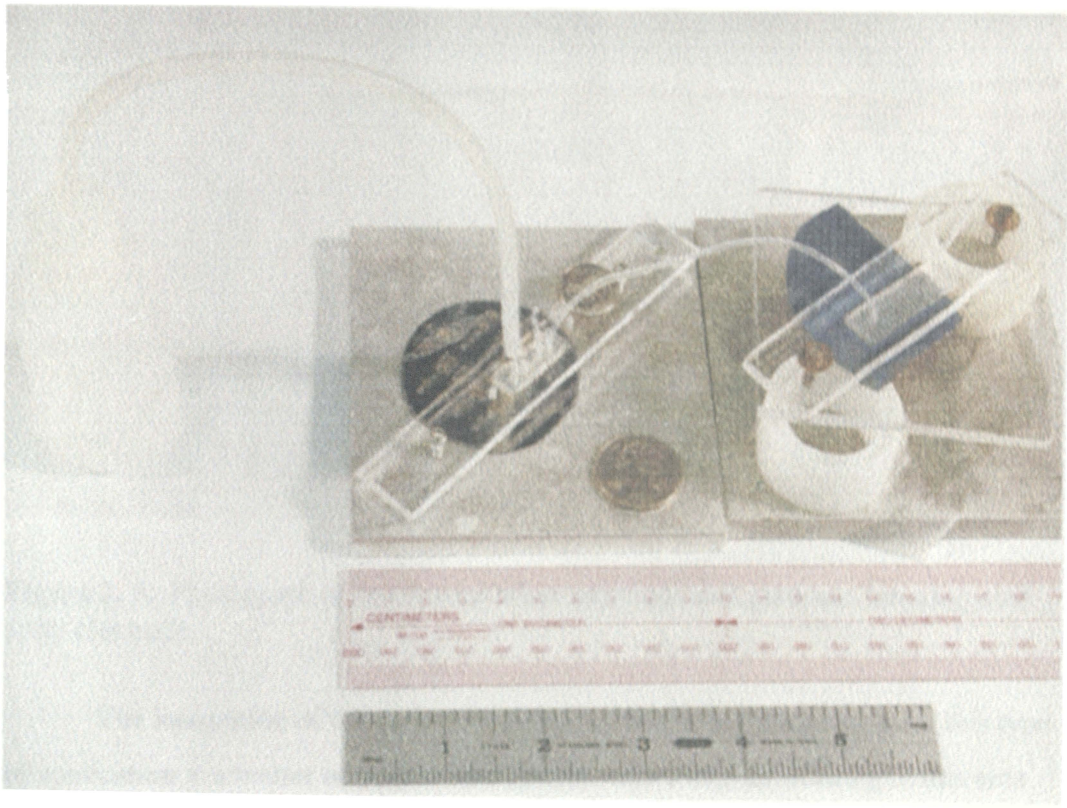

Figure 2. 4. Photograph of micropump connected to micro flow cell.

The flow cell incorporated thin film technology for the deposition of electrodes on the glass, which was anodically bonded to a silicon wafer with channels chemically etched into it. The two electrode system was on-channel, and a picture of the two electrodes in the channel is seen in Figure 2.5.

Figure 2.5

Two Electrode On-Channel Detector

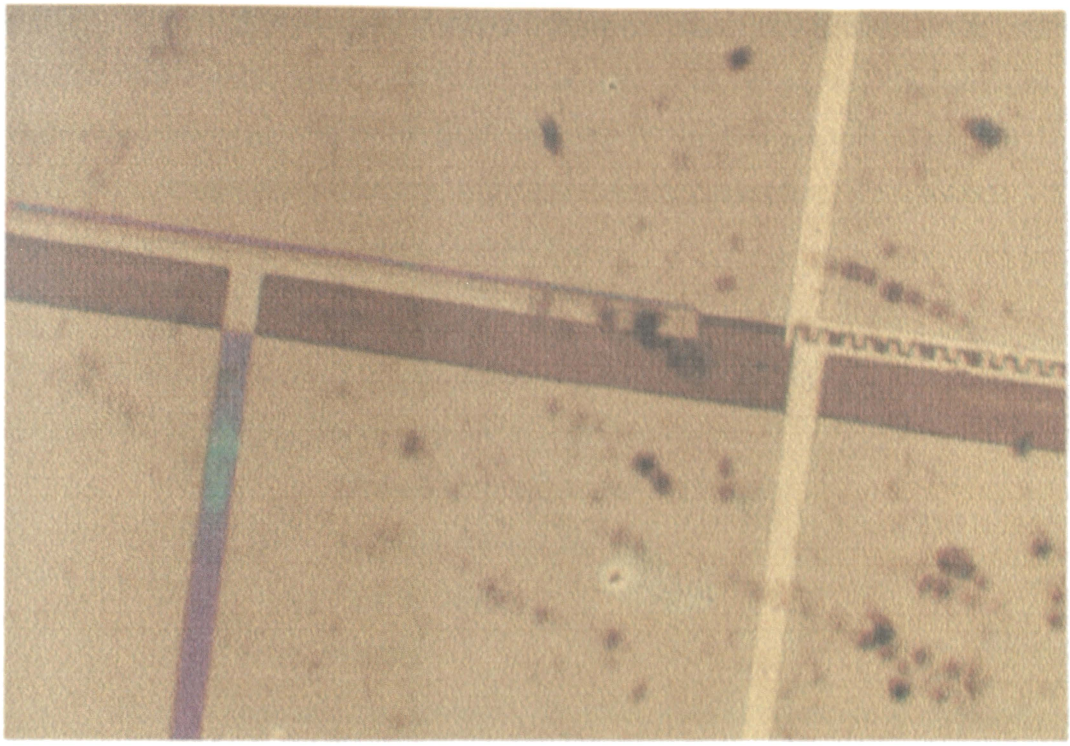

Figure 2. 5. Photograph of on-channel silver electrode and platinum interdigitated array electrode.

The integration of the various materials and fabrication methods for this type of application is a matter of interest to engineers and chemists working in this area. This is discussed in some detail. Both the model system and microfabricated system were evaluated using hydrogen peroxide and glucose as test analytes. Finally, recommendations for the next level of research in this area are discussed.

3.2. Theory

3.2.1. Design Rationale

The final design of the microfabricated flow cell was determined using a two-pronged strategy. The first was to evaluate the use of an immunomembrane in a

channel array that consisted of two plates that could be clamped. This was accomplished using a Plexiglas ™ model prior to any microfabrication (Figures 2.2 and 2.3). The performance of and recommendations based on this model are given in the first section of the Results and Discussion. The second prong was the evaluation of the dimensions required for the flow cell using the theories governing fluid mechanics, protein immobilization, and electrochemical detection. The theories, equations, and results are presented below.

3.2.2. Hydrodynamic

Several considerations were evaluated prior to determining the final channel dimensions. In order of importance, these parameters were:

1. Pressure drop, ΔP, across the channel
2. Reynolds number, Re
3. Flow profile
4. Mixing

The most important consideration, ΔP, resulted from the desire to eventually use the flow cell with a miniaturized pump. The maximum back pressure that could be pumped with this device was 5 KPa. In order to determine the appropriate dimensions (width, height, and length), Poiseuille's equation was employed. The equation is as follows:

$$\Delta P = 8\eta u L/\pi r^4 \qquad (2.1)$$

where η is the kinematic viscosity, u is the linear velocity, L is the length, and πr^2 is the cross-sectional area. The cross-sectional area of a v-shaped channel and a circular pipe are within ten percent of each other, therefore, for this and all following calculations a circular pipe is assumed.

The dependence of ΔP on channel diameter and channel length was tabulated. In an effort to standardize devices, a channel width of 100 μm was chosen. Based on

preliminary etching results, we determined that for a 100 μm wide feature, the etch depth was 50 to 70 μm. From this, a length of 9 cm was determined to give a ΔP of 4.7 KPa if the diameter used was 60 μm.

The Reynolds number was calculated for the "ideal channel" proposed above. The equation is as follows:

$$Re = \rho u L/\eta \qquad (2.2)$$

where the parameters are density, velocity, diameter, and kinematic viscosity, respectively.

The Reynolds number is significant because it predicts the type of flow in a tubular channel. Reynolds numbers below approximately 2300 indicate laminar, non-turbulent flow. The flow profile is parabolic (Figure 2.6). Between 2300 and approximately 5000, there is a transition between laminar and turbulent flow. This region is to be avoided, as the flow profile will not be reproducible. Above 5000 the flow is turbulent, and the flow profile is plug (Figure 2.6).

Figure 2.6

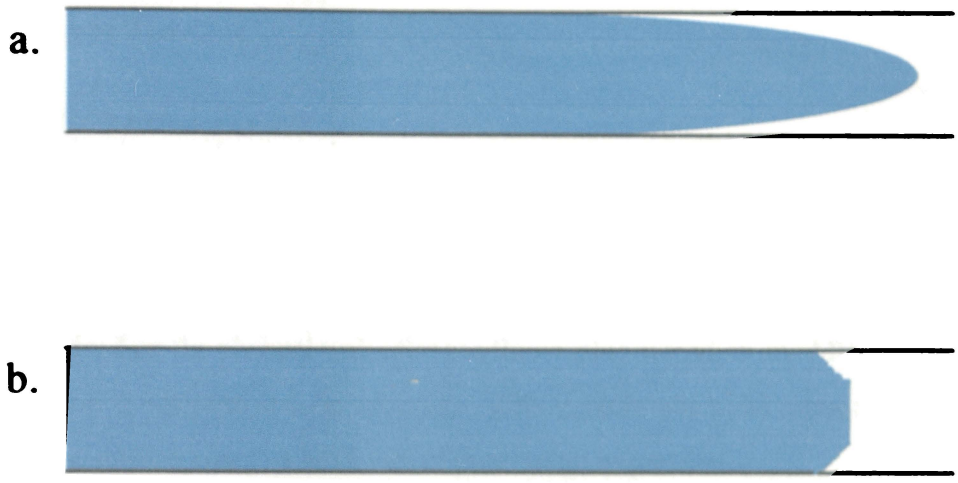

Figure 2. 6. Illustration of flow profiles at a. Low Reynolds numbers and b. Re>5000.

For these channels, the Reynolds number was on the order of 0.1 to 10 depending on flow rate. Clearly, the flow would be solely laminar. Because of this, it is impossible to induce turbulence within the 90 ° turns used to fit several channels onto one silicon wafer. Therefore, the mechanism for mixing would be diffusion.

Based on the linear velocity calculated for a 100 μm wide, 70 μm deep, and 9 cm long channel, the approximate time for a molecule to move through the channel at a flow rate of 1 μL/min was 16 seconds. The time for a small molecule at the center of the parabola to travel to the wall (maximum distance, l = 50 μm) based on a diffusion constant, D, of 10^5 cm^2s^{-1} is 2.5 seconds, approximately one-sixth the total time required for the channel length to be traversed (Equation 2.3).

$$t = l^2/D \qquad (2.3)$$

Based on the considerations discussed above, the final dimensions of a channel etched in silicon were determined. These dimensions were 100 μm wide by 70 μm deep by 9 cm long.

3.2.3. Protein Immobilization

The results from the model flow cell indicated that it was not feasible to proceed with a removable immunomembrane in the final design. The use of high temperature anodic bonding to seal the flow cell required that either the MRE must be immobilized on the channel wall after the flow cell is sealed, or the MRE must be introduced on an alternative solid substrate. If the protein was to be immobilized on the wall, the surface area available was of paramount importance.

The typical microtiter plate well adsorbs 1 pmol of antibody per square centimeter. Using this as the maximum possible amount of active antibody immobilized on the wall of the channel, the maximum amount of antibody in the channel would be 0.15 pmol. The LOD is usually three orders of magnitude below the amount of antibody immobilized *(10)*. A factor of ten would bring up the amount of antibody in the channel to that found on the microtiter plate. Surface roughness created by etching in CsOH doubles the surface area. Other approaches such as oxidative treatments in nitric acid and HF gave a ten fold increase in surface roughness on planar structures.

An additional issue introduced was that of regeneration. Immobilization in the channel rather than on a replaceable membrane required that the flow cell become either disposable or reusable. An increase in surface roughness did not address the issue of regeneration of the immobilized antibody. For this reason, it was proposed to test the micro flow cell using protein immobilized on 1 μm magnetic particles. This offered several advantages: 1. Increased surface area, 2. Decreased diffusion distance, 3. Renewable surface.

3.2.4. Electrochemical Detection

Our requirements for an on-channel two-electrode amperometric detector were good signal-to-noise ratio (S/N), flow rate independence, rapid response time, and electrical insulation between reference and working electrodes. The electrical insulation was provided by passivating the silicon wafer onto which the electrode contacts and leads would be pressed in the sandwich configuration with a thin (150 nm) layer of silicon dioxide. To achieve the remaining parameters, the interdigitated array was chosen as the geometry for the Pt working electrode. To prevent limiting the current by the surface area of the reference electrode, Ag/AgCl, was designed so its surface area was four times that of the working electrode. Below is a detailed discussion of the determination of the working electrode dimensions.

3.2.5. Interdigitated Array Electrode

In order to determine the dimensions of the electrode, several calculations were made. An explanation of the theories employed, and a summary of the results is presented below.

Interdigitated array electrodes are useful in situations where a relatively high surface area and relatively small total electrode area or volume is required. Supposedly, the S/N advantage derived from a microelectrode array results from the signal current arising from the geometric and surface active area, while the noise arises from the surface active area only *(16-18)*. A better explanation is that in the situation where diffusion is nonlinear, the diffusion layer is hemispherical. This occurs when the electrode has a characteristic comparable dimension to the thickness of the diffusion layer. At large-area continuous electrodes, diffusion is generally linear. At an interdigitated array of microelectrodes, each electrode has a hemispherical diffusion layer, and therefore, improved mass transport. However, the noise arises from the charging current, which depends only on the surface active area of the electrode. The noise then, is the same for both the array and the large electrode, but mass transport at the array electrode is improved, therefore the array

gives a higher S/N than the large electrode. An added advantage of the array is that mass transport is so efficient by the time the sample plug has reached the end of the array, the sample has been completely depleted by the electrode. As a consequence, electrode response is relatively independent of flow rate. An analogous situation is a porous electrode, or electrode sponge. Because of the high surface area and transport efficiency, the sample is in intimate contact with the electrode as it travels through the sponge. Accordingly it is completely electrolyzed. It is immaterial if the flow through the sponge is fast or slow.

In order for a micro electrode array to provide these benefits, however, several conditions must be met. Assuming the thickness of the metal electrode is several hundred angstroms, and therefore negligible, the dimensions of the array must be considered. For example, the individual electrodes in the array have to be small enough to guarantee hemispherical diffusion. Secondly, the gaps between the electrodes have to be spaced such that no shielding takes place. Shielding occurs in situations of prolonged electrolysis where the diffusion layers of two closely spaced electrodes overlap. In that case, one electrode depletes the other's depletion zone, and the net result is a signal smaller than if the array were a macroelectrode of the same total area. This requires a fairly accurate estimate of two things: 1. Diffusion layer thickness and 2. Electrolysis time. For all estimations and calculations a flow rate of 1 μL/ minute and a channel width of 100 μm are assumed. A Reynolds number, Re, has been estimated for both a circular and elliptical channel, and it falls below the critical number in both cases, therefore laminar flow is assumed.

The diffusion layer thickness was estimated using the relationships that follows in Equations 2.4 .

$$\delta \approx (D/v)^{1/3}\ \delta_{II} \qquad (2.4)$$

Using $D \approx 10^{-5}\ cm^2s^{-1}$ and $v \approx 10^{-2} cm^2s^{-1}$ Eq. 2.4 simplifies to Eq. 2.5:

$$\delta \approx 0.1\delta_H \qquad (2.5)$$

where δ is the diffusion layer thickness and δ_H is the thickness of the hydrodynamic layer. The hydrodynamic layer is defined as the layer within which all velocity gradients occur. This can be estimated as the width of the flowing stream defined by the physical boundaries of the structure it flows through *(19)*.

Based on a flow rate of 1 μL/ minute in an elliptical channel of dimensions 100 (width) by 30 μm (depth), the linear velocity is 0.11 m/s. Assuming that one electrode in the array is 10 μm in width ($1x10^{-5}$ m), then a 10 μm segment of the sample plug will be past the electrode in 1 microsecond. If the sample plug were to broaden so it occupied a length of 6 cm, the total electrolysis time is approximately 7 milliseconds. According to Huangxian *et al.*, if the electrolysis time is less than $3x10^{-5}$ seconds, the mass transport is by semi-infinite linear diffusion, and the diffusion layers do not overlap *(20)*. However, with an increase in electrolysis time, the radial term or edge effect cannot be neglected and the diffusion layer thickness is calculated from the following equations:

$$\theta' = Dt/We^2 \qquad (2.6)$$

$$\delta = We/\{(\pi\theta')^{1/2} + 0.97 - 1.10 \exp[-9.9/|\ln(12.370')|]\} \qquad (2.7)$$

where D = 7.1 10-6 cm^2s^{-1}, t = electrolysis time, and δ = diffusion layer thickness.

A diffusion layer thickness of 3.8 μm is determined from Eqs. 2.6 and 2.7. This was determined for the worst case scenario - a molecule with a large diffusion constant. Based on this calculation there would be no partial overlap and shielding would not occur if the gap dimension is 10 μm *(20)*.

In order to determine if the thin film electrode will provide enough current, it was important to evaluate the current density for the electrode. The current density is given by the following equation *(21)*:

$$j = i/A \qquad (2.8)$$

where i is the steady state current, and A is the surface area.

The steady state current can be calculated from the following equation *(21)*:

$$i = nFA(D_o/\delta)C^*_o \qquad (2.9)$$

where n is the number of electrodes, F is Faraday's constant, D_o is the diffusion constant, δ is the diffusion layer thickness, and C^*_o is the bulk concentration of O.

The current density for the array was calculated using $\delta_o = 3.8$ μm. The current density was calculated to be 5.6 $AM^{-1}cm^{-2}$. It was determined that a 32 electrode array with 10 μm wide and 20 μm long digits and 10 μm gaps would provide the appropriate geometry so that radial diffusion would occur at each electrode without overlapping. An array of 32 pairs provided a surface area of 0.013 cm^2, giving a predicted total maximum current of 730 μA for a 1 M solution.

3.2.6. Final Micro Flow Cell Specifications

A summary of the final flow cell specifications for microfabrication are presented here. The dimensions given are the dimensions for the masks used for photolithography.

The channels are v-shaped grooves anisotropically etched in a three inch diameter <100> silicon wafer 300-380 μm thick. The mask dimensions for the channel are 100 μm wide and 9 cm long. The mask is shown in Figure 2.7.

Figure 2.7

Mask for Channels Etched in <100> Silicon

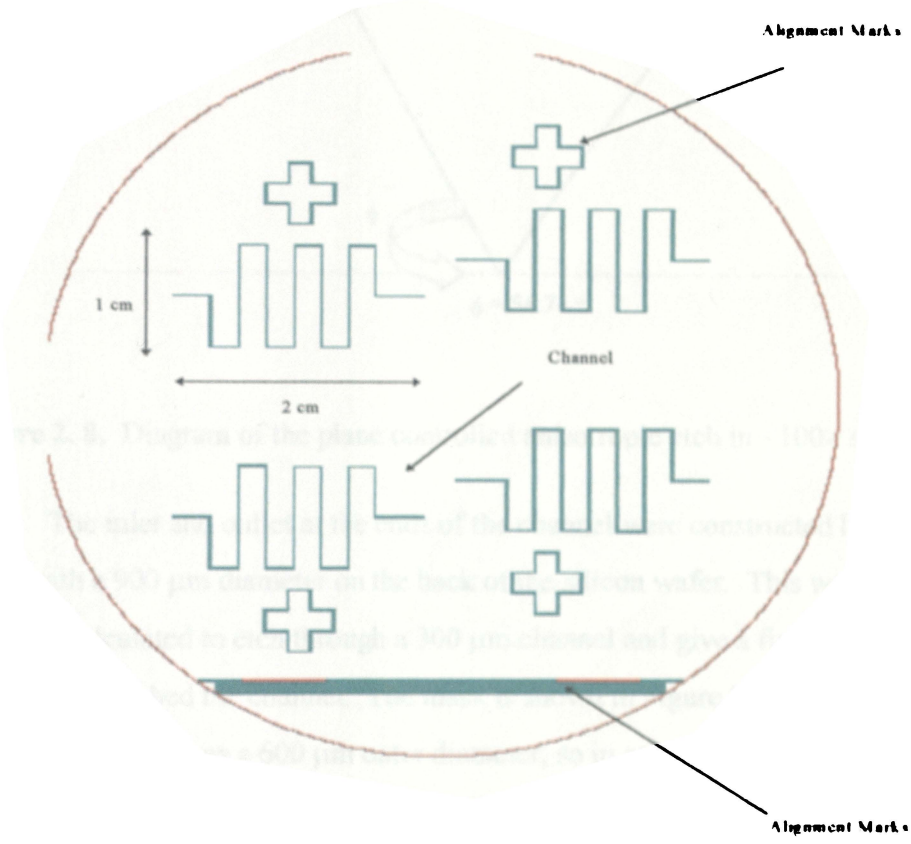

Figure 2. 7. Mask for channels etched in a silicon wafer.

A diagram of the expected results is shown in Figure 2.8. The depth, controlled by the <111> silicon plane, is calculated to be 70 μm. These dimensions were determined to be optimum by assuming a circular pipe and determining the

pressure drop from Poissueille's equation. The pressure drop falls under the 5 KPa operating drive pressure of the micropump.

Figure 2.8

Results of an Anisotropic Etch in <100> Silicon

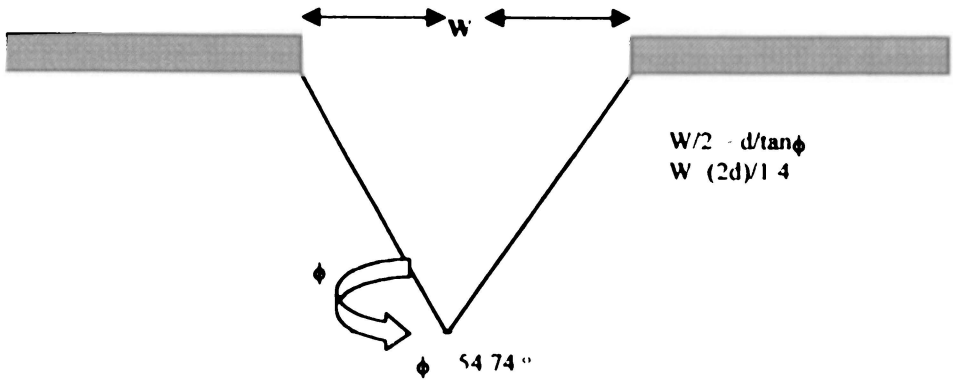

Figure 2. 8. Diagram of the plane controlled anisotropic etch in - 100 - silicon.

The inlet and outlet at the ends of the channel were constructed by etching holes with a 900 μm diameter on the back of the silicon wafer. This was the width that was calculated to etch through a 300 μm channel and give a final diameter of 600 μm once it reached the channel. The mask is shown in Figure 2.9. The PEO tubing used for the pump has a 600 μm outer diameter, so in principle the tubing should fit the hole at the channel termini. Figure 2.10 shows a picture of the outlet holes.

Figure 2.9

Mask for Inlet/Outlet to Channels

Holes Patterned on Opposite Side of the Wafer with Channels

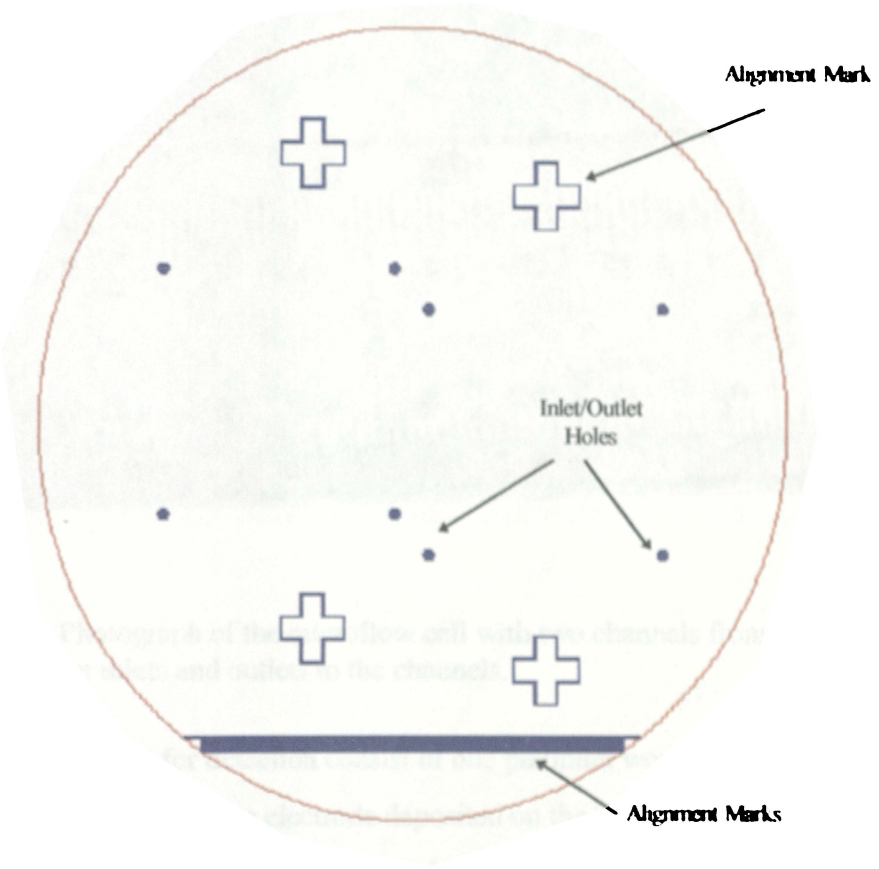

Figure 2. 9. Mask for inlet/outlet holes etched through the back of the silicon wafer with channels.

Figure 2.10

Picture of Back of Flow Cell - Inlet/Outlet Holes in a <100> Si Wafer

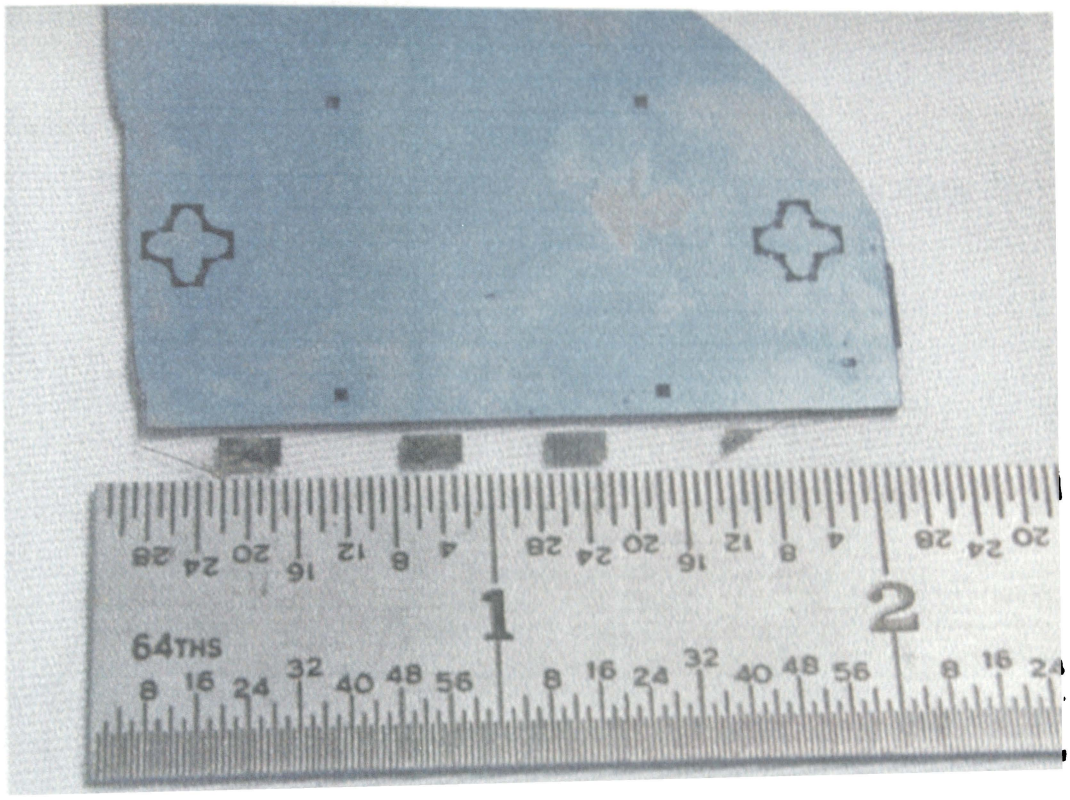

Figure 2. 10. Photograph of the microflow cell with two channels from the back The holes are the inlets and outlets to the channels.

The electrodes for detection consist of one platinum working electrode and a silver/silver chloride reference electrode deposited on the same side of a 250 μm thick three inch glass wafer. The Pt electrode is an interdigitated array with the dimensions for each digit being 20 μm long, 10 μm wide, with 10 μm gaps between digits. The electrode backbone width is 10 μm, and the total array length is 1100 μm and total width is 50 μm. The total area is 0.013 mm^2. The silver electrode dimensions are 1.2 mm by 0.050 mm giving a surface area of 0.06 mm^2. The Pt

electrode is placed before the Ag electrode. The silver electrode is followed by the channel outlet. Both electrodes are aligned in the center of the silicon channel. Figures 2.11 and 2.12 show the entire mask for each electrode; the Pt array is shown in detail on Figure 2.13.

Figure 2.11

Mask for Platinum Interdigitated Array Electrodes on Glass Wafer

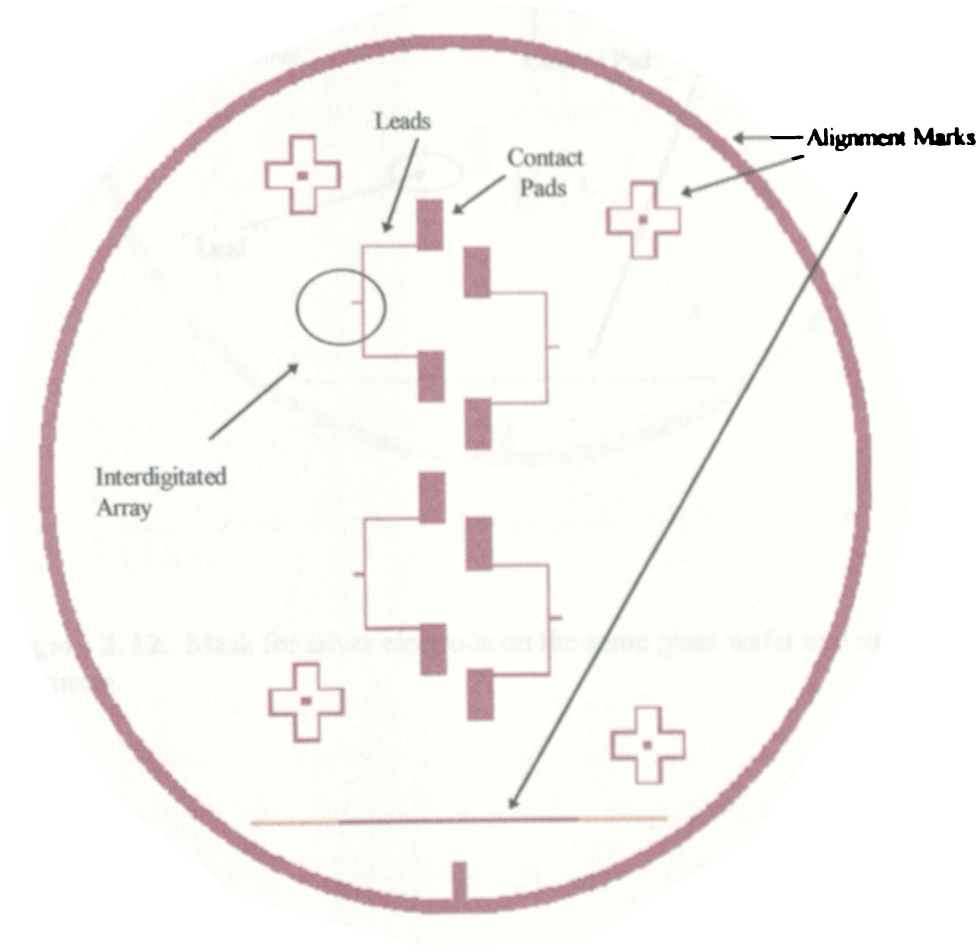

Figure 2. 11. Mask for the platinum interdigitated array electrode deposited on Pyrex™.

Figure 2.12

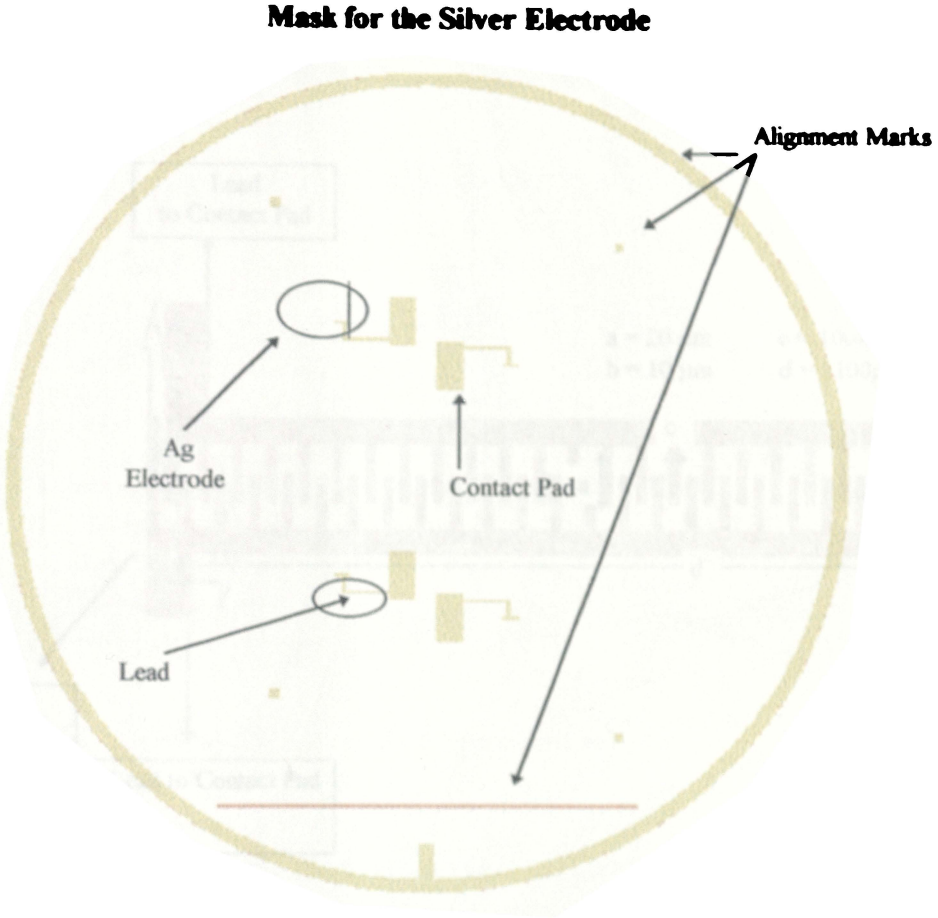

Figure 2. 12. Mask for silver electrode on the same glass wafer and same side as the platinum.

Figure 2.13

Close-up View of Platinum Interdigitated Array Electrode

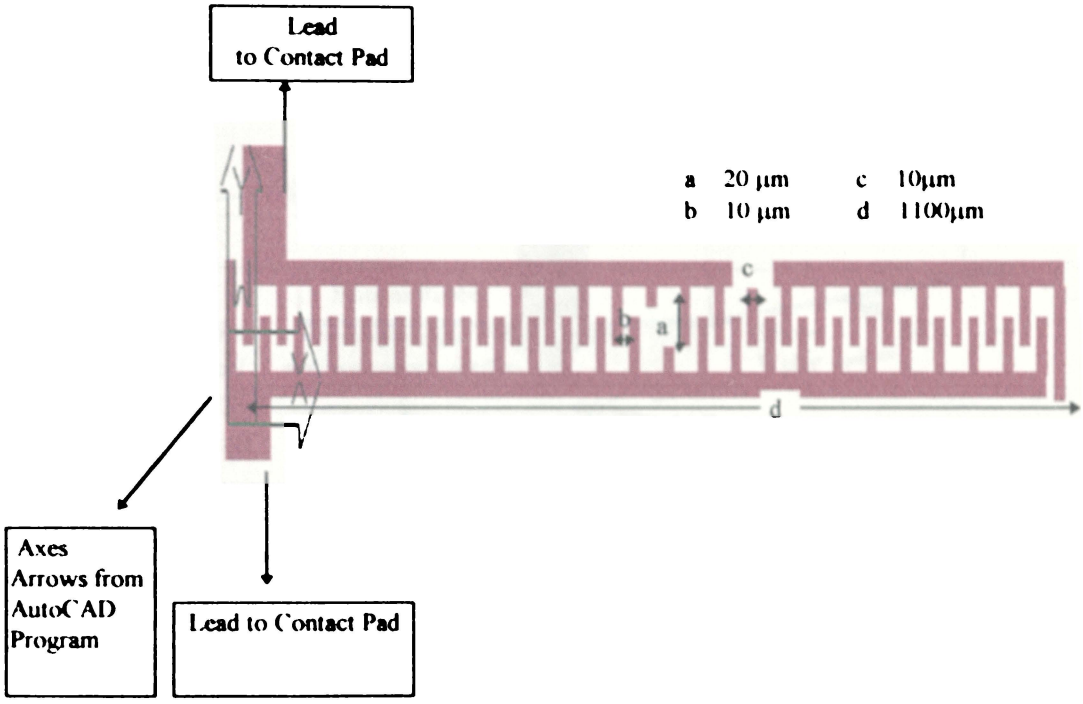

Figure 2. 13. Close-up view of platinum interdigitated array electrode feature of platinum electrode mask.

Anodically bonding the glass wafer with the electrode side facing the channel in the silicon wafer provides a permanent seal for the flow cell. In order to electrically isolate the electrodes (Si is a semi-conductor) a 130 nm oxide layer was grown over the channel after it had been etched and stripped of the original oxide layer. Refer to Figure 2.14 for a diagram of the assembled flow cell.

Figure 2.14

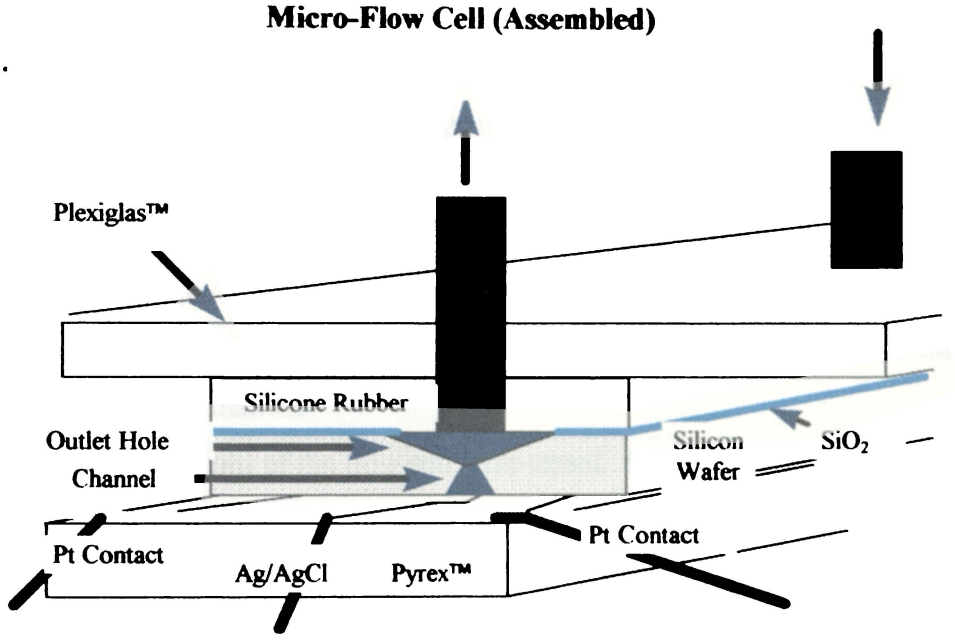

Figure 2. 14. Drawing of the assembled micro flow cell.

3.2.7. Microfabrication

An explanation of the theories and practices involved in photolithography, anisotropic etching, metal deposition and lift-off, and anodic bonding are found in the Appendix 2.1.

3.3. Experimental

3.3.1. Plexiglas™Model

3.3.1.1. Materials and Equipment

All reagents were obtained from Fisher Chemical (St. Louis, MO) with the following exceptions. Glucose oxidase and horse radish peroxidase IV (HRP-4,

I.U.B 1.11.1.7, 246,670 U/g) was obtained from Biozyme Laboratories International, Ltd. (San Diego, CA). The UltraBind membrane was obtained from Gelman Sciences (Fisher, St. Louis, MO). The reagents for Pierce BCA protein determinations were from Pierce (Rockland, IL). TMB solution was obtained from Kirkegaard & Perry (Gaithersburg, MD). Quarter inch thick clear Plexiglas™ was obtained from Allied Glass and Metal (Lawrence, KS). PEEK™ tubing of the following inner diameters: 0.005,0.01,0.02 in. was obtained from Upchurch Scientific (Oak Harbor, WA). Low pressure 0.125 inch fittings were also obtained from Upchurch Scientific. A Molecular Devices plate reader (Menlo Park, CA) was used for protein determinations.

Two configurations of the flow cell were tested. Please refer to Figures 2.2 and 2.3 for details. Injections were made with a Valco (Austin, TX) Cheminert 5000 valve with an internal sample loop of 20 nL. Two potentiostats were used. Configuration I used a BioAnalytical Systems (BAS) LC-4A (W. Lafayette, IN) amperometric detector, BAS dual syringe pump, and a Linear chart recorder. Configuration II used micropotentiostats (2x2 inches) built by the Instrument Design Lab (IDL) at KU, a KD Scientific 220 multi-syringe pump (Fisher), and a 486 computer with potentiostat control and data collection software written by the IDL. All experiments were done with 0.1 M phosphate buffered saline (PBS) pH 7.4 as the carrier buffer and the standard diluent buffer. Both 2mm Pt foil and 180 μm diameter Pt wire were used with a 280 μm diameter Ag/AgCl reference.

3.3.1.2. Methods

3.3.1.2.1. Plexiglas™Model Flow Cell Fabrication

The flow cell was made by using conventional machining. The channels were formed by scratching the Plexiglas ™ surface with the tip of a drill bit. Final

channel dimensions were estimated from a microscope and are shown in Figure 2.2. In summary, the channels themselves are 1 inch long by 500 μm wide and 50 microns deep. The channels are separated by 2 cm. The 0.5 inch thick Plexiglas™ plate is 3.2 cm wide by 3.8 cm long. It is sandwiched to another Plexiglas ™ plate of the same dimensions. Note Configurations I and II in Figure 2.3.

3.3.1.2.2. Protein Immobilization

The glucose oxidase was covalently immobilized to Gelman UltraBind membrane for the glucose assay. The manufacturer's procedure was followed with some modifications. It is summarized here.

A 4 mm by 2.54 cm strip of UltraBind was cut out with a scalpel. It was coated with 60 μL of a 10 mg/mL solution of glucose oxidase. It was left covered to dry at room temperature (typically 5 to 15 minutes). The active sites were blocked with a 0.1 M glycine solution in 0.1 M PBS (pH 7.4) at 37 °C for 1 hour without agitation. Non-specifically adsorbed protein was removed by rinsing the membrane in a 0.1% Tween 20 (v/v) in 0.01 M PBS (pH 7.4) at room temperature. The protein is attached covalently to the UltraBind membrane through its amine group to an aldehyde on the membrane surface.

3.3.1.2.3. Determination of Protein Loading

The determination of protein loading was made using the Pierce BCA assay. This is based on the biuret assay for protein. Cu^{2+} is reduced to Cu^{1+} in the presence of amino acids such as tyrosine. Bicinchoninic acid (BCA) forms a 2:1 complex with Cu^{1+}. The complexation of the copper ion causes a color change from green to purple. The procedure is as follows. A 13 mm diameter hole was punched out of the membrane using an office hole punch. This was cut in half with a razor blade or scalpel. Each half was placed in the well of a microtiter plate. Standards of concentration 0.0625 mg/mL to 1 mg/mL were prepared in 0.1 M phosphate buffered saline (PBS). To each well 50 μL of standard or blank (PBS) was added. To the

wells with a membrane, 50 μL of PBS was added. To all wells, 200 μL of Pierce BCA work reagent prepared according to the manufacturers specifications were added. After mixing and incubation for 30 minutes at 37 °C or two hours at room temperature, the absorbance was measured on a Molecular Devices plate reader at 550 nm. Prior to reading, the solution over the membrane was moved to empty wells.

3.3.1.2.4. Determination of Glucose Oxidase Activity

The activity of glucose oxidase after covalent attachment to the UltraBind membrane was compared to soluble glucose oxidase standards using the following method. A solution containing 120μl of 200 μg/mL HRP-4 and 240 μL of 1 M glucose (mutarotated overnight) was diluted to 2.5 mL using TMB. On a microtiter plate six disks with glucose oxidase immobilized on the surface and 100 μL of PBS were added to six wells. Six disks with no protein and 100 μL of PBS were added to six wells. Six wells had 0.1 M PBS only. Six wells had 100 μL of a 1.5 μM glucose oxidase solution. To all wells 100 μL was added. The reaction was incubated at room temperature for 15 minutes and stopped with 50 μL 1 M HCl. The absorbance was measured at 450 nm on a molecular devices plate reader. The ratio of the absorbance units to the concentration of glucose oxidase was used to compare the activities of the bound and free enzymes. The blanks were subtracted prior to this calculation.

3.3.1.2.5. Detection of Peroxide and Glucose

Peroxide and glucose were detected by making injections into a flowing stream of flow rate 2 μL/min. The scale of the potentiostats were varied to obtain the best peak height and width to work with for visualization purposes. These changes were accounted for in all calculations.

3.3.2. Microfabricated Flow Cell

3.3.2.1. Materials and Equipment

All photolithography chemicals including primer, photoresist 1818, Microposit 351 developer, and Microposit 110 remover were obtained from Shipley (Newton, MA). Buffered oxide etch (BOE), acids, bases, and Summa Clean™ were obtained as electronic grade from Ashland Chemicals, Inc. (Columbus, OH). Cesium hydroxide was obtained at 50% by weight from Aldrich Chemicals (St. Louis, MO). All water used for wafer processing was deionized and filtered to a purity measured as 12-18 MOhm resistance. Three inch diameter, 300 μm thick, 3-7Ω <100> silicon wafers were obtained from NOVA Electronic Materials, Inc. (Richardson, TX). Three inch diameter, 250 μm thick Pyrex™ 7740 wafers were obtained from Vogelin Company (Norwood, NH).

Mask designs were generated using a two dimensional design program, AutoCAD by Autodesk, Inc. (San Rafael, CA). The masks were made using a GCA MANN 3600F/3696 pattern generator (GCA; Novi, MI). A Varian electron beam evaporator in an ultra high vacuum system (San Fernando, CA) was used to evaporate silver and gold. A Norton NRC 3117 Evaporation System was used to evaporate Pt (NRC; Newton, MA). Masks were examined with a Nikon microscope in the clean room (Melville, NY). Photoresist was deposited using a Headway Research PWM101 photoresist spinner (Headway Research; Richardson, TX). The photolithography of the photoresist used a Karl Suss MJB 3 infrared mask aligner (Waterbury, VT). Etch depths were obtained using a Tencor P1 long scan surface profiler. Silicon oxide was deposited using a Thermco (Thermco Systems; Orange, CA) diffusion furnace. The thickness of the oxide layer was determined using a Gaertner ellipsometer from Gaertner Scientific Corporation (Chicago, IL). The alignment of the glass and silicon wafers prior to bonding was done using a Karl Suss vacuum arm with a Nikon transmission microscope. The anodic bonding apparatus was composed of two 500 V maximum power supplies, a hot plate

(Corning; Corning, NY), positioning arm (Karl Suss) in a in-house produced purgeable box.

3.3.2.2. Fabrication Procedures and Results

All processing occurred in a Class 1000 clean room with the exception of the following procedures : Platinum evaporation, wafer dicing, and anodic bonding.

3.3.2.2.1. Silicon Processing

3.3.2.2.1.1. Method 1

Etch of Inlet/Outlet Holes In Silicon Wafer. A 0.9 μm oxide layer was grown on 6 wafers prior to photolithography. Photoresist 1818 was then spun on the rough side of all 6 wafers at 4000 rpm for 30 seconds following treatment with an adhesion promoter (10 sec stand, 10 sec spin at 4000 rpm). A 30 second pre-bake on a hot plate at 115°C followed. Then, using the UV mask aligner, the back side (unpolished) was exposed for 12 seconds with the inlet/outlet mask. Alignment to the flat was somewhat difficult because there were no alignment marks on the mask to indicate if the mask was centered on the wafer. After development in developer for 60 seconds and a 3 minute rinse, the wafers were baked for 5 minutes at 120°C . The polished side was then protected with photoresist 1818, and a 25 minute bake at 125°C followed. All 6 wafers were then left in 6:1 buffered oxide etch (BOE) for 20 minutes. This left the pattern of the channels etched into the oxide layer.

Following a quick rinse, only 3 wafers continued to a 50% CsOH etch bath with stirring at 80°C . The etch rate was determined to be 1.1 μm/min using the Tencor profiler. After 205 minutes, the holes were etched to an average depth of 230 μm, so the etch was stopped. The etch was stopped to make it easier to apply photoresist in the next step. The presence of holes made it very difficult to apply an

even layer of photoresist, and thus compromises the oxide layer during the BOE etch of the SiO_2.

Etch of Channels in Silicon Wafers. Three of the wafers processed as above were further processed. Again, photoresist 1818 was used to protect the polished side. This was aligned to the channel mask and to the pits already etched on the back using the infrared aligner. The alignment marks were too far from the center of the chuck for good alignment using them, but the channels were aligned to the holes themselves. The exposure time was as above. The protection of the back with the pits was accomplished two ways. On one wafer, photoresist was spun as usual, but patches that were not covered with photoresist were covered by hand then respun. This survived a 10 min. BOE dip with the only features exposed being on the edge of the wafer. The other wafers were protected with a 100 Å layer of titanium then 5000 Å of silver. Tiny pinholes that were not covered by silver were then protected by using the conventional photoresist 1818 coating. After the postbake, the wafers were left in BOE for 10 minutes with no evidence of incomplete protection of the oxide layer. The photoresist was removed with photoresist remover, and the silver was removed with nitric acid (25 seconds). The titanium was removed with a 30 second dip in 10:1 BOE. The first wafer (coated only by photoresist 1818) was etched for 2 hours in 50% CsOH, with a rate of 20 μm/hour. Not satisfied with this rate, we increased the temperature to 70-75 °C . The wafers coated with silver as well as photoresist were then etched in CsOH at 75 °C. The etch was finished after 3 hour at this temperature. The final dimensions of all three wafers were a channel width of 140-150 μm and a depth of 80 to 90 μm.

The oxide was stripped after the etch using 6:1 BOE. The wafers were then oxidized using a dry oxidation to form a 130 nm layer of oxide prior to bonding. The wafers were cut in half with a diamond scribe, then cleaned in 3:1 sulfuric acid to hydrogen peroxide (piranha) for 15 minutes immediately prior to bonding.

3.3.2.2.1.2. Method 2

The procedure was as above with the following exceptions. The protection of the rough side prior to the BOE oxide removal step was achieved using only photoresist 1818 applied in patches to areas still exposed after the usual application and spin at 4000 rpm. The final dimensions were as above.

3.3.2.2.1.3. Method 3

Method 2 was followed with the following exceptions. After the first etch of the inlet/outlet holes, there was a significant amount of white particles on the surface of the wafers. The wafers were cleaned in Summa Clean for 15 minutes with sonication at 40°C . This broke the thin silicon film at the bottom of the pits, so the holes were etched through. In order to apply photoresist to each side for the subsequent photolithography and BOE oxide removal step, the following changes were made.

Blue contact paper used for wafer dicing was applied with heat (50°C) to the polished side of the wafer. Photoresist was then applied as in Method 1. The contact paper was removed, and a 30 second pre-bake on a hot plate a 115°C followed. The same piece of contact paper was reapplied to the photoresist coated, unpolished side. Photoresist 1818 was then applied without promoter and spun off at 4000 rpm. The contact paper was removed, and the wafer was pre-baked at 125°C for 15 minutes. Then, the polished side was exposed with the channel mask using the IR mask aligner as in Method 1. The wafer was developed as in Method 1. 6:1 BOE was used as above for the removal of the exposed oxide layer, but the duration was 15 minutes. The CsOH etch that followed was at 80 °C and the etch time was 2 hours. The final channel dimensions were 100 μm wide by 80 μm deep.

3.3.2.2.2. Glass Processing

Six Pyrex wafers were annealed using the manufacturers recommendations. These shattered in the deionized water cascade, so no annealing was used for the glass wafers.

3.3.2.2.2.1. Method 1

Platinum Electrode Photoresist was deposited on one side of the glass wafers as described above. The alignment to the mask for the Pt electrodes was somewhat difficult without a mark dead center, however, this did not present a problem in the final results. A twelve second exposure time was used.

Chromium was first evaporated onto the glass to yield a 75 Å thick layer, followed by an 803 Å Pt layer. This was lifted off by emerging 30 seconds in acetone, leaving the electrodes. The fragments of Pt that stuck to the wafer were easily removed by 1:3 H_2O_2:H_2SO_4 in 10 seconds with no adverse effects to the Pt array.

Silver Electrode After cleaning, a second layer of photoresist was deposited on the Pt, this time exposed with the silver electrode mask. A 10 second exposure was sufficient. This time, the photoresist was not post-baked. A 2000 Å layer of silver was deposited on the Varian on a 25 Å Cr layer. Unfortunately, the wafers were rotated during deposition, and good step coverage was achieved. As a result the lift-off in acetone took 2.5 hours. This also may have compromised the resolution of the Pt interdigitated array. The wafer was cut in half with a dicing saw, then cleaned with piranha prior to bonding (10 seconds).

3.3.2.2.2.2. Method 2

Platinum Electrode The photolithography procedures varied as follows. UV exposure times were varied from 6 seconds to 12 seconds. The optimum time was

determined to be 8 seconds. Additionally, a vacuum contact was used to make contact between the mask and the wafer to improve resolution. Finally, the developer used was mixed in the high resolution formula of 5:1 deionized water to Microposit 351 developer as recommended by the manufacturer. Metal deposition, lift-off, and anodic bonding pre-treatment were not varied from Method 1.

Silver Electrode The only variations were that a 100 Angstrom Cr adhesion layer was used, and Ag was deposited to a thickness of 5000 Å.

3.3.2.2.2.3. Method 3

Platinum Electrode All procedures were as in Method 2 except that there was no photoresist post-bake. After initial problems with piranha removing the Pt, the wafers were cleaned in sonicated 40 ° C nanopure water for several seconds with no ill effects to the Pt.

Silver Electrode No silver electrode was deposited

3.3.2.2.2.4. Method 4

Gold Electrode All procedures are as in Method 2 except that Au was used instead of Pt.

Silver Electrode No silver electrode was deposited.

3.3.2.2.3. SiO_2-Glass Bonding

Figure 2.15 is a drawing of the anodic bonding apparatus used for both methods described below.

3.3.2.2.3.1. Method 1

The halves were aligned by aligning the electrode in the channel under the microscope using a positioning arm with vacuum suction to hold both the glass wafer and the silicon wafer in place during the alignment. The alignment was held in place with an aluminum bracket on a quarter inch thick, four inch square aluminum plate placing ceramic pieces between the aluminum bracket and the aluminum plate and the bracket and the wafer to prevent electrical contact. The vacuum was turned off. The entire bracket and holder was transferred to the hot plate. Glass with Pt and Ag, just Pt, and just glass were used to make a total of 4 bonded flow cell arrays (2 flow cells per half). The bonding conditions did not vary. The applied voltage was 1KV and the temperature was 400 - 450 °C. Total bonding time was 1 hour. The electrode for bonding was moved once during bonding after 30 minutes. The Pt was unaffected, but the Ag disappeared after 20 minutes of bonding. The current hypothesis is that it oxidized and diffused into the glass to replace the sodium ions moving into the silicon.

3.3.2.2.3.2.Method 2

The procedure followed was as above except that the anodic bonding chamber was purged with nitrogen gas for 30 minutes prior to the introduction of the wafers into the chamber, then throughout the bonding procedure itself to minimize oxidation of the Ag.

Figure 2.15

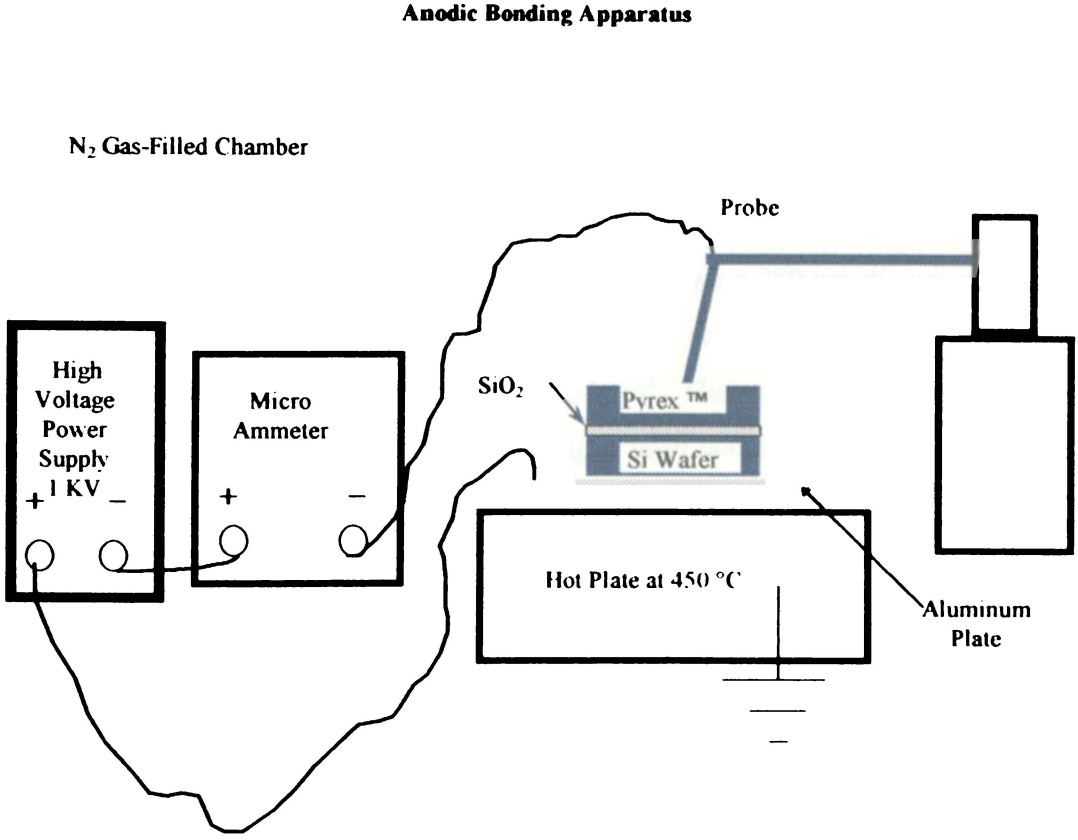

Figure 2. 15. Schematic of anodic bonding apparatus.

3.3.2.2.4.Bracket

A 4 x 4 inch 0.25 inch thick Plexiglas™ square with two holes drilled on opposite diagonal corners is used as the base. A 3.5 inch long, 0.5 inch wide Plexiglas™ with one hole drilled on either end and two holes aligned for use with the inlet/outlet holes on the flow cell in the center forms the top piece. The top piece also has a 0.25 inch thick silicone rubber piece also with two holes for the inlet/outlet

holes on the channel. These center holes accommodate 0.125 in. o.d. tubing. The top piece is held to the base using two allen head screws.

3.3.2.2.5. Ag/AgCl Electrode

In order to form a Ag/AgCl electrode in the channel, a 3 M $FeCl_3$ (in 0.1 M HCl) solution was pumped through the channels containing a Ag thin layer electrode. The voltage was measured vs. an external reference electrode to determine if a AgCl electrode had been formed. Additionally, pieces of anodically bonded Pyrex were treated in the same way. The reference electrode used was a 280 μm diameter silver wire (1.5 inches long) immersed for a minimum of 30 seconds in a 3 M $FeCl_3$ (in 0.1 M HCl) solution. The surface area was 0.33 cm^2. The surface was stable for approximately 24 hours of use. The surface AgCl layer could be refreshed several times on the same wire using the same $FeCl_3$ solution.

3.3.2.3. Protein Immobilization

3.3.2.3.1. Materials

The glucose, glucose oxidase, and BCA reagents were obtained from the same sources as for the Plexiglas™ model. Bovine serum albumin (BSA) was obtained from Aldrich (St. Louis, MO). One μm diameter magnetic beads, Dynabeads M-450, were used with an 11,000 Gauss magnet in a 24 well plate configuration both from Dynal (Lake Success, NY). Hydrogen peroxide (31.9% v/v), sodium chloride, hydrochloric acid, sodium phosphate, potassium phosphate, and phosphate buffer (pH 7.4) were obtained from Fisher Chemical (St. Louis, MO).

3.3.2.3.2. Immobilization of Glucose Oxidase to Magnetic Beads

3.3.2.3.2.1. Method 1

In a 24- well plate, approximately 1 ml of tosyl activated magnetic beads ($4x10^8$ beads/mL) were added. After placing the plate on a magnetic plate, the

supernatant was withdrawn. The beads where then washed with 1 mL of 0.1 M borate buffer (pH 9.5)(Buffer A) and resuspended in 0.5 mL of the same buffer. To this solution was added 0.5 mL of 0.4 mg/mL GOx in borate buffer and incubated at room temperature for 24 hours on an orbital shaker at 210 rpm. The supernatant was removed and the beads were washed twice with 1 mL of 0.1 M PBS (pH 7.4) for 5 minutes on the orbital shaker. After discarding the wash solution, the beads were then resuspended in 10% ethanolamine in Buffer A (Buffer B) and incubated for 2 hours at room temperature. After washing as above in 0.1 M PBS, the beads were resuspended in 0.5 mL of PBS.

3.3.2.3.2.2. Method 2

Method 1 was followed except for the following two differences. The buffer used for the washes and final resuspension was 0.1% (w/v) BSA in 0.1 M PBS (pH 7.4). The second incubation lasted 24 hours instead of 2 hours using 0.1 % (w/v) BSA in 0.2 M Tris (pH 8.5).

3.3.2.3.2.3. Determination of GOx Loading on Magnetic Beads

The Pierce BCA test (Pierce, Rockford, IL) was used to determine the amount of protein immobilized on the magnetic beads. The procedure is as follows. Ten microliters of either soluble glucose oxidase standard, PBS blank, or magnetic beads are added to 0.6 mL microcentrifuge tubes. To this, 200 microliters of Pierce BCA work reagent prepared according to the manufacturers specifications are added. After mixing and incubation for 30 minutes at 60 °C, the absorbance is measured at 542 nm on a Beckman DU 640B (Beckman Instruments). The tubes containing magnetic beads were spun down prior to UV detection in a microcentrifuge at 200 rpm. The concentration and mass of GOx immobilized is determined using a calibration curve measured from soluble GOx standard solutions 0 to 250 µg/mL in 0.1 M PBS (pH 7.4) in increments of 50.

3.3.2.3.2.4. Determination of GOx Activity on Magnetic Beads

The trials were performed at room temperature with constant stirring using a bent glass rod attached to a mechanical stirrer. The working electrode was a Teflon coated Pt wire with approximately 1 cm of Teflon removed and then dipped twice into a 4 % cellulose acetate solution. The reference electrode was Ag/AgCl. The applied potential was + 600 mV.

After obtaining a stable current baseline at the applied voltage in 4.0 mL of 0.1 M PBS, 10 microliters of GOx-magnetic beads were added. After the current stabilized, 10 microliters of an 18% glucose solution (in water) was added for a final concentration of 2.5 mM. The current change was measured as a function of time.

3.3.2.4. Flow Cell Evaluation

3.3.2.4.1. Materials and Equipment

The materials and equipment used here are the same as in the Plexiglas™ flow cell with the following exceptions. The valve was connected to a syringe pump and to the flow cell with 780 μm i.d., 1 mm o.d. Teflon FEP tubing (Cole-Parmer). To reduce dead volume, all the data collected using the Au interdigitated array electrode (IDA) flow cells was collected using 200 μm i.d. PEO tubing threaded through the above Teflon tubing (Cole-Parmer). A micropump made by Jim Cunneen at UIC was used. The pump was connected using the same Teflon FEP tubing as above.

3.3.2.4.2. Peroxide Determinations

All solutions were prepared fresh daily from 31.9% hydrogen peroxide (as received from manufacturer) in 0.1 M PBS (pH 7.4).

3.3.2.4.3. Glucose Determinations

Glucose was prepared as an 1 M stock solution in 0.1 M PBS, mutarotated overnight at 4°C .

3.3.2.4.3.1. Method 1

10 microliters of magnetic bead stock solution were diluted to 1 mL in 0.1 M PBS. The flow cell was filled with the solution and held with a magnet. Then a 18% glucose solution was injected using the Valco valve described above.

3.3.2.4.3.2. Method 2

10 microliters of magnetic bead stock solution diluted to 1 mL of 0.1 PBS was mixed with an aliquot of 1 M glucose solution prepared in 0.1 M PBS. After a 30 second incubation, this solution was injected.

Method 3. Same as Method 3, but the solution was used as the carrier stream.

3.3.2.4.4. Determination of Sensitivity

Since calibration curves were not generated, sensitivity was determined by taking the ratio of nA current to mM peroxide or glucose at a particular concentration.

3.3.2.4.5. Determination of Flow Rate Independence

Using both PBS and peroxide as the flowing stream, the flow rate was varied from 0.5 microliters/min to 40 microliters/min while recording the baseline current.

3.4. Results

3.4.1. Plexiglas™ Model

The protein immobilization on the UltraBind membrane was first evaluated. The average loading was 850 pmol/cm^2 ± 2.5%. This was close to the monolayer coverage calculated to be 900 pmol/cm^2. On one channel, the amount of protein was

11 pmoles. This is ten times higher that what could be immobilized on the surface of the microfabricated channel walls if maximum coverage is achieved. The activity, shown in Table 2.1, only decreased one order of magnitude as a result of immobilization. Thus, the membrane possessed good qualities as a potential immunosorbent surface.

Table 2. 1

Results from the Immobilization of Glucose Oxidase on UltraBind Membranes

	Soluble Glucose Oxidase	Immobilized Glucose Oxidase
Density		850 pmol/cm^{2**}
Activity	2.0 x 10^{-3} au/nM	2.5 x 10^{-4} au/nM

**** This is the surface coverage divided by the geometric area of a 13 mm diameter disk of membrane (0.283 cm^2)**

The Plexiglas™ model in Configuration I was demonstrated to detect low concentrations (250 nM) of glucose in 20 nL sample volumes in a channel with a total volume of 6 mL with a current density of 4 pA nM-1 mm-2 (Figure 2.3). Low limits of detection for glucose were achievable using a sandwich flow cell with narrow, shallow channels and a high surface area MRE-bound membrane. However, the advantages of using a high surface area membrane with reproducible covalent surface coverage by protein were offset by the irreproducible nature of water absorption, and membrane deformation.

The presence of the membrane resulted in problems with reproducibility, linearity, and detection limits due in part to the following:

1. Uptake of liquid by the MRE-membrane
2. Uneven flow cell seal due to MRE-membrane

3. Mechanical instability of membrane (tearing)
4. Increased dead volume at the detector (Pt electrode) observed in Configuration II.

Immobilization of the electrodes was required for a reproducible electrode area in contact with the sample plug. However, immobilization of the electrodes is further complicated by the presence of any membrane or spacer. This is illustrated by the results obtained from Configuration II. The dilution at the detector by having the membrane act as a spacer between the electrode and the channel is evident in the lower LOD obtained. The results from both configurations are listed in Table 2.2. It is seen that the addition of the spacer causes a decrease in LOD from 250 nM to 10 mM. The dramatic decrease in LOD and non-linear behavior reflect an additional complication of Configuration II - leaks around the detector due to the presence of the membrane.

The unsealed sandwich flow cell that was modeled above proved to be cumbersome. In spite of the obvious advantages afforded by the ability to switch out a high density immunomembrane, the design for the microfabricated flow cell was reevaluated. Based on the requirements determined from the Plexiglas™ model, a new flow cell design was proposed to eliminate the above problems using the microfabrication technology available. The new design called for the following:

1. No removable membrane
2. Anodically bonded sandwich system - minimize leaks
3. Two Channels - 600 nL volume per channel
4. Coplanar micro lithographic indicating/reference electrode.

For a detailed explanation of the final design dimensions and fabrication methods refer to the Theory and Experimental sections.

Table 2. 2

The Detection of Glucose in Two Model Plexiglas™ Flow Cell Configurations

	Configuration I	Configuration II
Analytical LOD	250 nM	10 mM
Sensitivity	4.8 nA/μm	not linear
Linear Range	250 nM to 1 μM	not linear

3.4.1.1. Micromachined Micro Flow Cell

3.4.1.1.1. Etch

The yields of the different fabrication methods are listed in Table 2.3. The results from etching were good, but there were problems meeting original specifications. The dimensions obtained with Method 1 resulted in channels that were 50 % wider and 30% deeper than designed. The presence of metal was not the cause, since the first wafer was never coated with metal. This leaves two factors, the elevated temperature or the length of the etch time. No evidence exists for the fact that the elevated temperature should adversely affect the channel dimensions *(22).* Method 3, the shortest etch time, met specifications closely, therefore it is concluded that the etch time alone prevented the channels from meeting the dimension specifications in Methods 1 and 2. Additionally, it was shown that using silver to protect the backside of the wafer where the inlet/outlet holes were etched was not an improvement over using photoresist 1818 spun and hand applied.

A top view of the bonded flow cell is shown in Figure 2.16. Note the 90 ° corners are over-etched. This acts as a velocity diffuser allowing more time for

molecules to diffuse to the wall but also broadens the sample plug. While this can be corrected using corner compensation, we decided to leave the corners broader to allow for the option of trapping beads or molecules in the corners.

Figure 2.16

Top View of Bonded Flow Cell - Channels Etched In Si Viewed Through Pyrex™ Cover

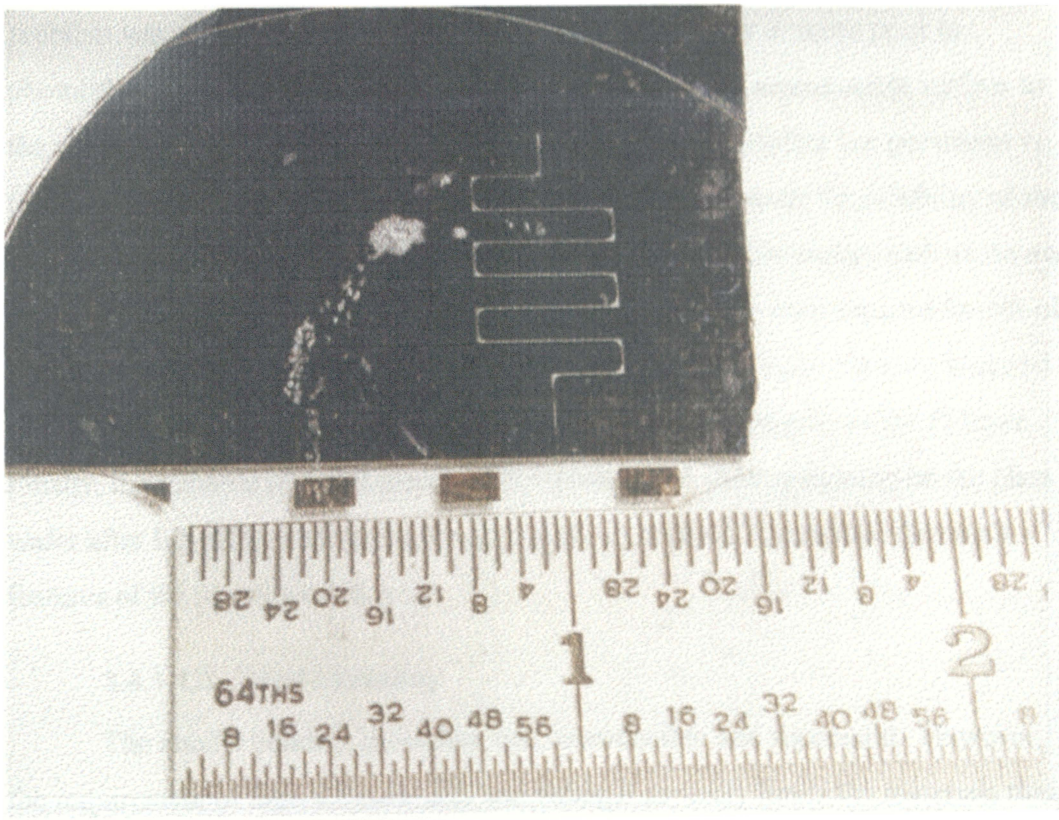

Figure 2. 16. View of channels etched in silicon throught the Pyrex top (anodically bonded).

3.4.1.1.2. Metal Electrodes

Of specific interest is the fabrication of the thin film Pt and Au electrodes. While Au is a much less sensitive surface for electrochemically detecting peroxide, it has the advantage that the thin film is quite rugged compared to platinum. The lift-off method of depositing electrodes requires that the surface in the area developed be free of photoresist. Unlike Pt, the Au adhesion to glass is very good, and minor differences in the surface of the glass do not effect it. Platinum, a much better metal for detecting peroxide, gives more variable results. While good adhesion was observed for Methods 1 and 3, Method 2 gave very poor results. One solution to this problem was to bake the Pyrex wafers at 150°C for an hour or more prior to photolithography to dehydrate the surface. This presents a reproducible surface to the photoresist, whose solubility is affected by moisture. Another key parameter is the omission of the post-bake. The post-bake serves to decrease the solubility of the photoresist, making the lift-off step in acetone prolonged. For metals such as Au and Ag where adhesion is strong, this significantly decreases the time required for lift-off. Additionally, in the case of Pt where adhesion is poor, it prolongs the time required and increases the need for agitation, thus jeopardizing the integrity of the Pt layer. Finally, the removal of small pieces of Pt + photoresist 1818 remaining on the glass wafer after lift-off by sonicating in warm water in Method 3 preserved the small features of the interdigitated array.

3.4.1.1.3. Anodic Bonding

The anodic bonding procedure was reproducible and successful. However, the requirement of high temperatures and voltages severely limits the materials that may be incorporated in this type of flow cell. This was evident in the survival of silver. While a thicker silver layer, as in Method 2, did not disappear on bonding, it did oxidize. Treatments with a 25 % sulfamic acid solution to dissolve the oxide layer after bonding did not provide a surface that reacted with the iron chloride solution to form the Ag/AgCl layer. This was also demonstrated on Ag deposited on

Pyrex that had not been sealed in the flow cell. However, an external Ag/AgCl wire used as a reference did work well, with background currents in the range of 0.5 to 10 nA.

Anodic bonding was attempted at various temperatures and voltages. However, complete bonding over the entire surface area did not occur below 400°C at 1 KV.

3.4.1.1.4. Final Assembly

The bracket for making connections was leak free for approximately 10 to 15 uses. After this point, the Plexiglas™ top piece became too flexible. The silicon seal was effective for about the same period of time, but flipping it over increased its lifetime. While replacement of these pieces is possible, this behavior suggests that the seals and interconnects should be designed first, then the flow cell made to fit them. This is also consistent with the observations made while evaluating the flow cell.

Electrical connections to the flow cell were made using Ag epoxy cured at 150°C for 1 hour. This made good electrical contact. However, the combination of the bracket and the weight of the epoxy on the brittle glass resulted in breakage after 2 to 5 days of continual use. Flow cells tested only for flow characteristics, and therefore, not connected to the potentiostats, did not exhibit this fragility, and were able to survive weeks in the bracket without cracking. This suggests that a circuit board connector should be designed to make electrical contact.

Table 2. 3

Fabrication Yield

Substrate	Procedure †	Theoretical Device Total	Actual Device Total	Percent Yield
Silicon	Etch 1	12	10	83
Silicon	Etch 2	12	10	83
Silicon	Etch 3	24	20*	83
Pyrex	Pt 1	12	0**	0
Pyrex	Pt 2	24	3	12.5
Pyrex	Pt/Ag 3	24	21	87.5
Pyrex	Au 4	12	12	100
	Anodic Bonding 1	3	3	100
	Anodic Bonding 2	12	12	100

*** Loss due to dropping and breaking a wafer**

**** Loss reflects the loss of interdigitated array resolution. The Pt electrode still functioned as a macro working electrode in further tests.**

† Nomenclature is the name of the process and the method number from the Experimental section.

3.4.1.2. Performance Evaluation

3.4.1.2.1.Demonstration of Micropump, Micro Flow Cell, and Micropotentiostats.

Initially the flow cells with the macro Pt electrode were evaluated using a microfabricated pump designed and made by Jim Cunneen at UIC (Figure 2.17). A schematic of the pump and how it works is found in Figure 2.18. A photograph of two micropumps is shown in figure 2.19. Note the scale.

Figure 2.17

Schematic Cross-Section of a Micropump

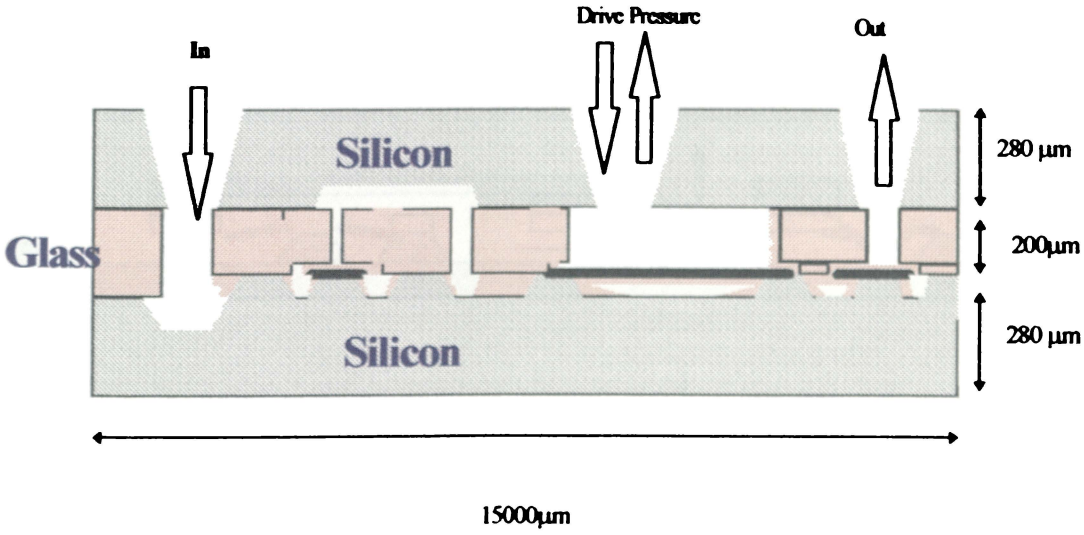

Figure 2. 17. Drawing of micropump.

Figure 2.18

Schematic Diagram of Pump Operation

Order of Scheme:

1. Quiescent State 2. Empty Chamber 3. Valves Change State 4. Fill Chamber 5. Valves Change State

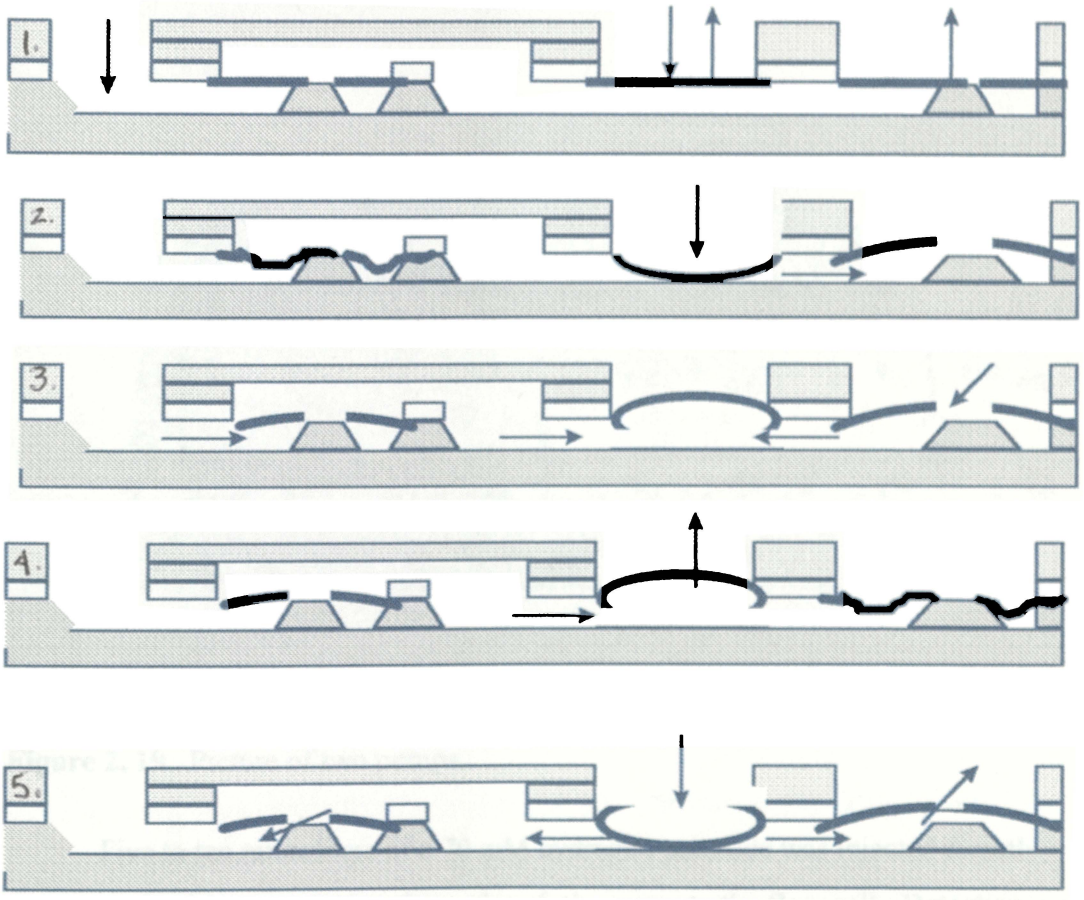

Figure 2. 18. Schematic of pump operation.

Figure 2.19

Two Micropumps from a Two Inch Pump Wafer (8 Pumps/Wafer)

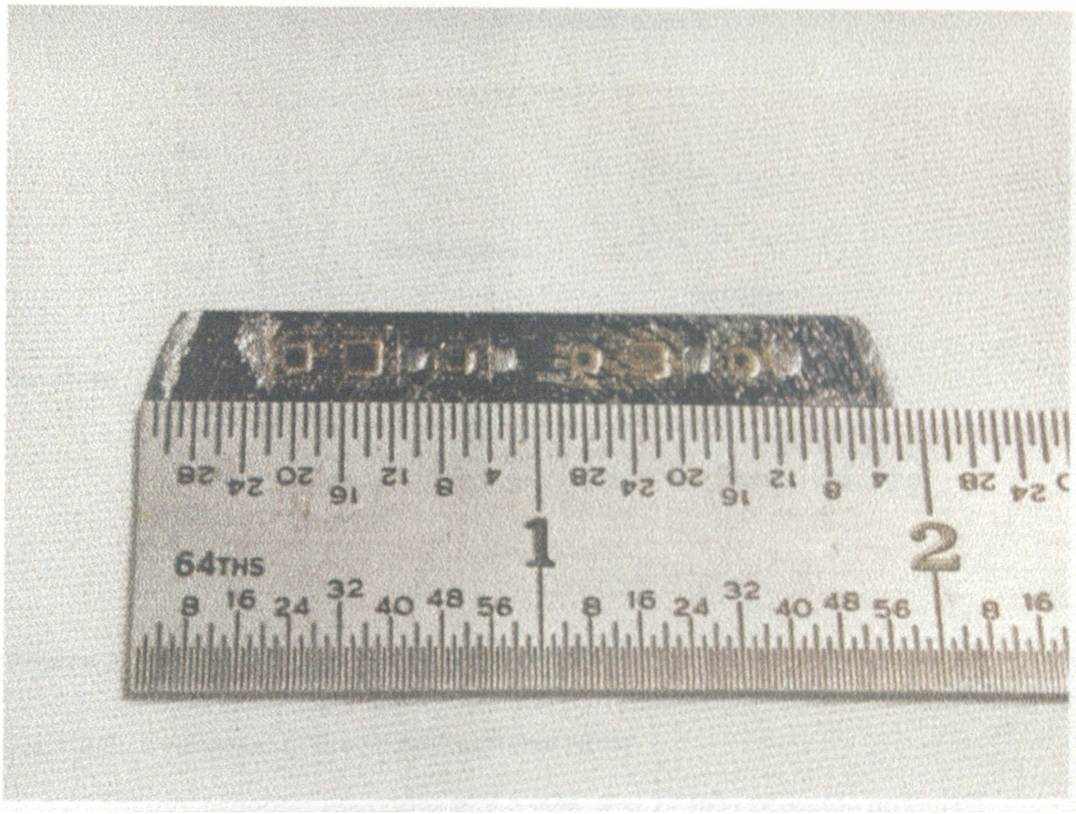

Figure 2. 19. Picture of two pumps.

Five to ten microliters of a 70 mM hydrogen peroxide was injected directly into the soft tubing connecting the outlet of the pump to the flow cell. Detection was at 660 mV applied voltage versus an external Ag/AgCl electrode. A photograph of the system is shown in Figure 2.4. The results from this type of injection is shown in Figure 2.20. It shows a left-skewed Gaussian peak. The flow rate was approximately 5 microliters/min. Injection of buffer produced peaks that were significantly smaller, and looked like spikes from air bubble introduction. Only one pump could be operated at a time, because only one pneumatic drive was available.

In addition, the injection was not reproducible, so the remaining experiments used the Valco valve and syringe pump described in the Experimental section.

Figure 2.20

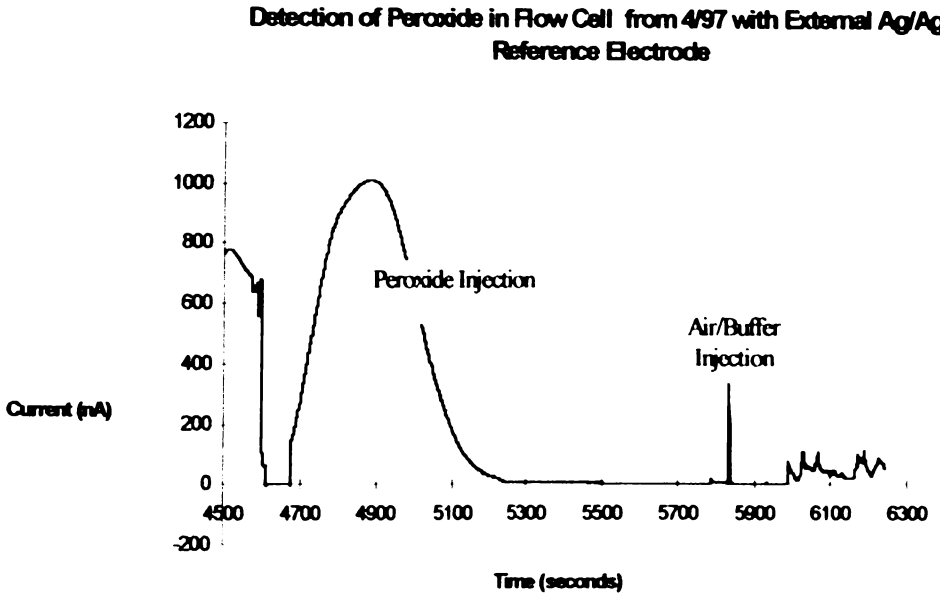

Figure 2. 20. Detection of peroxide using the micropump and micro flow cell.

3.4.1.2.2. Evaluation of the Pt Interdigitated Array

Twenty nanoliter injections of 8.5 mM and 17 mM peroxide produced reproducible peaks. Table 2.4 shows the peak heights, widths, and areas. Injections of 17 mM were also reproducible, and the results were not linear. This is perfectly consistent with what has been reported in the literature *(23)*. The current density for the thin film interdigitated array reported in Table 2.5 is 1000-fold lower than calculated value and 400 fold lower than the current density observed in the Plexiglas ™ model.

The calculated value does not take into account differences in electron transfer rates at different metals. Therefore it is more reasonable to compare the interdigitated array (IDA) with the Plexiglas ™ model than the calculated value. The

difference could be accounted for by two explanations: 1. The oxidation potential of peroxide is different on the thin layer Pt IDA than the bulk electrode or 2. Dilution of the sample plug.

The first case is the least likely. Prior to injecting peroxide, the flow cell was filled with 85 mM peroxide. The current was off scale at 0.6 V vs. Ag/AgCl. The background current, however, was low, so it is not likely that water was being oxidized. Thus it is confirmed that the peak maximum is at the appropriate voltage.

The second case is highly probable. The 100 μm i.d. Peek™ tubing used with the Plexiglas ™ model was too heavy and inflexible to use with the microflow cell. The Teflon ™ FEP tubing used had an inner diameter of 280μm. Recall that the volume is proportional to the cube of the diameter. Thus a 3 fold increase results in a 27 fold dead volume increase.

Before the remainder of a calibration curve could be produced, the flow cell broke at the electrode contacts. The baseline current did not vary with flow rate, as was observed with the macro electrode. Following this, a lower weight of silver epoxy was used to minimize the pressure on the glass.

Figure 2.21

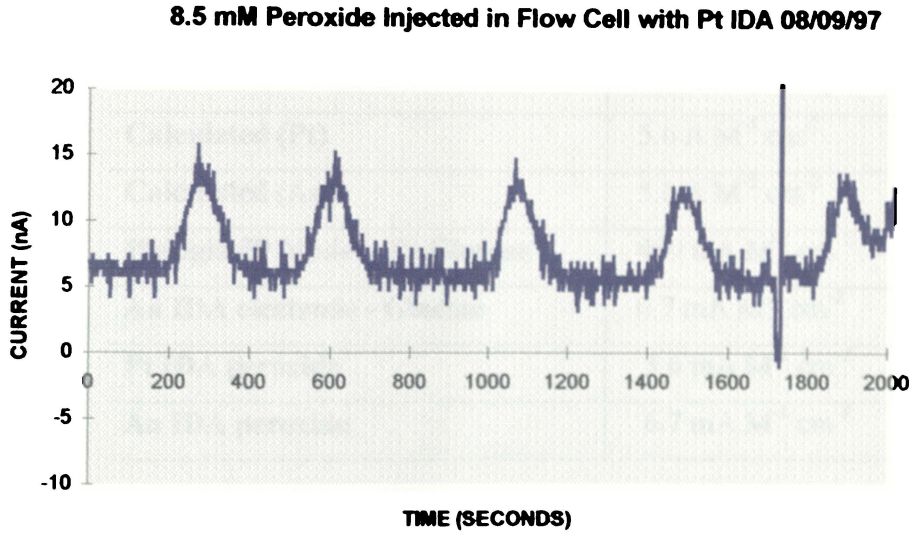

Figure 2. 21. Evaluation of platinum interdigitated array.

Table 2. 4

Summary of Data from Pt Interdigitated Array Electrode

Concentration	Av. Peak Height (nA)	Av. Peak Area (nA sec)
8.5 mM 0.17 nmoles	7.41 ± 0.2	652 ± 17
17 mM 0.34 nmoles	7.43 ± 0.1	465 ± 47

Table 2. 5

Calculated and Actual Current Densities for Peroxide and Glucose

	Current Density
Calculated (Pt)	5.6 A M^{-1} cm^{-2}
Calculated (Au)	5.6 A M^{-1} cm^{-2}
Plexiglas™ Model - Pt Glucose	400 mA M^{-1} cm^{-2}
Au IDA electrode - Glucose	0.7 mA M^{-1} cm^{-2}
Pt IDA peroxide	5.6 mA M^{-1} cm^{-2}
Au IDA peroxide	6.7 mA M^{-1} cm^{-2}

3.4.1.2.3. Evaluation of Au Interdigitated Array.

An 85 mM solution of peroxide was used to evaluate the flow cell. Since results using the injector were uneven, the flow cell was evaluated by switching from a PBS run buffer to the peroxide solution. Table 2.6 lists the results. The flow rate was varied from 0.1 to 40 μL/min with both PBS and peroxide. The average current determined from the second peak in Figure 2.22 reported in Table 2.6 below was determined during the period of 1 minute while the flow rate was varied. The 7 % standard deviation reflects the flow rate independence of the electrode. After one minute the current decreased steadily, again even while varying flow rate, as the Pt oxide layer was saturated. Again, the signal is shown to be flow rate independent. The true limit of detection could not be determined, as injections produced irreproducible results.

Figure 2.22

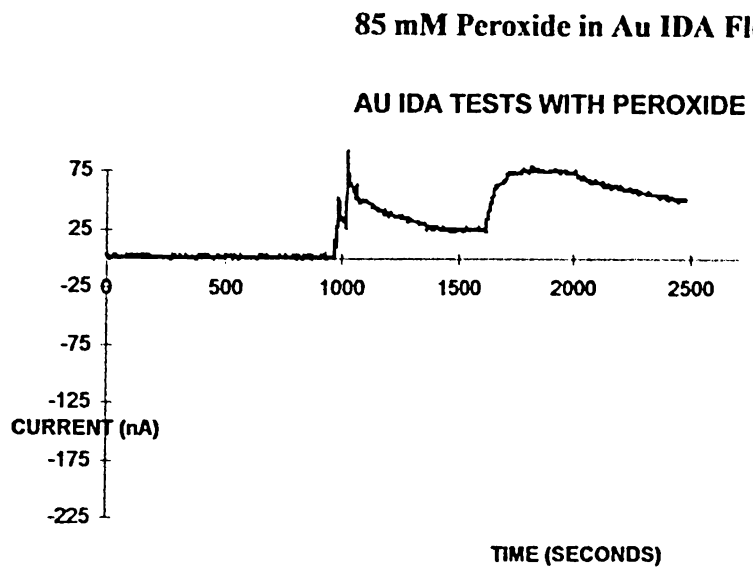

Figure 2. 22. Evaluation of gold interdigitated array electrode.

The current densities given for the Au and Pt interdigitated arrays in Table 2.5 are approximately the same. This is surprising, since Au gives about five times less current than Pt for peroxide detection *(23)*. This is most likely due to the fact that in the case of the Pt electrode, the currents were determined from injections while in the case of the Au electrode, the current was determined by filling the flow cell with peroxide. Thus the steady state is reached in the case of gold.

Table 2. 6

Average Current for a Flow Cell with a Au IDA Electrode

Concentration	**Average Current at Plateau n=5**
85 mM	75 ± 5.4 nA

3.4.1.2.4. Evaluation of the Au Electrode Using GOx Labeled Magnetic Beads

3.4.1.2.4.1. Magnetic Bead Immobilization

The primary difference between the two methods used to immobilize material on the magnetic beads was the block step. It seems that the use of a bovine serum albumin solution (BSA) to block the remaining active sights gave better results than the ethanolamine block. However, it is worth noting that the two methods were only demonstrated once. Therefore, differences could also be attributed to experimental technique at this point.

It is also worth noting that the activities, given in Table 2.7, are one order of magnitude higher for the soluble protein than for the magnetic beads. This suggests that further optimization of the immobilization method must be done to attempt to bring the activity up.

Table 2. 7

Protein Loading and Activity of Glucose Oxidase Immobilized on Magnetic Beads

Biomolecule	*Protein Concentration in Electrochemical Cell*	*Rate (Response to 2.5 mM Glucose) in nA/min*	*Activity (nA min^{-1} M^{-1})*
10 µL GOx-beads (Method 1)	9.7 nM	1.54	0.16
10 µl GOx-beads (Method 2)	37 nM	2.41	0.24
10 µL 200 µg/mL GOx	3.1 nM	63.2	20
5 µL 50 µg/mL GOx	0.78 nM	8.07	10

3.4.1.2.4.2. Evaluation of Beads in the Flow Cell

First, the beads with GOx were added to the flow cell by pumping a solution of 10µl beads diluted to 1 mL in PBS through the cell. Then, the flow cell was placed on top of the magnet array. The flow was stopped to allow the beads to settle. After 5 minutes, the beads were assumed to be settled. After the addition of the magnetic beads, an increase in current was observed at 8500 seconds (Figure 2.23).

Figure 2.23

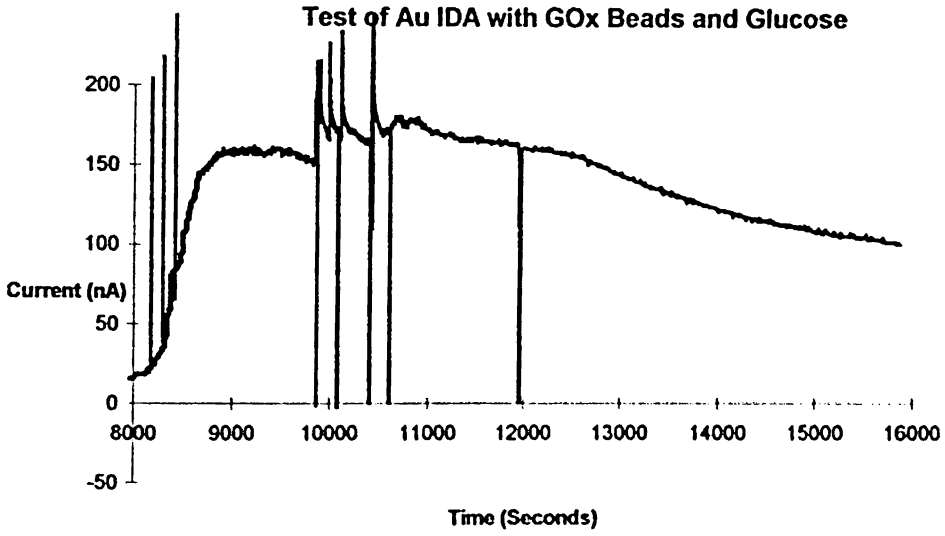

Figure 2. 23. Evaluation of gold interdigitated array using glucose and glucose oxidase labeled magnetic beads.

An increase in current was also observed in the determinations of glucose oxidase modified magnetic bead activity when the beads were introduced into a 4 mL electrochemical cell with a Pt electrode at 600 mV vs. Ag/AgCl reference (Figure 2.24).

Figure 2.24

Injection of GOx-Labeled Magnetic Beads into a 4 mL Electrochemical Cell

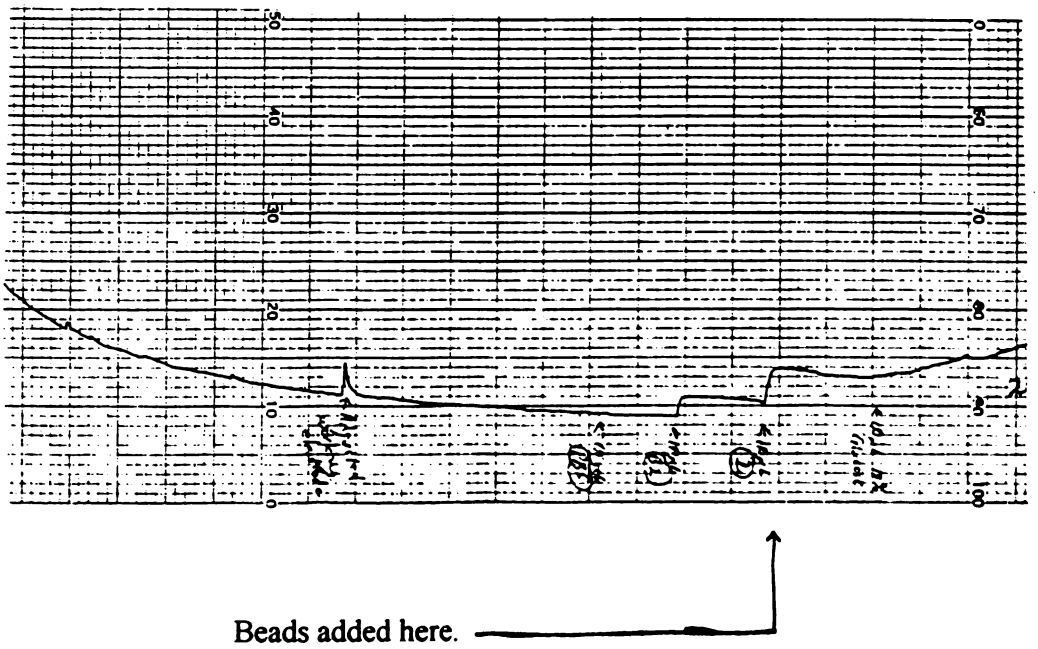

Figure 2. 24. Injection of glucose oxidase - labeled magnetic beads to a 4 mL electrochemical cell.

Injection of 20 nL of a 1M glucose solution in PBS into the flow cell gave no response. Then 0.5 mL of 1M glucose was then mixed with the 0.5 mL of the beads off-line at time 9700 seconds. A 1 minute incubation time was allowed. The channel was filled with this solution. This gave a 50 nA response. Before further experiments could be performed, again the flow cell broke at the electrode contact. The current density, however, given in Table 2.5, was also 1000 fold less than what was obtained from the Plexiglas™ flow cell. This is consistent with the behavior observed for just peroxide. It suggests that the problems with injecting glucose when beads were in the channel (i.e. no signal) resulted from solvable problems such as the interconnects or the geometry of the magnet.

3.5. Discussion

The fabrication template determined from the results of the silicon and glass processing relies on using Etch Method 3, Pt Deposition Method 3, an external Ag./AgCl reference electrode, and Anodic Bonding Method 2. The critical steps, respectively, are: 1. Protection using photoresist only; 2. Final rinse of Pt electrode in warm water with sonication; 3. Omit an on-channel reference electrode; 4. Use a nitrogen purge to prevent oxidation of sensitive metals. The total estimated time for one person to fabricate 6 wafers (24 flow cells) is five days.

While the fabrication of the flow cell is now a standard procedure, the evaluation was necessarily incomplete. The interconnection of the fluid and electrical components was a limiting factor. Jury-rigging, of course, could have produced more data, but its reproducibility would still be in question. This points to the next step - a rationale design of the interconnects - both fluid and electrical. Following this, any changes in the design of the flow cell could be made. Since design changes would effect primarily geometry, the fabrication methods outlined here could be used. Thus, this work describes a blueprint for the fabrication of further flow cells, to be tested using appropriately designed interfaces.

Wilson and Zhang's work shows that at greater than 1 mM peroxide, the behavior of the Pt electrode is non-linear *(23)*. They attribute this to the saturation of the surface oxide with peroxide or oxygen. Thus the surface concentrations are no longer dependent on the bulk concentration. Our results from the micro flow cell with the Pt electrodes are perfectly consistent with this observation. Unfortunately, the LOD was too high, so work at lower concentrations was out of the question.

Some of the differences in the calculated and actual current density probably reflect dilution. The dead volume of the cell was limited by the number and volume of interconnects required. This supports our first conclusions regarding the interconnects. The current density difference was approximately 1000 fold. A factor

of 100 could be derived from the total cell volume, if the sample completely diffused through the channel. It is somewhat unlikely, however, as the channel was also filled with solution. This suggests a truly reduced current density. A high dead volume does, however, explain the difficulty in detecting injected volumes. This could have easily been caused by the tubing used to connect the valve to the flow cell.

Janata suggested that the presence of adhesion layer would adversely effect electrochemistry on platinum and gold thin films *(24)*. However, the reported difficulties are an increased response time, and a change in potential. The change in potential was not observed, as hydrodynamic studies showed maximums at the expected potentials. Response time was not measured, but depending on the application, it is not necessarily a concern. Also, in this case the solution resistance with PBS filling the channel was high, 10 MΩ, so the time constant for response is most likely dominated by this.

It is more likely that instability in the connections are directly responsible for the uneven evaluation. Therefore, the best solution to the observed problems is to repeat the evaluation of the flow cell with new connectors, both fluidic and electrical. So far, the results can not be readily explained by insufficient electrode area or defects in the thin film electrodes.

The issue of the use of the magnetic beads is separate. Again, the evaluation shows simply that the presence of the magnetic beads does not interfere with the electrochemical detection. The lack of signal at this point in the injection mode cannot be directly linked to the beads themselves, when the evaluation of the flow cell itself is still in question. The result with the beads in a stirred solution and the high current density suggest that this method is promising. The geometry of the magnet, a series of one centimeter circles, was not the optimum geometry to hold the beads in a triangular channel. Future work for this should use a more appropriate magnet geometry, such as rectangular. Additionally, studies of the use of other beads such as latex, and their manipulation in channels would provide insight into the

use of particles to provide higher surface area. Finally, the immobilization of receptors on large molecules, such as dextrans, rather than beads, could provide the simplest solution, as no particle manipulation would be required.

3.6. Conclusion

In conclusion, described here is a basic microflow cell with on-channel electrochemical detection that is flow rate insensitive. This provides a template for the fabrication of more flow cells for use in a miniaturized flow injection analysis immunoassay array. The fabrication procedure is general enough to sustain changes in geometry, size, and electrode composition as long as the following steps are remain constant:

1. Regardless of the etchant used, the silicon wafer is coated with a thin silicon oxide layer.
2. Nothing is deposited prior to anodic bonding that cannot sustain temperatures above 400°C.

The evaluation of the flow cell with peroxide and glucose suggests that further work must be done designing connectors for both fluid and current. The ruggedness of the cell must be significantly improved in order to accurately evaluate the flow cell for future use with enzyme based assays such as ELISA. However, preliminary results indicate the thin film electrode does not display a decreased response time or change in oxidation potentials as predicted by Janata.

3.7. Future Work

Electrical connectors making use of circuit board technology should be relatively easy to design. Prior to this, serious thought must be given to the fluid connectors. Considerations such as minimizing pressure and dead volume should determine the final design of the fluid connectors. Two types of connectors should be designed, one for the real world sizes of the Valco valve and syringe pumps, and one for a micromachined sampling valve.

With respect to manipulating particles, it would be of interest to model the flow of various sized particles and particle densities, then choose particles based on these results. The use of magnetic particles also requires an estimation of the particle size and density, and corresponding magnetic field strength and geometry. Once this has been designed, the use of the magnetic particles could prove to be of tremendous advantage, because the flowing stream will not determine the movement of the particles unless the magnet is not present. This also offers the potential for counter current measurements where the flow of the magnets is perpendicular to the channel. This could be used to bring something on the surface of the magnet in contact with either the solution, so the diffusion speed of molecules in solution is immaterial. A secondary advantage is that it is possible to incorporate an electromagnet into a microfabricated structure. Thus the particle manipulation, channel array, and detector could be integrated onto one structure.

Further miniaturization of channel dimensions would allow us to take better advantage of the low Reynolds number flow. A sheath of viscous liquid could surround a faster moving carrier stream. Receptors would favor the outer sheath based on hydrophobic interactions, but the active site would be accessible or even in the hydrophilic center stream. The sample in the carrier stream could then interact with the receptors, and an enzymatic reaction would lead to a slug of product that could be detected at the end of the column.

3.8. References

1. Brody, J.P. Yager, P. *Sensors and Actuators A* **1997**, *58*, 13-18.
2. Blankenstein, G.; Scampavia, L.; Branebjerg, J.; Larsen, U.D.; Ruzicka, *J. AMI* 1996 Special Issue Proceedings of the 2nd International Symposium on Miniaturized Total analysis Systems μTAS'96, 82–84.
3. Brody, J.P.; Yager, P.; Goldstein, R.; Austin, R.H. *Biophysical Journal* **1996**, *71*, 3430-3441.
4. Murakami, Y.; Takeuchi, T.; Yokoyama, K,; Tamiya, E.; Karube, I; Suda, M. *Analytical Chemistry* **1993**, *65*, 2731-2735
5. Woias, P.; Richter, M.; Yacoub-George, E.; Wolf, H.; Abel, T *AMI* **1996** Special Issue Proceedings of the 2nd International Symposium on Miniaturized Total Analysis Systems μTAS'96, 256.
6. Laurell, T.; Drott, J.; Rosengren, L. *Ibid.*, 100-103.
7. Egodage, K.L. *Designing Antibodies to Defined Epitopes: Immunoassays as Structural and Analytical Probes*, Ph.D. Dissertation, The University of Kansas, 1996, pp. 109-113.
8. Pollema, C.H.; Ruzicka, J. *Analytical Chemistry* **1994**, *66*, 1825-1831.
9. Willumsen, Christian, G.D.; Ruzicka, J. *Analytical Chemistry* **1997**, *69*, 3482 - 3489.
10. Liu, H.; Yu, J.C.; Bindra, D.; Givens, R.S.; Wilson, G.S. *Analytical Chemistry* **1991**, 63, 666-669.
11. Harrison, D.J.; Manz, A.; Fan, Z.H.; Lüdi, N.; Widmer, H. M. *Analytical Chemistry* **1992**, *64*, 1926- 1932.
12. Verpoorte, E.M.J.; van der Schoot, B.H.; Jeanneret, S.; Manz, A.; Widmer, H.NM.; de Roij, N.F. *Journal of Micromechanics and Microengineering* **1994**, *4*, 246-256.
13. Bard, A.J.; Crayston, J.A.; Kittlesen, G.P.; Shea, T.V.; Wrighton, M.S. *Analytical Chemistry* **1986**, *58*, 2321-2331.

14. Josowicz, M.; Janata, J.; Levy, M. *Proceedings of the Symposium on Chemical Sensors* **1987**, *87-89*, 352-359.

15. Chidsey, C.D.; Feldman, B.J.; Lundgren, C.; Murray, R.W. *Analytical Chemistry* **1996**, *58*, 601-607.

16. Penner, R.M.; Martin, C.R. *Analytical Chemistry* **1987**, *59*, 2625-2630.

17. Reller, H. Kirowa-Eisner, E.; Gileadi, R. *Journal of Electroanalytical Chemistry and Interfacial Electrochemistry* **1984**, *161*,247.

18. Cassidy, J.; Ghoroghchian, J.; Sarfarazi, F.; Smith, J.J.; Pons, S. *Electrochimica Acta* **1986**, *31*, 629.

19. Brett, C.M.A.; Brett, A.M.O. *Electrochemistry Principles, Methods, & Applications* Oxford University Press, NY:1993, pp. 97-98.

20. Huangxian, J.; Hongyuan, C.; Hong, G. *Journal of Electroanalytical Chemistry* **1992**, *341*, 35-46.

21. Bard, A.J.; Faulkner, L.R. *Electrochemical Methods*, John Wiley & Sons, Inc., NY:**1980**, p. 280.

22. Chambers, F.A.; Wilkiel, L.S. *Journal of Micromechanics and Microengineering* **1993**,*3*,1-3.

23. Zhang,Y; Wilson, G.S.; *J. Electroanalytical Chemistry* **1993**, *345*, 253-271.

24. Lin, Y.C.; Hesketh, P.J.; Maclay, J.G; Cocco, T. *EECS 449 Laboratory Manual*, University of Illinois – Chicago,**1996**.

25. Hesketh, P.J.; *Short Course On Principles of Microfabrication*, The University of Kansas Higuchi Biosciences Center for Bioanalytical Research Fifth International Workshop on Bioanalysis, **1996**.

26. Vossen, J.E.; Kern, W. eds., *Thin Film Processes*, Academic Press, Inc. NY, NY: **1978**, 12 – 204.

4. Chapter 3: Non-Conservative Behavior of Bromide and Cyanazine in Wetland Mesocosms

4.1. Introduction

A major source of non-point pollution in surface- and ground-water is agricultural chemicals *(1)*. Cyanazine, a pre-emergent herbicide from the s-triazine family, is climbing in usage in the United States as atrazine is being phased out *(2)*. In 1991, cyanazine was listed as the fourth most applied herbicide in the Midwest with an application rate of 9×10^6 kg/yr *(3)*. While it is less persistent in soil than atrazine, it is regulated at levels lower than atrazine, 1 µg/L *(4)*. Most of the year, the concentration of cyanazine falls well below the EPA level, but during the spring flush levels as high as 20 µg/L have been measured in ground water *(5)*. Additionally, systematic studies of the metabolites of cyanazine and other herbicides have proven metabolite monitoring to be a useful geochemical indicator *(2,5,6)*.

One approach to minimizing non-point source pollution (NPS) is the addition of wetland buffer strips where water from crop run-off collects, degrades, and then redistributes as purified water into the surface and ground water *(7)*. While discussions of the experimental design and need to determine the reciprocal effects of wetland structure and pesticides *(8)*, Lee's study examining the effect of mesocosm structure on atrazine and alachlor degradation is the first effort to characterize this problem on actual compounds of interest in a real world setting *(10)*. Cyanazine is rapidly replacing atrazine in the Midwest. Therefore, it is important to determine the degradation pathway of cyanazine in wetlands and the effect of wetland structure on degradation.

This study examines the effect of wetland structure on the half-life of cyanazine and the metabolites formed. The specific objectives of this study were to (1) determine the effect of wetland structure on the degradation of cyanazine and (2) determine the effect of wetland structure on metabolite profiles. Two wetland

structures were chosen, three emergent and three submergent ponds. Additionally, a set of three fiberglass tanks with no soil or rooted plants was treated along with the wetlands to determine if photolysis and hydrolysis were significant pathways for degradation. A set of three fiberglass tanks treated with only potassium bromide (KBr) served as blanks. The parent compound and two metabolites, deethyl cyanazine and cyanazine amide, were determined by gas chromatography/mass spectrometry (GC/MS). Potassium bromide was applied to all systems as a conservative tracer *(11,12)*.

4.2. Theory

4.2.1. Cyanazine

Cyanazine, a preemergent herbicide applied extensively in the Midwest, blocks the P450 electron transfer step in photosynthesis. The first literature report of cyanazine was as a new, test compound, SD 15418, by Hughes, *et al.*, in 1967 *(13)*. Its half-life in soil, 11 to 31 days *(14-18)*, makes it an attractive alternative to atrazine, which has a half-life of 45-60 days, in areas where crop rotation is used. In colder climates where crop rotation is practiced; herbicide residues may persist and interfere with crop growth *(15)*.

The following degradation pathways have been proposed based on M. Meyer's extensive study of cyanazine in run-off, field plots, and the Mississippi River *(4)*. Figure 3. 1 shows the herbicide and its metabolites.

Figure 3.1

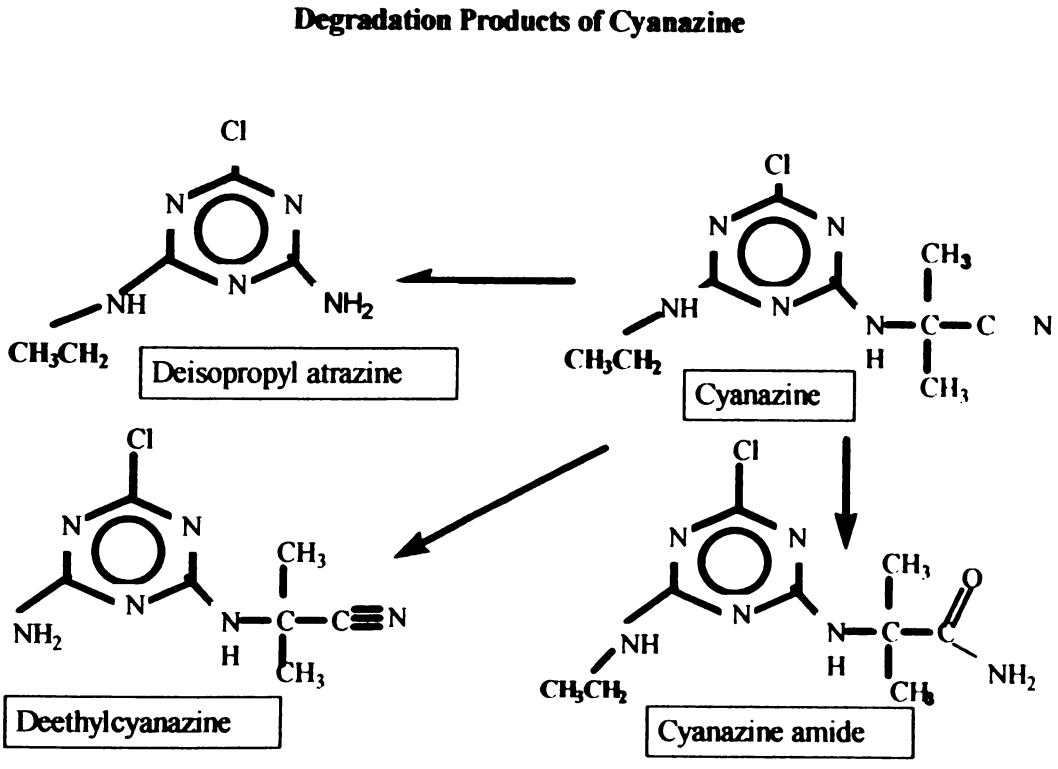

Figure 3. 1. Degradation pathways of cyanazine.

4.2.2. Volume Tracers

The use of bromide as a method of correcting for volume fluctuations is widespread in hydrology *(11,12)*. Typically it is used for studies in lakes or rivers. It has also been used in run-off studies and a similar mesocosm study *(10)*.

The principle behind the use of bromide as a volume tracer is simple. The best volume tracers are not nutrients, so they will not be sequestered by flora, bacteria, or protozoa. The natural background level should be low. Additionally, they should not form precipitates with other ions likely to be present (e.g. Ca^{2+}). Also, hydrolysis, photolysis, adsorption, evaporation, oxidation, or reduction should not be significant pathways of degradation. It must be readily detected, bearing in

mind that in may cases it will diluted several orders of magnitude with rain events or transport to larger volume areas. Finally, the tracer should be non-toxic.

The bromide ion (Br^-) meets these requirements *(11)*. Detection by ion chromatography or with an ion selective electrode at the part per million level is trivial *(19,20)*.

The volume correction of the concentration of the analyte of interest (AOI) using a volume tracer (VT) is made as follows:

$$[VT] = MASS_1/VOLUME_1$$

$$[AOI]_{RAW} = MASS_2/VOLUME_1$$

$$[AOI]_{RAW}/[VT] = \{ MASS_2/VOLUME_1\} * \{ VOLUME_1/ MASS_1\}$$

$$[AOI]_{ADJ} = MASS_2/ MASS_1$$

Therefore, the corrected "concentration" really is a ratio of the mass of the AOI to the mass of the VT. Since the mass is known, it is easy to calculate the actual mass of the AOI, which is not volume dependent.

4.2.3. Wetland Mesocosms

The definition of wetlands is of considerable importance legally as well as scientifically. There is no shortage of definitions, in fact over 50 federal and state wetland definitions exist *(21)*. A useful, although disputed, working definition is provided by the U.S. Army Corps of Engineers and the U.S. Environmental Protection Agency in their dredge and fill permit under SS 404 of the Clean Water Act (33 CFR SS 323.2, and 40 CFR SS 230.3):

> "The term 'wetlands' means those areas that are inundated or saturated by surface or ground water at a frequency and duration sufficient to support, and that under normal circumstances do support, a prevalence of vegetation typically adapted for life in

saturated soil conditions. Wetlands generally include swamps, marshes, bogs, and similar areas."

Therefore, an area is considered a wetland if it has water at or near the surface for a period of time, wetland plants, and periodically anaerobic soils resulting from prolonged saturation. The U.S. Fish and Wildlife Service uses the same definition except an area has only to meet one of the above three criteria to be considered a wetland. Wetlands are further classified into types such as swamps, marshes, bogs, and fens, based on characteristic vegetation, soils, atmospheric and geological conditions, and/or water quality.

Wetlands function to maintain both the volume and quality of surface and ground water. They intercept nutrients, sediments, and contaminants, providing clean water that percolates beneath the surface as groundwater. As almost all drinking water is obtained from groundwater, the health benefits are obvious. The presence of aquatic plants, fungi, and bacteria contribute significantly to the removal of contaminants. Additionally, the ability of wetlands to store storm runoff for long periods and gradually return it as surface flow prevents flooding. It is of interest to determine their utility in the degradation of commonly used herbicides.

Wetlands, by definition, are uncertain ecosystems. Natural wetlands can remain dry for years, even decades. Many are porous, so tracing water is difficult. However, aquatic ecosystems created in the controlled environment of the laboratory rarely approximate the natural conditions. The use of a wetland mesocosm, a constructed wetland mimic in the outdoors, is a reasonable compromise. The structure of the wetland mesocosms should be as follows:

1. Water tight
2. Controllable flora and fauna
3. Filled with water from a well characterized source
4. Known soil composition

The utility of wetland mesocosms, or controlled, constructed wetland mimics, has been well documented *(22)*. The wetland mesocosms at the Nelson Site in Tonganoxie, KS meet the above requirements. The progression of the mesocosms at the Nelson Site is well documented, and more information is available in the reference listed *(23)*.

These mesocosms can be structured in a variety of ways. Two common variations are to include emergent vegetation in one subset, and only submergent vegetation in another. A subset with no vegetation or fiberglass tanks can be used as a control. It is of interest to observe any influence of the actual mesocosm structure on the degradation pathway and half - life of cyanazine.

4.3. Experimental

4.3.1. Materials and Methods.

Methanol and ethyl acetate (Fisher, St. Louis, MO) were reagent grade solvents. Cyanazine, deethyl cyanazine, deethyl cyanazine amide, cyanazine amide, deisopropyl atrazine, and deethyl atrazine were obtained from Supelco (Bellefonte, PA). Potassium bromide (KBr) was obtained from Aldrich (St. Louis, MO). All standards were prepared in methanol. Phenanthrene-d_{10} (EPA, Cincinnati, OH) and terbuthylazine (EPA, Research Triangle Park, NC) were used as internal and surrogate standards, respectively, for GC/MS quantitation. The C_{18} cartridges (Sep-Pak from Waters, Milford, MA) contained 360 mg of 40- µm C_{18} bonded silica. Deionized water was charcoal filtered and glass distilled prior to use.

The C_{18} cartridges were prepared by sequential washes with 3 mL of methanol, 3 mL of ethyl acetate, 3 mL of methanol, and 2 mL of distilled water. Filtered water samples (123 mL) were manually spiked with a recovery surrogate standard (terbuthylazine) and were passed through the Sep-Pak cartridges using a

Millipore Workstation (Waters, Milford, MA) at 20 mL/min. The cartridge was eluted first with air to remove residual water and then eluted with 2.0 mL of ethyl acetate. The ethyl acetate was spiked automatically with phenanthrene-d_{10}, then evaporated under nitrogen at 50°C to 100 µL and analyzed by GC/MS. Recovery of the parent and each metabolite was determined by comparison of the GC/MS results from standard-spiked water that had been extracted by SPE to the results from standard-spiked ethyl acetate.

4.3.2. GC/MS Analysis

GC/MS analyses of the eluates were performed on a Hewlett-Packard (Palo Alto, CA) Model 5890A GC / 5970A quadrupole mass selective detector (MSD). Operating conditions were as follows: ionization voltage at 70 eV; ion source temperature at 250°C, electron multiplier at 2200 V above autotune; direct capillary interface at 280°C, daily tunes with perfluorotributylamine, and a 50 ms dwell per ion. For sample analysis, the solvent delay was 2 min. For each sample, three ions were selected for a positive compound identification (214, 225, 240 amu). The base peak ion current was measured for the quantification curve versus the response of the 188 ion of phenanthrene-d_{10} *(4)*.

A fused silica capillary column with a C_{18} bonded phase and 5% phenyl methyl silicone with a film thickness of 0.33 µm, 12 M x 0.2 mm i.d. (Ultra-2, Hewlett-Packard) was used for the GC separation. Helium was the carrier gas with a flow rate of 1 mL/min and a head pressure of 35 kPa. The samples were injected in the splitless mode by the autoinjector (Hewlett-Packard). The column temperature was held at 120 °C for 1 min and programmed to 250°C at 11°C/min and held at the final temperature for 0.3 min. Injection port temperature was 210°C *(7)*.

4.3.3. Field Study.

A schematic of the experimental design is shown in Figure 3.2. Two wetland structures were chosen; three emergent and three submergent ponds, and these were

treated with Bladex at approximately 5 µg/L and KBr at 15 mg/L. Additionally, a set of three fiberglass tanks with no soil or rooted plants was treated along with the wetlands . A set of three fiberglass tanks were treated with KBr only and served as blanks. The ponds were approximately 10 m across, and 1 - 1.5 m deep. They were located at the Nelson site in Tonganoxie, KS and were maintained by the Kansas Biological Survey. The water for the ponds and tanks was taken from the Tonganoxie, KS ground water, then aged for 6 months at the Nelson site reservoir. **Figure 3.2**

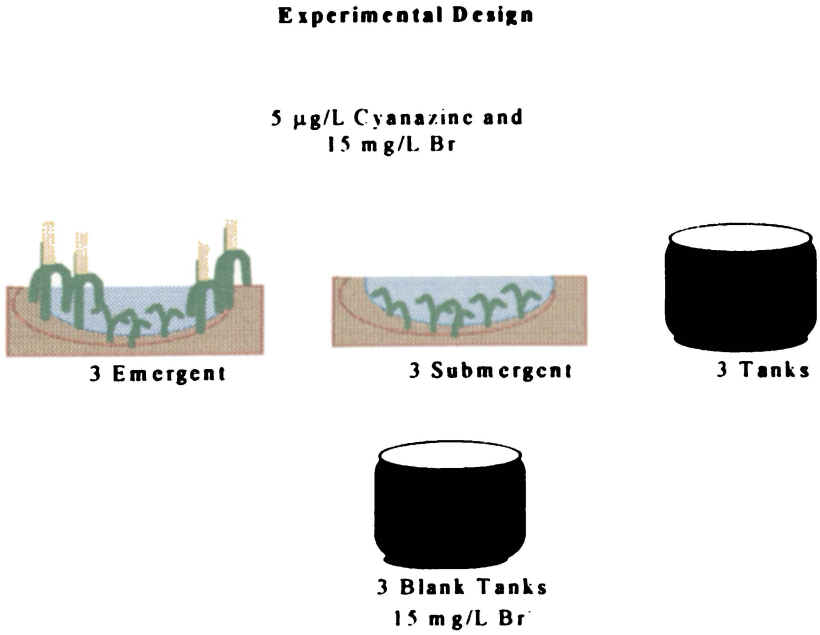

Figure 3. 2. Schematic of mesocosm treatments.

Collection bottles were baked amber 1 L bottles. Dissolved oxygen, pH, conductivity, temperature, and turbidity were measured in the field with a U-10 Water Checker (Horiba Instruments International, Irvine,CA) on the same days that water samples were taken. Each structure was divided into quadrants assigned numbers and letters. Using a random number table, water was sampled in three

randomly selected places in each pond and tank with a sampler constructed in-house. The sampler was constructed of 3" i.d. PVC pipe and a one-way valve. All water samples were vacuum filtered through Gelman 0.4 μm glass fiber filters (Fisher, St. Louis, MO) into three 125 mL baked amber glass bottles and stored at 4°C until extraction and analysis. Blanks of all ponds and tanks were analyzed two days prior to application. Application occurred June 30 1994, prior to the height of pond bioactivity. Samples were taken until October 1994, well past the senescence of the ponds. Sampling occurred most frequently the first month when degradation was predicted to be most rapid, then only every other week until September. In September and October the ponds were sampled once.

4.3.4. Anion Analysis

Chloride, sulfate, bromide, nitrate, nitrite and phosphate were analyzed using a Dionex ion analyzer. Two 123 mL samples were filtered through a 0.2 μm pore size glass fiber filter, and stored in amber glass bottles at 4°C until analysis. Analysis was performed by the ecotoxicology lab at the Kansas Biological Survey (KBS). With the exception of bromide, the results were unremarkable, and will not be discussed in detail here.

4.3.5. Preparation of Bromide Solution from Cattails.

1000 ppm KBr and 5 M $NaNO_3$ stock solutions were used as standard solutions prepared from the dry chemicals diluted in deionized water. 100 to 500 g of cattail roots taken from three places in all the emergent ponds and from the reservoir (untreated with Br^-) were rinsed in tap then deionized water. They were air dried at stored at 4°C . The plant matter was further dried at 105 - 115 °C for 2 hours except for samples coded EN3A-C which were dried for 3 hours total. 50 g of the dried sample was weighed and homogenized with 400 mL deionized water using an Oster 10 - speed blender set on "liquefy" (Wal-Mart, Lawrence, KS). The solution was first filtered through HandiWipes then a 0.45 micron glass fiber filter *(20)*. This did

not seem time effective, so it was abandoned and the samples were analyzed without filtration after the sediments were allowed to settle.

4.3.6. Bromide Analysis.

An Orion Research microprocessor analyzer 1901 (Fisher, St. Louis, MO) was used set on the mV scale with a bromide ion selective electrode vs. Ag/AgCl (Fisher, St. Louis, MO). Each standard and solution was prepared as follows for analysis. 50 mL of the sample was mixed with $NaNO_3$ to adjust the ionic strength. The standards were prepared from a 1000 ppm stock solution at the following concentrations: 0.0, 5, 10, 50, 100, 500 ppm. From these data a calibration curve was generated. The correlation coefficient was 0.996, and the equation for the line, $y = 2.98x - 0.015$, was used to calculate the concentration of the sample solutions.

4.4. Results and Discussion

4.4.1. Disappearance and Re-appearance of Bromide

Figure 3.3 shows the bromide ion concentration over time in the submergent pond, emergent pond, and tank structures. The concentration of bromide remains relatively constant in the treated tanks until day 64 where it begins to rise until day 93 where it remains constant until the end of the study. In the submergent ponds, there is a slight decrease over the same time, with an increase observed at day 93 and continued increase until the conclusion of the study. In the emergent ponds, however, there is a sharp decrease in Br^- almost immediately after application.

Figure 3.3

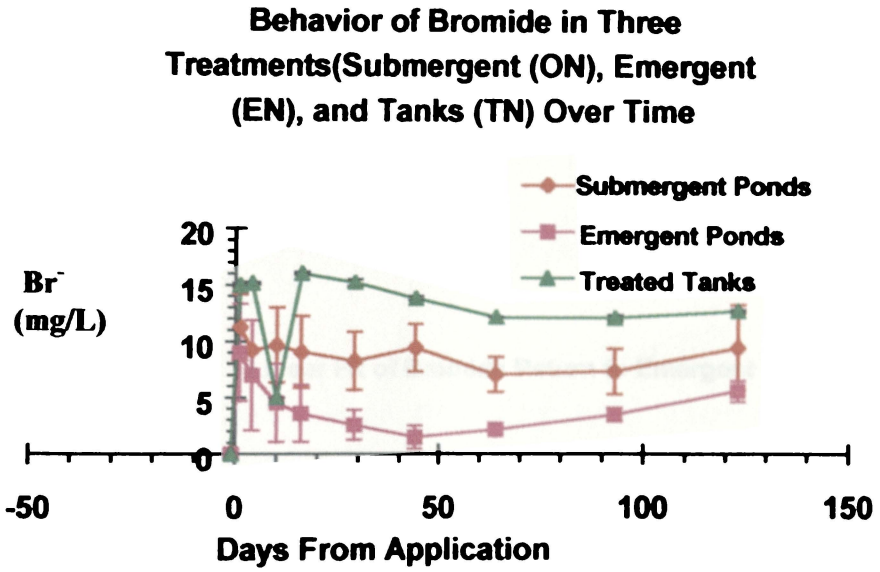

Figure 3. 3. The concentration of bromide (volume corrected) over the course of the study.

The decay is exponential until day 44 which represents the lowest point, then increases linearly until the last day of the study (Figure 3.4). The exponential decay suggests a mediated process, such as active transport, while the linear increase suggests a first order process such as diffusion.

Figure 3.4

a.

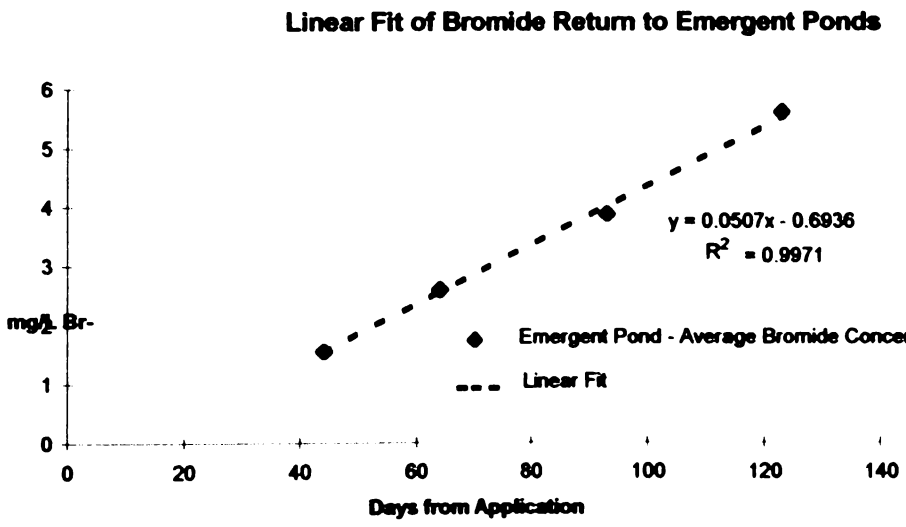

b.

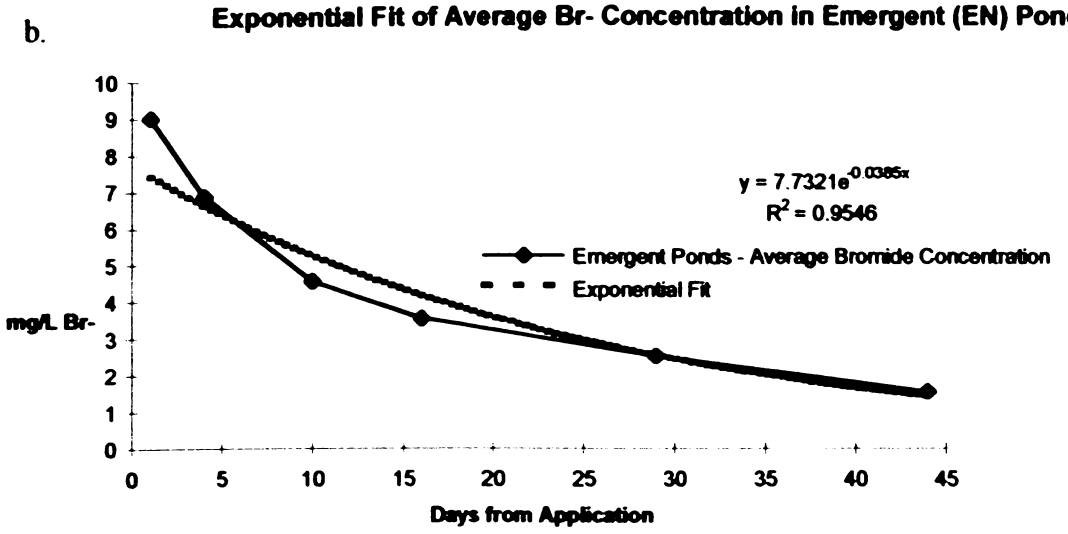

Figure 3. 4. The return and disappearance of bromide in the emergent ponds fit to a a. linear and b. exponential curve, respectively.

The tanks were filled with reservoir water, but the water was not sterilized, so a modest amount of algal growth on the sides of the tanks was observed, as was algae on the water surface. This suggests that the cattails, a tuber plant, found only in the emergent ponds, selectively sequestered the bromide ion, and released it upon decay. It is established that chloride ion competes with nitrate for the nitrate ion transfer protein in plant nutrient uptake *(25)*. Bromide might also compete for the same binding sight.

The above hypothesis is supported by two observations. K.J.S. Kung observed the uptake and release of bromide ion in a field experiment involving potato tubers *(20)*. Additionally, bromide measurements of the cattail roots themselves were made 290 days after bromide was first applied. The results, shown in Table 3.1, show that the biomagnification of bromide ion by the tubers is 20 to 30 times what is observed naturally in the untreated cattails and also observed in the water of the treated ponds.

Cattails taken from the reservoir, which had only 1.5 ppm bromide, showed a biomagnification factor of 8. Another pond, 1E, that was not treated with bromide, showed the same biomagnification in the cattail roots as those taken from the reservoir. However, the roots taken from each of the three emergent ponds in the study (EN1, EN2, EN3) gave a bromide concentration of 300 ppm while the water in the ponds was between 11 and 15 ppm.

Table 3. 1

Sample	Br^- concentration (mg/L)
reservoir blank - water	1.53 (n=1)
pond 1E blank - water	1.47 (n=1)
reservoir blank - cattail roots and stem	12.36 (n=1)
pond 1E blank - stem	2.82 (n=1)
pond 1E blank - root	11.7 (n=1)
EN1 - water	11.7 (n=1)
EN2 - water	12.2 (n=1)
EN3 - water	14.2 (n=1)
EN1 - root (AVERAGE)	296 ± 64 (n=3)
EN2 - root (AVERAGE)	313 ± 93 (n=3)
EN3 - root (AVERAGE)	277 ± 49 (n=3)

4.4.2. Dissipation of Cyanazine.

Figures 3.5 - 3.7 shows the disappearance of cyanazine as a function of time from application in the submergent and emergent ponds, and the treated tanks. The concentrations were volume corrected using the conductivity due to the non-conservative behavior of bromide.

Figure 3.5

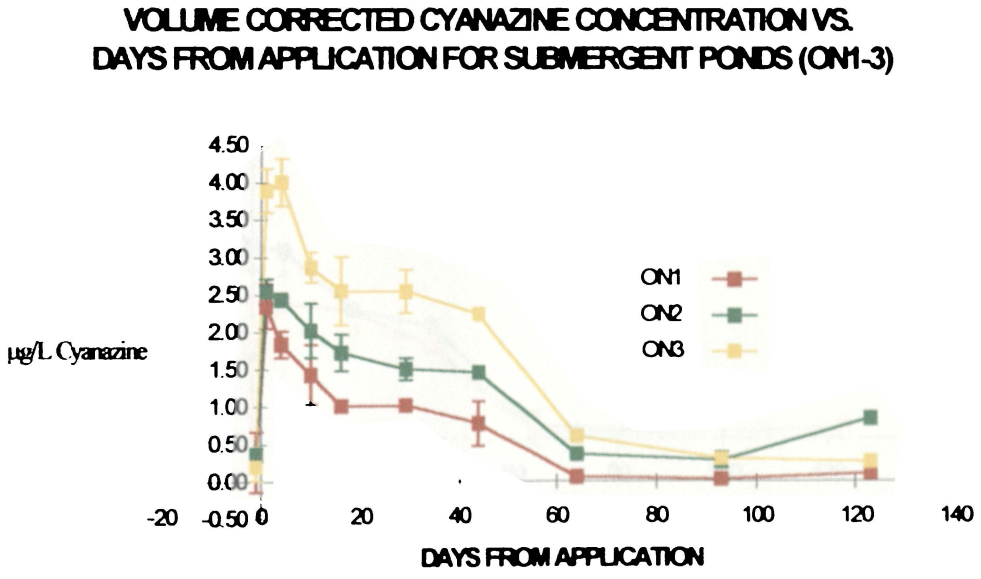

Figure 3. 5. Plot of cyanazine concentration changes in all three submergent ponds (ON1, ON2, ON3).

Figure 3.6

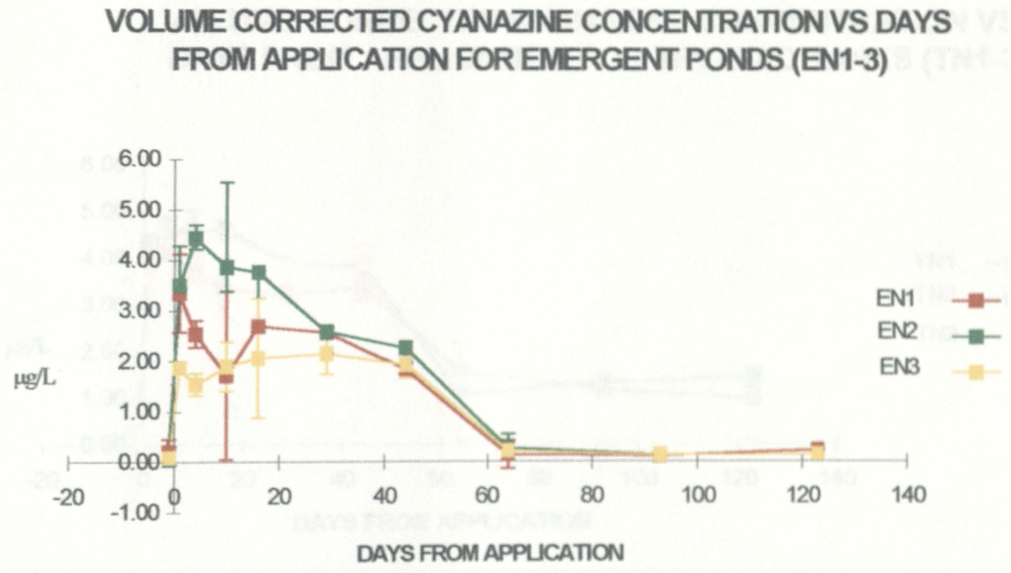

Figure 3. 6. Plot of cyanazine concentration changes in all three emergent ponds (EN1, EN2, EN3).

Figure 3.7

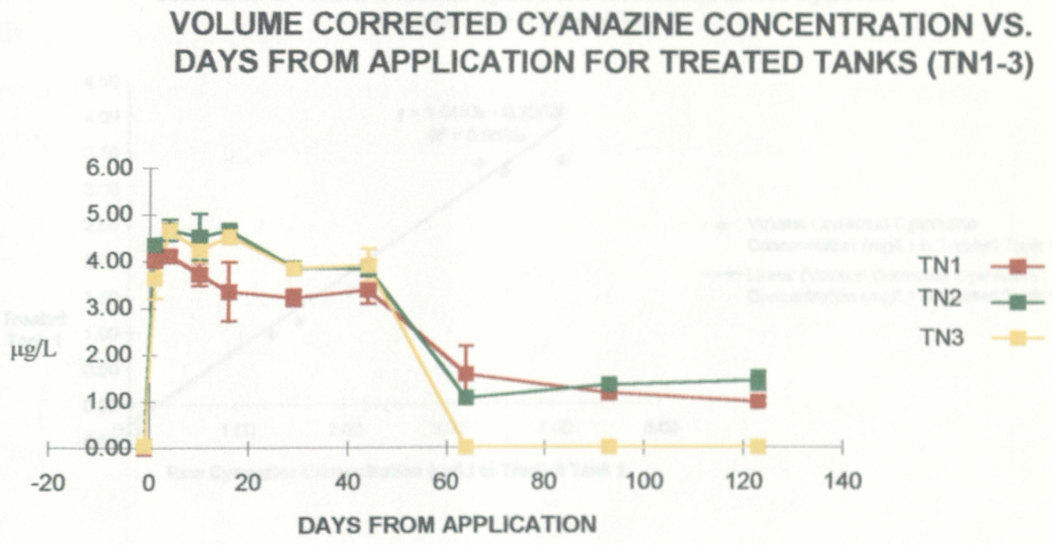

Figure 3. 7. Plot of cyanazine concentration changes in all three treated tanks (TN1, TN2, TN3)

4.4.2.1. Volume Correction Using Conductivity

Conductivity increases as a function of increased ions. Assuming no leakage, changes in conductivity correspond to changes in volume. As a check for this assumption, volume correction when applied to the treated tanks, where bromide uptake was not observed, did not produce any significant difference in the results (Figure 3.8). By multiplying the concentration of cyanazine (or any other analyte of interest) by the ratio of the conductivity on that day to the conductivity at the start of the study, any dilution or concentration is reflected. While this serves only as an estimate, it is useful for standardizing the data, and for estimating mass balance.

Figure 3.8

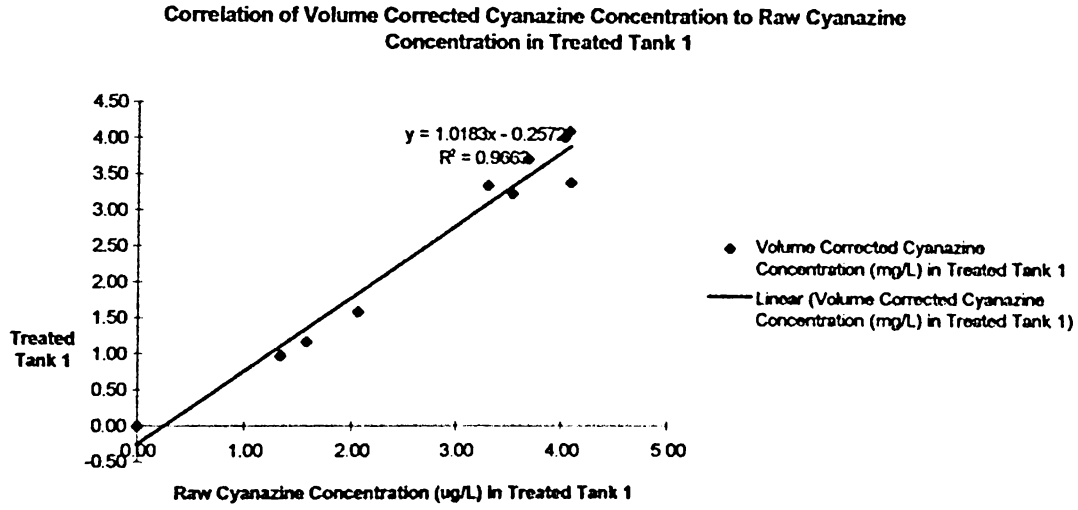

Figure 3. 8. Correlation of the volume corrected cyanazine concentrations to the raw cyanazine concentrations in Treated Tank 1.

A table of half-lives is found in Table 3.2. Typically, disappearance follows first order kinetics, therefore the half-life is determined by plotting the natural log of the concentration versus time, and finding the slope, -k. If kinetics are first order, then the half-life is determined using the equation t = -.693/k. Log plots of the emergent and treated tanks data did not yield linear plots. The half-lives could only be calculated based on a first-order kinetics assumption for the submergent ponds, and those calculations did not reflect the fact that two kinetic events (two distinct slopes) led to disappearance. Therefore, the half-life was determined by graphically finding the point in time where half the concentration remained. In one plot, for ON1, this result was extremely low, on the order of 10 days. This point was discarded as an outlier. A comparison of the half-lives using the analysis of variance supports the null hypothesis that the mean half-lives are not significantly different despite different wetland structures. The results of the ANOVA are shown in Table 3.3.

The results in Table 3.3 show that the F number, 3.05, is less than the F critical, 5.78. Therefore, at the 95% confidence level there is no difference between the mean disappearance half-lives for each treatment. This suggests that the degradation *rate* is not affected by the wetland structure. It does not necessarily follow that the degradation *pathway* is the same for each treatment.

Table 3. 2

Treatment	Cyanazine Half-Life (Days)
Submergent Ponds	
ON1	2 slopes
ON2	52
ON3	48
AVERAGE FOR ON (n=2)	50 ± 2
Emergent Ponds	
EN1	52
EN2	55
EN3	50
AVERAGE FOR EN (n=3)	52 ± 2.5
Treated Tanks	
TN1	80
TN2	62
TN3	55
AVERAGE FOR TN (n=3)	66 ± 13

Table 3. 3

Anova: Single Factor

SUMMARY

Groups	*Count*	*Sum*	*Average*	*Variance*
on	2	100	50	8
en	3	157	52.33333	6.333333
tn	3	198	66	156

ANOVA

Var. source	*SS*	*df*	*MS*	*F*	*P-value*	*F crit*
Btw.Groups	406.2083	2	203.1042	3.052668	0.136018	5.786148
W/in Groups	332.6667	5	66.53333			
Total	738.875	7				

4.4.3. Appearance and Fate of Cyanazine Metabolites.

Shown in Figures 3.9 and 3.10 is the appearance and disappearance of the two metabolites detected in this study, cyanazine amide and deethyl cyanazine. Deisopropyl atrazine was not detected during the study. Cyanazine amide was not detected in the treated tanks (TN), but deethyl cyanazine was found at concentrations at the detection limit of the instrument. Additionally, cyanazine amide is present at a much greater degree in the emergent ponds (EN) than in the submergent ponds (ON). It is not immediately obvious what the reason for this could be, but it suggests that the emergent plant life impacts the degradation pathway. This is probably an indirect influence, for example, the microbes living near the cattail roots may be different than those near the submergent vegetation roots. A correlation plot (Fig 3.11) of the two metabolites shows there is no relationship between the two metabolites.

Figure 3.9

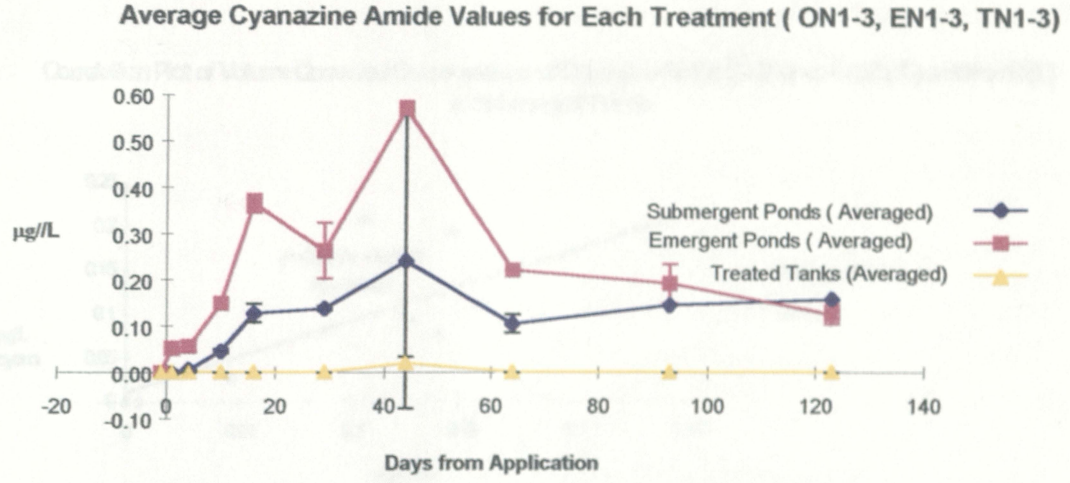

Figure 3. 9. Average cyanazine amide values for each treatment (volume corrected).

Figure 3.10

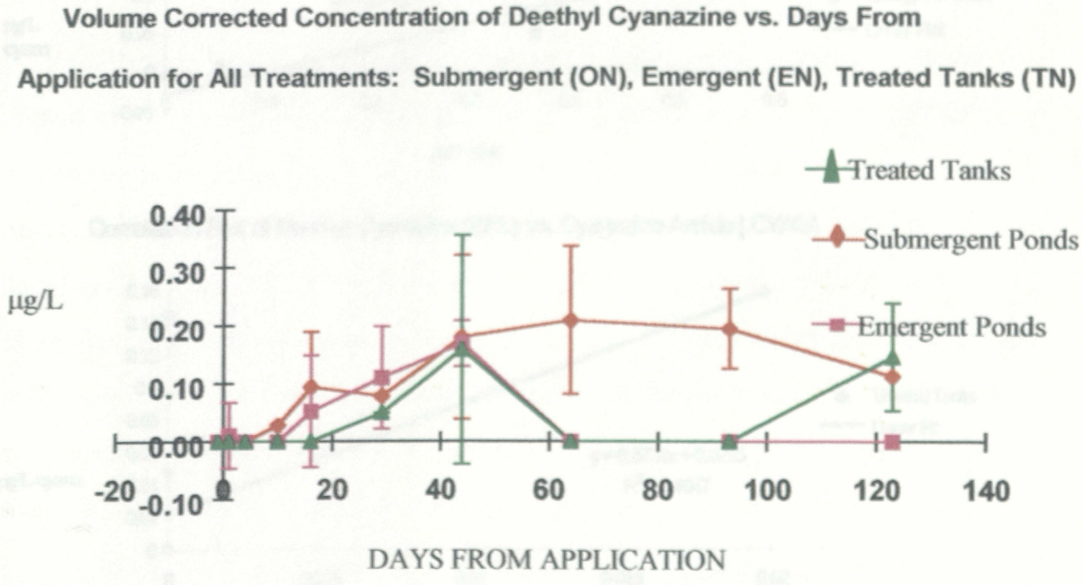

Figure 3. 10. Volume corrected concentration of deethyl cyanazine for all treatments.

Figure 3.11

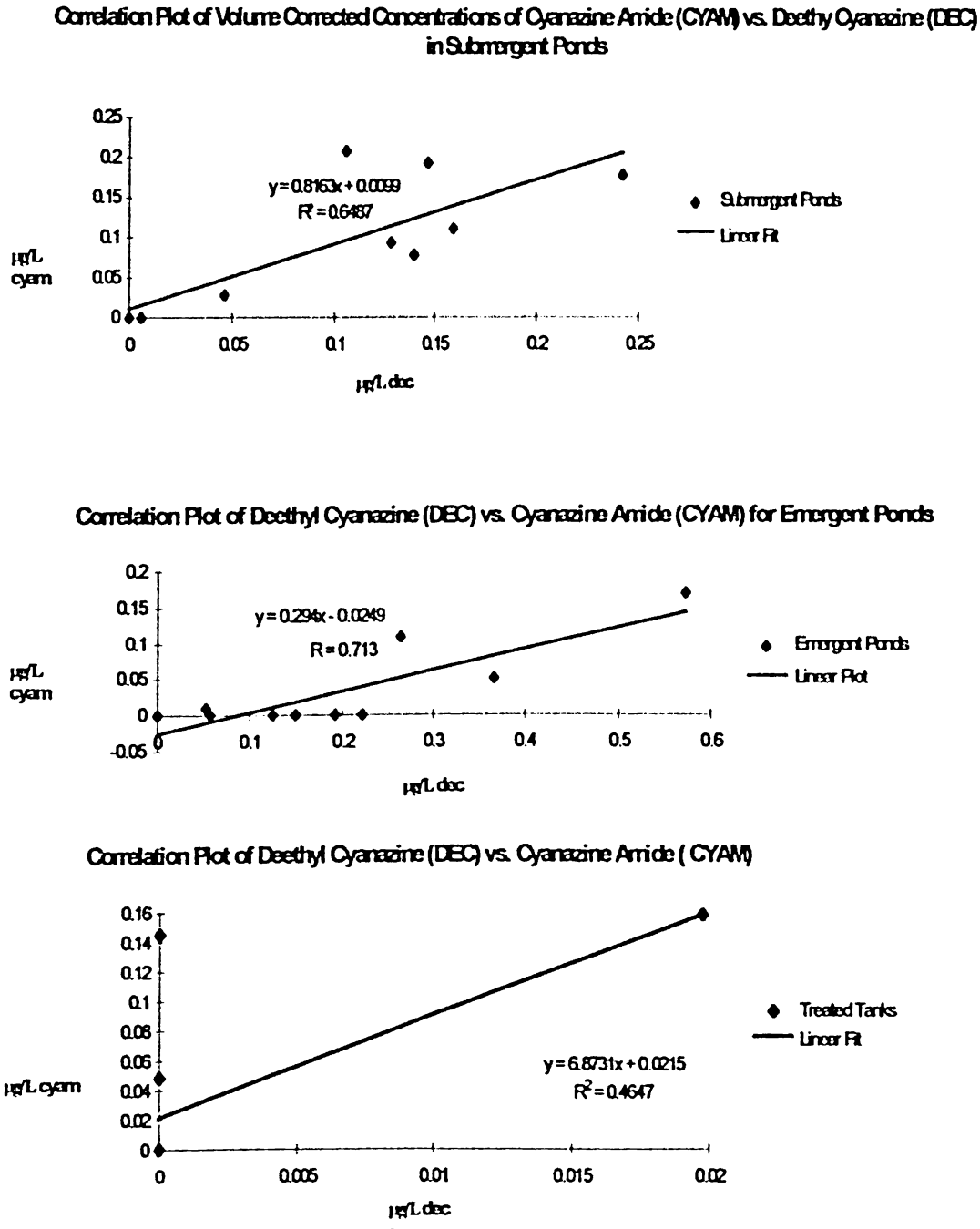

Figure 3. 11. Correlation plots of cyanazine amide and deethyl cyanazine for all treatments.

Figure 3.12

COMPARISON OF AVERAGE DISSAPEARANCE OF CYANAZINE IN ALL TREATMENTS: SUBMERGENT (ON), EMERGENT (EN), TREATED TANKS (TN) (Volume Corrected)

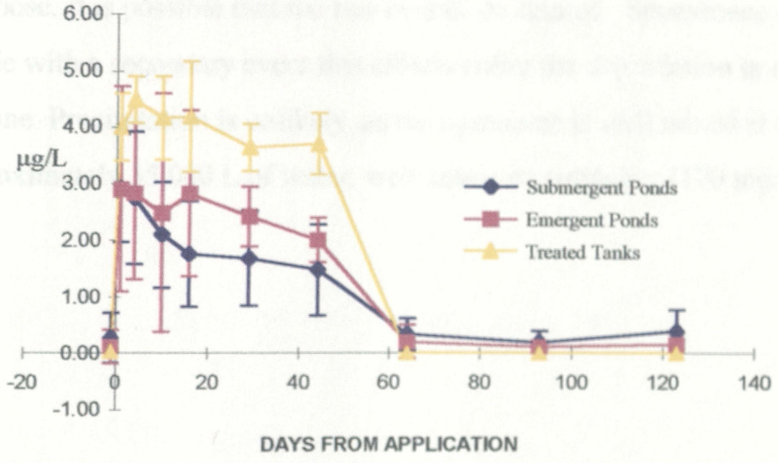

Figure 3. 12. Plots of the averaged cyanazine concentration over time for all three treatments (volume corrected).

Possible causes of the sharp decrease in cyanazine concentration at day 64 shown clearly in Figure 3.12 include adsorption, degradation by hydrolysis to the carboxylic acid derivative, or a third complex ecological process heretofore not considered. Analysis is not the issue, because standards were run and show acceptable results. Furthermore, Lee's results for atrazine and alachlor also show a sharp decrease at the same point in the study *(10)*. Leakage is not probable, as the mesocosms are clay lined, and cyanazine has been shown by several researchers to be well contained by clay *(15)*. The carboxylic acid derivative was not found, however, the analytical method in place to analyze it gave very low recoveries.

In Figure 3.12 the averaged water quality data, including dissolved oxygen, conductivity, pH, temperature, and the bromide concentration are plotted for each treatment (emergent, EN, submergent, ON, treated tanks, TN). The respective units are all indicated on the y axis. It was hoped that along with the dramatic

concentration change at day 64 a measure of water quality would also change for all the treatments. The only change observed is a temperature drop at day 64 of 4 - 5 °C. This corresponds to the start of plant senescence, when plants begin to die and decompose. It is possible that the two events are related. Senescence could cause or coincide with a secondary event that effects either the degradation or sequestering of cyanazine. Precipitation is unlikely, as the cyanazine is well mixed at this point and in approximately 35,000 L of water, well above its solubility (170 mg/L).

Figure 3. 13

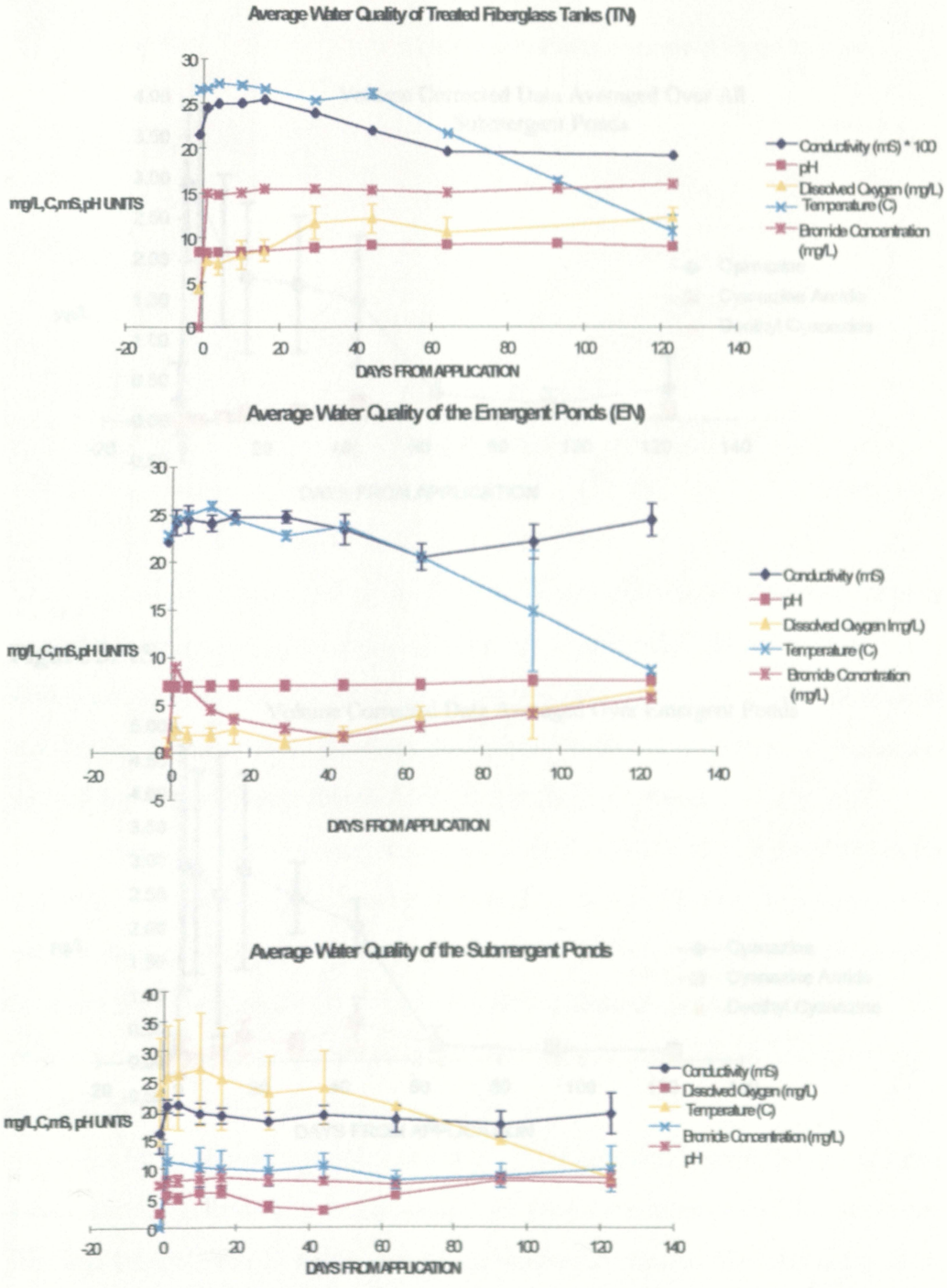

Also coinciding with day 64 is a beginning of the decay in the concentration of cyanazine amide and deethyl cyanazine observed in Figures 3.14-3.16.

Figure 3. 14

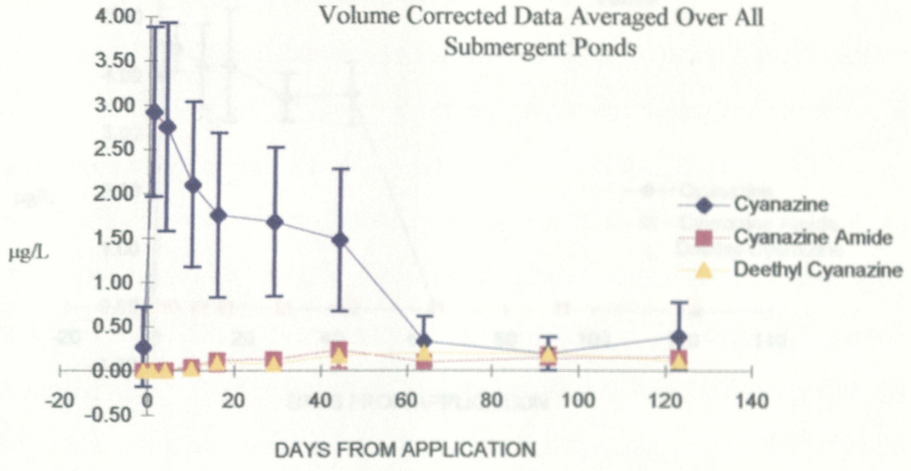

Figure 3. 15

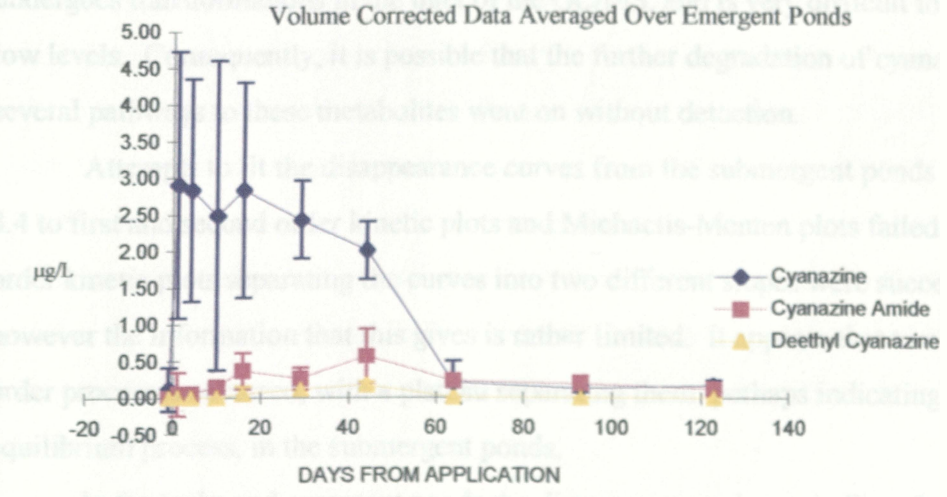

Figure 3. 16

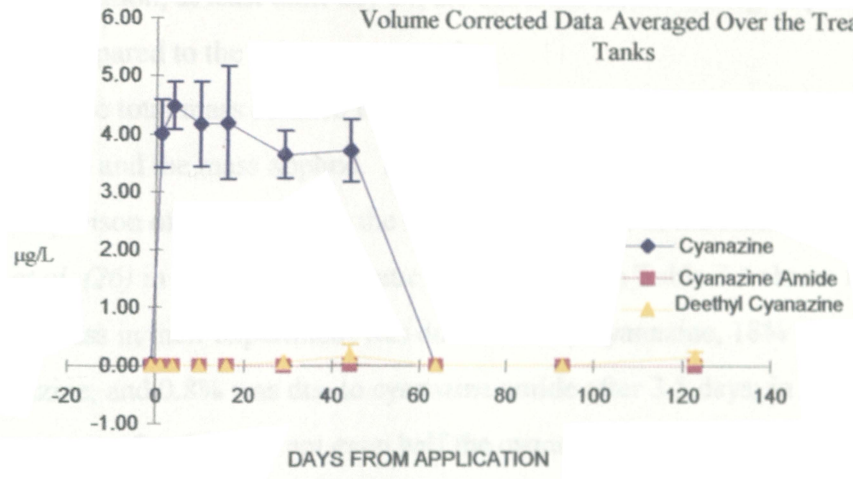

Cyanazine amide goes on to form the acid derivative, while deethyl cyanazine can lose the cyano group to form deethyl cyanazine amide. This compound undergoes transformations in the inlet of the GC/MS, and is very difficult to detect at low levels. Consequently, it is possible that the further degradation of cyanazine by several pathways to these metabolites went on without detection.

Attempts to fit the disappearance curves from the submergent ponds in Figure 3.4 to first and second order kinetic plots and Michaelis-Menten plots failed. First order kinetic plots separating the curves into two different slopes were successful, however the information that this gives is rather limited. It appears that two first order processes occurred, with a plateau separating them, perhaps indicating an equilibrium process, in the submergent ponds.

In the tanks and emergent ponds the disappearance shown in Figs. 3.5 and 3.6 have a plateau followed by a rapid decrease. However, attempts to plot the decay as first and second order kinetics, as well as Michaelis-Menten plots did not elucidate the kinetics. However, it appears that in these two treatments the equilibrium process occurred first, where there is a long initial plateau after treatment, followed by the

rapid decrease in cyanazine concentration around day 64. Clearly the mechanisms for degradation, at least until day 64, are different for the emergent ponds and treated tanks compared to the submergent ponds.

The total mass balance was estimated from the initial concentration of cyanazine and the mass applied. A table of the mass balance is shown in Table 3.4. A comparison of the data from the metabolites to that of the results obtained by C.C. Yu *et al. (26)* in a laboratory aquatic system listed in Table 3.4 shows that while 60% of the mass in their experiment was due to deethylcyanazine, 18% was due to cyanazine, and 0.8% was due to cyanazine amide after 3.5 days; in the outdoor mesocosms after 35 days not even half the cyanazine had disappeared in all but one pond. The remaining 28% of the mass was not accounted for. Both cyanazine amide and deethylcyanazine had peaked by day 45, and the maximum percentage of each was 10% CAM in submergent and emergent ponds but less than 1 % in the fiberglass tanks, and 6 - 7% DEC in the submergent and emergent ponds and 4% in the tanks. What is significant is that so much cyanazine amide was found in the emergent and submergent mesocosms, while the results from the treated tanks were much the same as Yu's microcosm experiment. Equally significant is the absence of deethyl cyanazine as a major component of the mass. This is true of all treatments, including the treated tanks, indicating that it did not migrate or adsorb to material not present in the microcosm study. It suggests that in the outdoors, the mechanism of degradation is different. This suggests that in the natural environment other factors such as exposure to sunlight may play a more important role than previously suggested by laboratory experiments.

Table 3. 4

Mass Balance

Mesocosm Study % Total Mass after 44 Days	Submergent Ponds Average (ON1-3)	Emergent Ponds Average (EN1-3)	Treated Tanks Average (TN1-3)
Cyanazine	55 %	55 %	87 %
Cyanazine Amide	10 %	11 %	0.71 %
Deethyl cyanazine amide	7.5 %	4.9 %	5.9 %

%Total Mass from C.C. Yu *et al.* after 35 Days	
Cyanazine	18 %
Deethyl cyanazine	60.4 %
Cyanazine amide	0.8 %
Deethyl cyanazine amide	0.3 %

4.5. Conclusions

This is the first study to determine the effect of wetland structure on cyanazine disappearance and degradation product profiles in outdoor wetland mesocosms. The observation of both the disappearance of cyanazine and the appearance of 10 % of the cyanazine as metabolites shows that the mechanism for disappearance was not merely adsorption, volatilization, or disappearance, but rather actual degradation of the parent compound. The half-life was observed to be 55 to 60 days in water, 50% longer than the half-life observed in soil of 18 to 31 days. In addition, new information regarding the use of a common conservative volume tracer, bromide, was obtained. Bromide was proven to be selectively sequestered by cattails in the root. This suggests potential for the use of cattails to selectively sequester other less desirable charged material, such as charged organic chemicals. However, bromide is not a suitable volume tracer for stagnant water systems with tuber plants.

The lack of a difference in mean disappearance half-life of cyanazine based on the wetland treatment suggests that wetland structure is not important if the half-life is the only measure. However, if the pathway of disappearance is important, wetland structure does play a role. This was observed in the apparent kinetics of disappearance and the differences in the appearance and disappearance of metabolites.

The mass balance showed that 80% or better of the cyanazine mass is converted to a compound or compounds that were not detected. This was true even in the treated fiber glass tanks that had no soil or flora, suggesting that a hydrolysis product, such as cyanazine acid, may be a predominant metabolite. Another hypothesis is that the plant senescence affected either the degradation, absorbance, or solubility of cyanazine.

The significantly longer half-life observed partially reflects the fact that the mesocosms were virtually water-tight. This means that very little pond water permeates the soil, and has low contact with the rizosphere where most of the

bacteria thought to degrade herbicides live. Additionally, most studies of cyanazine involve the disappearance of cyanazine from the site of application. Thus, the predominant mechanism of disappearance is the transport off a field by running water, in other words, it is physically removed. However, counter to this is Yu's aquatic study which showed significantly more degradation *(26)*. This highlights the importance of using a mesocosm to gather data for predictive models, where real world factors like UV light, seasonal changes, and ecological diversity not included in Yu's study play a role.

4.6. Future Work

Further investigations of this problem require a multidisciplinary approach. The analytical chemist is needed to focus on problems such as the detection of cyanazine acid, a charged compound, and the isolation of cyanazine and its metabolites from soil, plants, sediment, and insects. The microbiologist can focus on characterizing microbial populations and determining any effect of wetland structure on these populations. Additionally, the she could identify metabolic pathways using follow-up microcosm studies in the laboratory. Finally, the organic geochemist is needed to focus on the problem of modeling the transport and degradation of the compounds that are found.

4.7. References

(1) Humenik, F.J.; Smolen, M.D.; Dressing, S.A., *Environmental Science and Technology* **1987**, *21*, 737-742.

(2) Periera, W.E.; Rostad, C.E. *Environmental Science and Technology* **1990**, *24*, 1400-1406.

(3) Gianessi, L.P.; Puffer, C.M.; *Herbicide use in the United States; Resources for the Future, National Summary Report*, **1986**, Washington, D.C., 490.

(4) M.T. Meyer, *Geochemistry of Cyanazine and Its Metabolites: Indicators of Contaminant Transport in Surface Water of the Midwestern United States* Dissertation, The University of Kansas, 1995.

(5) Thurman, E.M. ; Goolsby, D.A.; Meyer, M.T.; Koplin, D.W., *Environmental Science and Technology*, **1991**, *25*, 1794-179.

(6) Goolsby, D.A.; Thurman, E.M.; Koplin, D.W., 1991, *Geographic and temporal distribution of herbicides of the upper Midwestern United States*, 1989-1990, U.S. Geological Survey Water-Resources Investigation Report: 91-4034, p.183-188.

(7) Baker, L.A. *Ecological Engineering*, **1992**, *1*, 1-26.

(8) Rodgers, J.H.; Dunn, A. *Ecological Engineering*, **1992**, *1*, 83 - 95.

(9) Vellidis, G.; Lowrance, R.; Hubbard, R.K. *Versatility of Wetlands in the Agricultural Landscape* **1996**, p. 191 - 200.

(10) Lee, K.E. *Atrazine and Alachlor Degradation in Wetlands: The Effect of Hydrophyte Community Structure*, The University of Kansas, 1995.

(11) Davis, S.N.; Thompson, G.M. ; Bentley, H.W.; Stiles, G. *Ground Water*, **1980**, *18*, 14 - 23.

(12) Bowman, R.S. *Soil Science Society of America Journal*, **1984**, *48*, 987 - 983.

(13) Hughes, W.J.; Chapman, T.; Jordan, D.; Schieferstein, *Proceedings N.C. Weed Control Conference*, 1967, p. 27.

(14) Muir, D.C.; Baker, B.E. *Weed Research*, **1978**, *18*, 111-120.

(15) Yoo, J.Y.; Muir, D.C.; Baker, B.E., *Canadian Journal of Earth. Science*, **1981**, *61*, 237-242.

(16) Helling, C.S.; Zhuang, W.; Gish, T.J.; Coffman, C.B.; Insensee, A.R.; Kearney, P.C.; Hoagland, D.R.; Woodward, M.D. *Chemosphere*, **1988**, *17*, 175-187.

(17) Smith, A.W.; Walker, A.; *Canadian Journal of Soil Science*, 1989, 69, 587-595.

(18) Frank, R.; Clegg, B.C.; Patni, N.K. 1991, *Archives Environmental Contamination and Toxicology* **1991**, *21*, 253-262.

(19) Onken, A.B.; Hargrove, R.S.; Wendt, C. W.; Wilke, O.C. *Soil Science Society of America Journal*, **1975**, *39*, 1223-1225.

(20) Kung, K.J.S. *Soil Sci. Soc. Am. J.* **1990**, *54*:975-979.

(21) Dennison, M.S.; Berry, J.F., *Wetlands*, Noyes Publication, Park Ridge, NJ: 1993., p.4.

(22) Detenbeck, N.; Hermanutz,R.; Allen, K.; Swift, M. C. *Environmental Toxicology and Chemistry*, **1996**, *15*, 937-946.

(23) Howick, G.L.; Giddings, J.M.; Denoyelles, F.; Ferrington, L.C.; Kettle, W.D.; Baker, D. *Environmental Toxicology and Chemistry*. **1992**,*11*, 107-114.

(24) Marschner, H. *Mineral Nutrition in Higher Plants*. Academic Press Inc. London :1986, pp.38-39.

(25) Yu, C.C.; Booth, G.M.; Larsen, J.R. *Journal of Agricultural Food Chemistry*, **1975**, *23*, 1014-1015.

5. Appendix 1.1

Figure 1.8

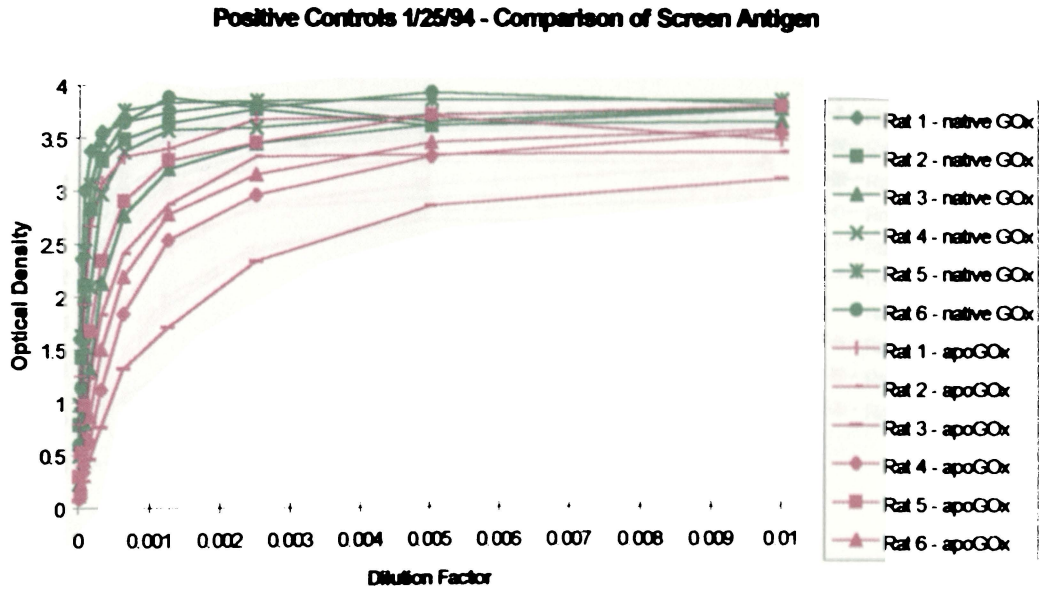

Figure 1.8. Sera from POS rats, rats injected with apoGOx, screened for the first time after the second boost against holo- and apoenzyme.

Figure 1.9

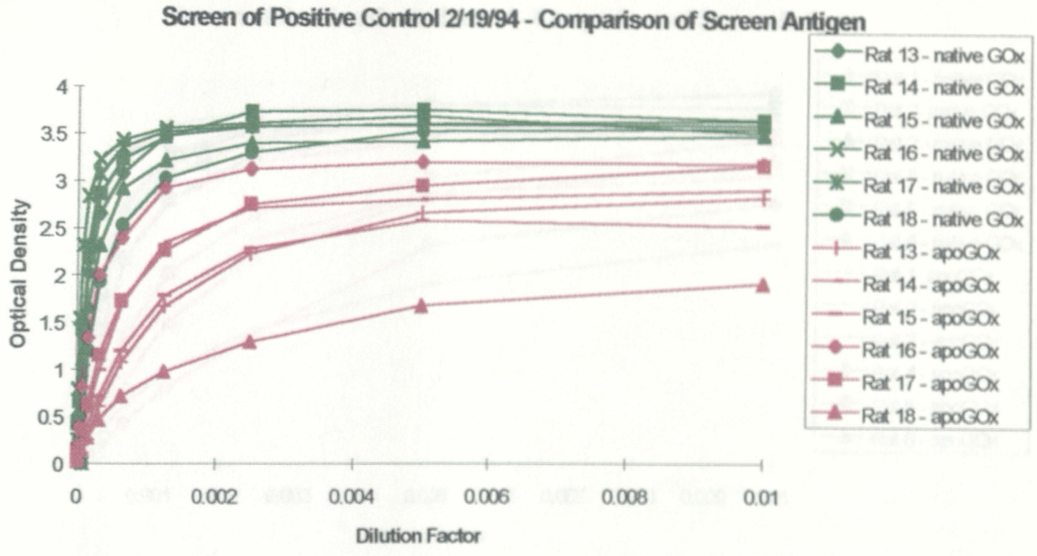

Figure 1.9. Sera from POS rats, rats injected with apoGOx, screened for the second time after the second boost against holo- and apoenzyme.

Figure 1.10

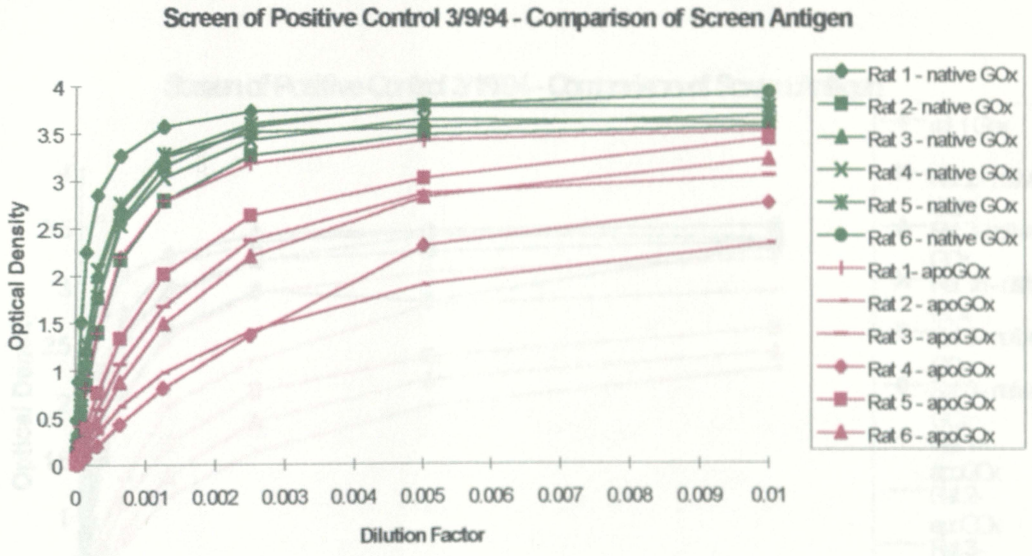

Fig. 1.10. Sera from POS rats, rats injected with apoGOx, prior to third boost screened against holo- and apo-enzyme.

Figure 1.11

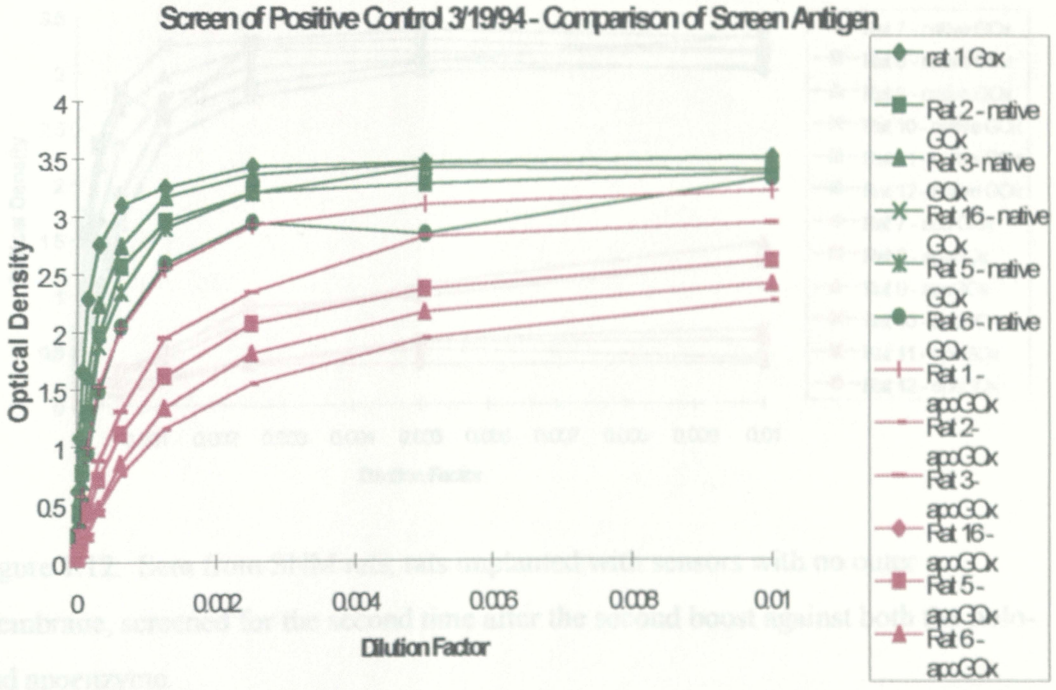

Figure 1.11. Sera from POS rats, rats injected with apoGOx, screened after the third boost against both the holo- and apoenzyme.

Figure 1.12

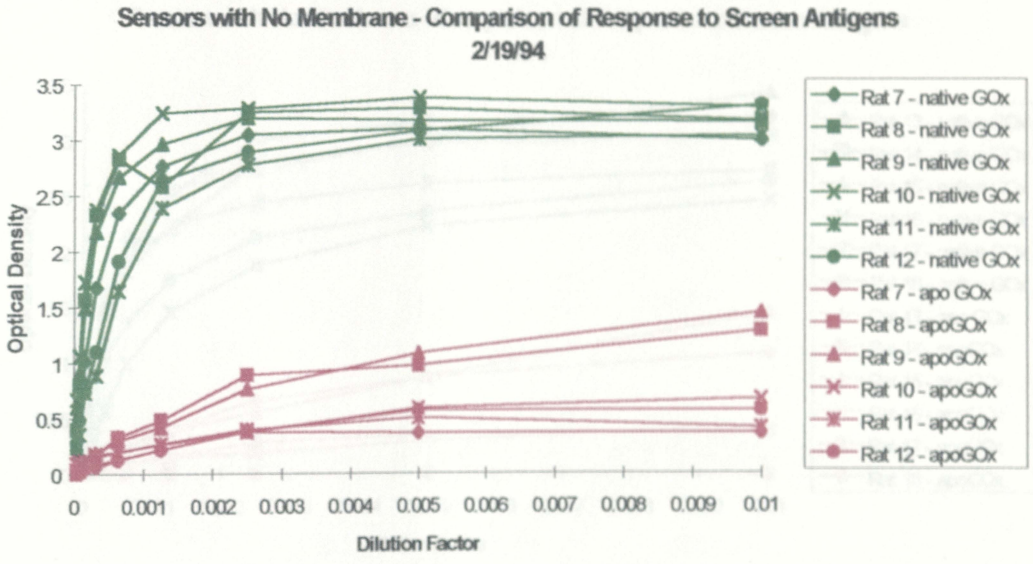

Figure 1.12. Sera from SNM rats, rats implanted with sensors with no outer membrane, screened for the second time after the second boost against both the holo- and apoenzyme.

Figure 1.13

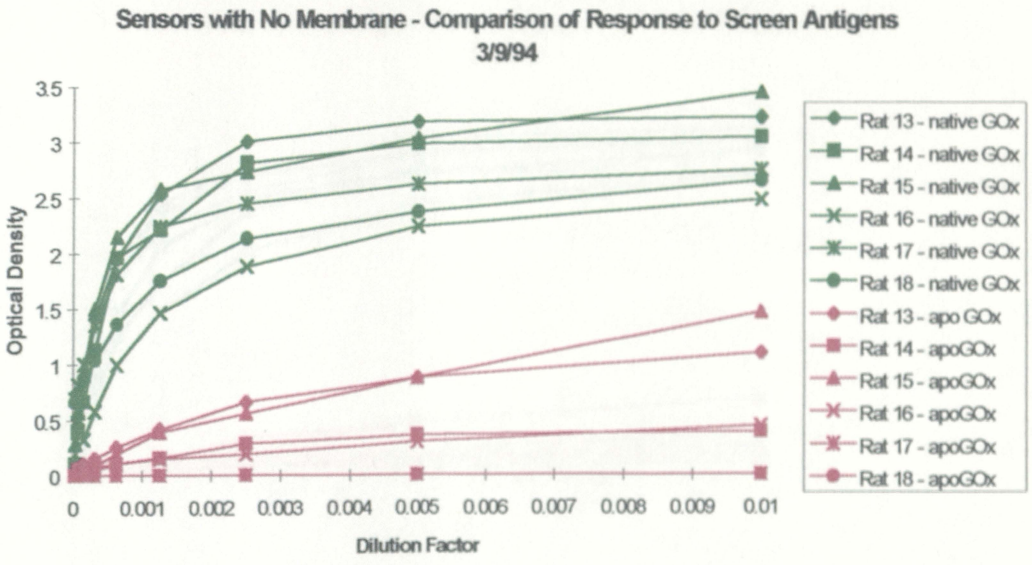

Figure 1.13. Sera from SNM rats, rats implanted with sensors with no outer membrane, screened before third boost against holo- and apoenzyme.

Figure 1.14

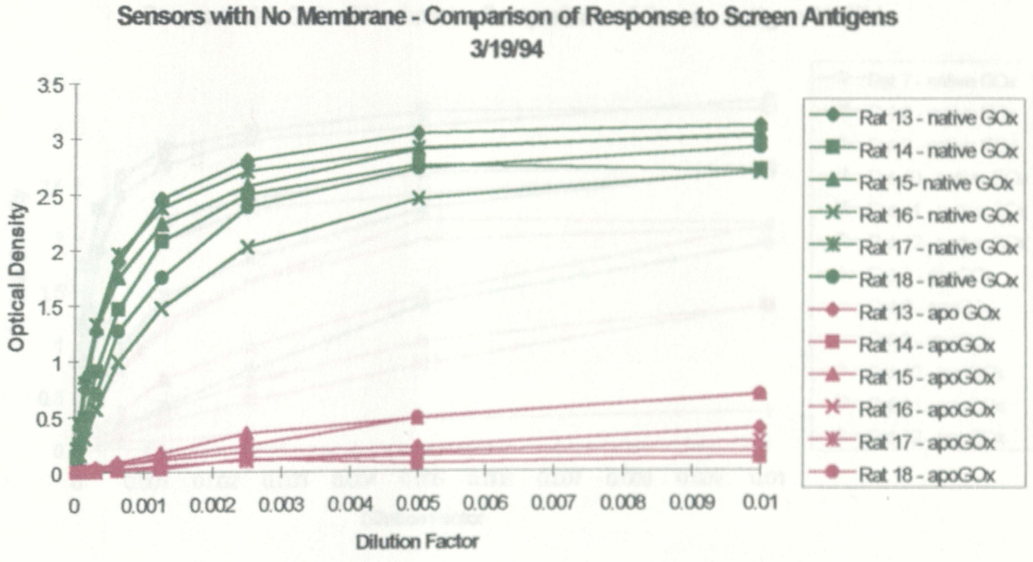

Figure 1.14. Sera from SNM rats, rats implanted with a sensor with no outer membrane, screened after the third boost against both holo- and apoenzyme.

Figure 1.15

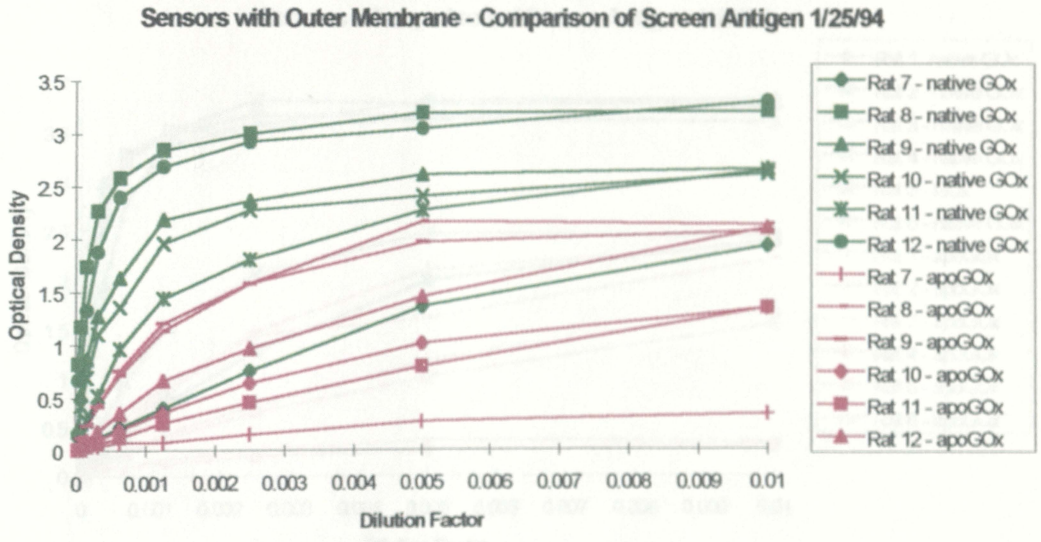

Figure 1.15. SWM rats implanted with complete sensor screened for the first time after the second boost against both holo-and apoenzyme.

Figure 1.16

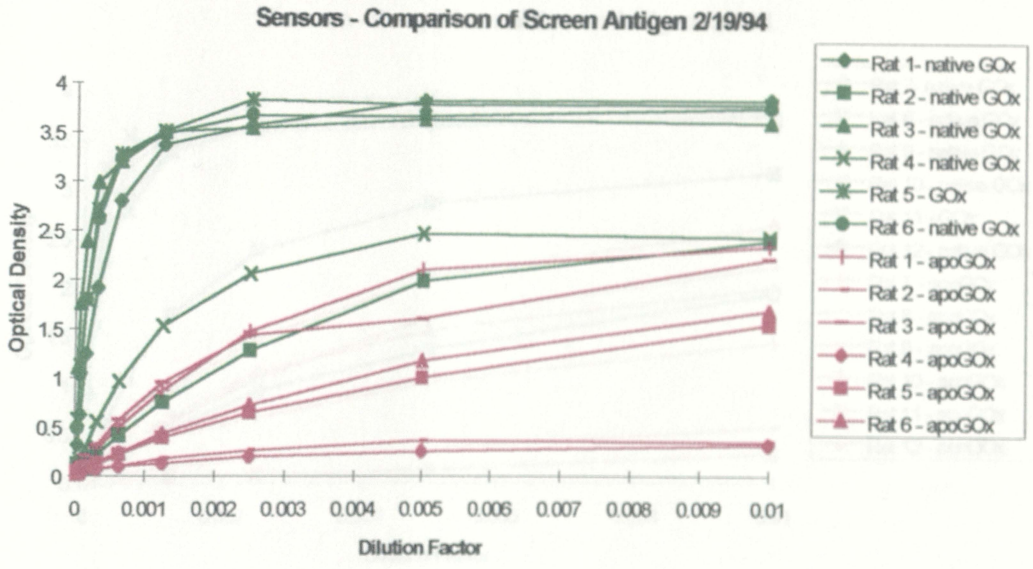

Figure 1.16. SWM rats implanted with complete sensor screened for the second time after the second boost against both holo- and apoenzyme.

Figure 1.17

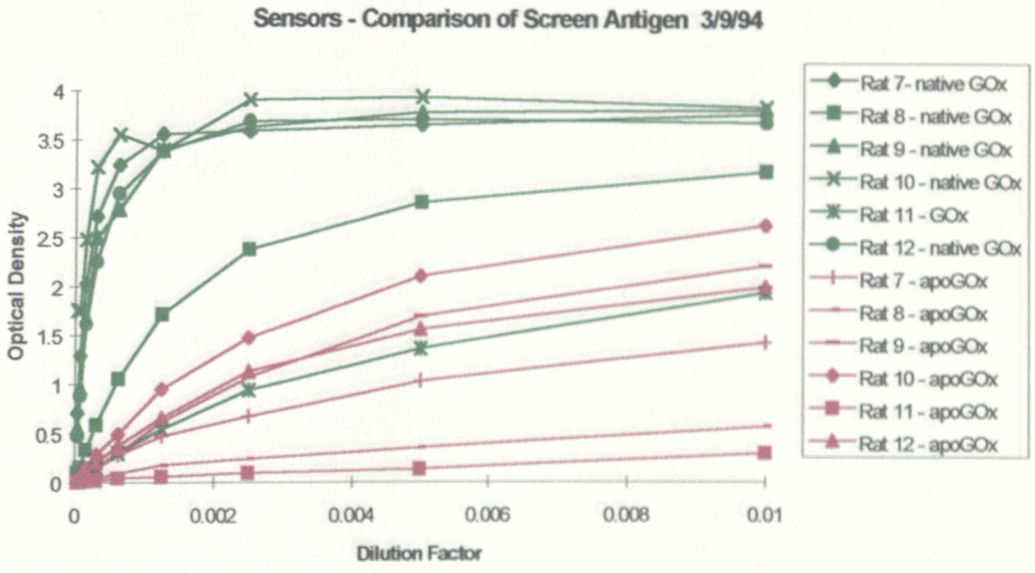

Figure 1.17. Sensor rats screened prior to third boost. Results from screens against holo- and apoenzyme are both shown.

Figure 1.18

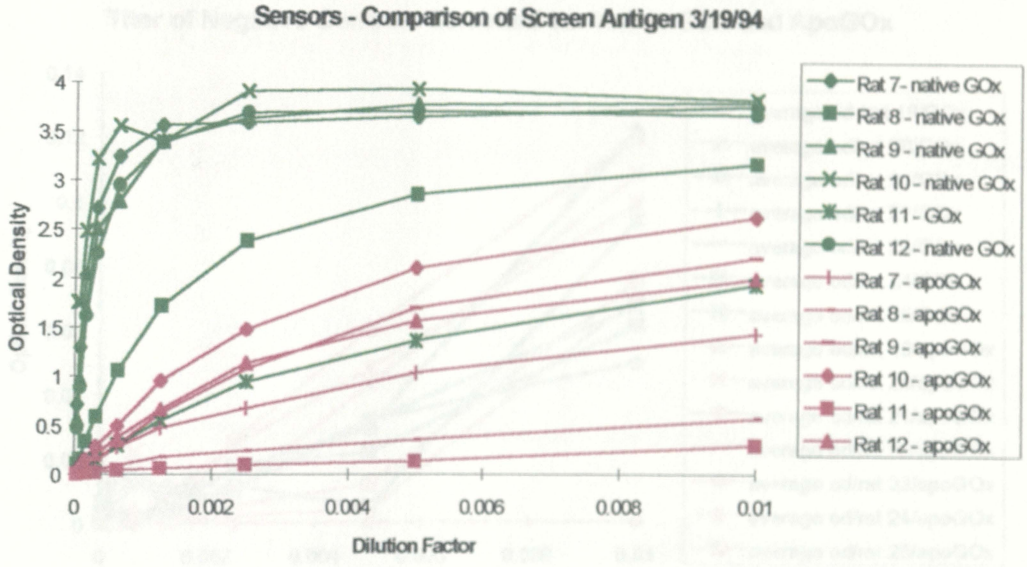

Figure 1.18. Sera of rats immunized with sensors after third boost. Results from both screens against the native and apo enzyme are shown.

Figure 1.19

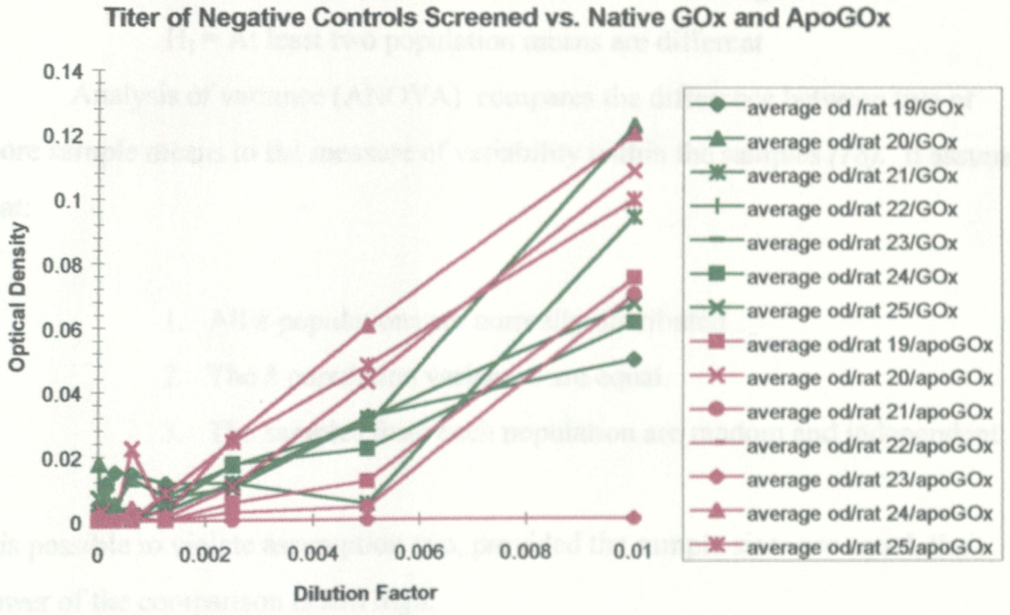

Figure 1.19. Negative control sera screened against both the holo- and apoenzyme are shown.

ANOVA Consider the two hypotheses, H_0 and H_1, that follow:

$H_0 = MEAN_1 = MEAN_2 = MEAN_3 = \ldots = MEAN_K$

H_1 = At least two population means are different

Analysis of variance (ANOVA) compares the difference between two or more sample means to the measure of variability within the samples *(18)*. It assumes that:

1. All *k* populations are normally distributed
2. The *k* population variances are equal.
3. The samples from each population are random and independent.

It is possible to violate assumption two, provided the sample sizes are equal, the power of the comparison is still high.

ANOVA determines if the variance observed between test groups results from more than the variance found within the groups. This is expressed in the F-ratio or F-number. The test statistic F, takes the ratio of the mean square for treatments (MST) to the mean square for error (MSE). MST is defined by taking the average of the sum of the squares (SS) for the treatments, and MSE is another name for the sample variance, s^2. If the F ratio is larger that the critical F value (determined by the degrees of freedom [df] and the α level [usually 0.05]), then the null hypothesis, H_0, is rejected. Figure 1.20 shows a pictorial representation of ANOVA *(19)*.

Figure 1.20

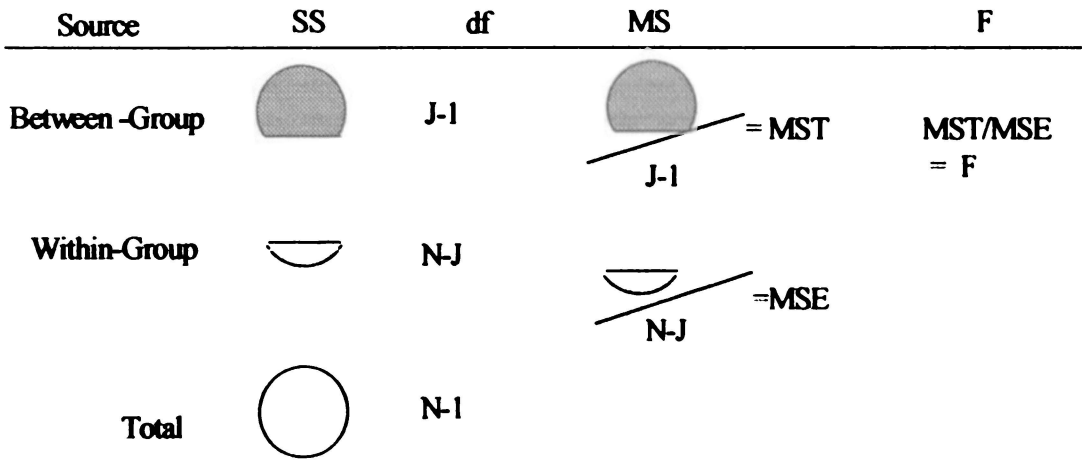

Fig 1.20 Analysis of variance(single-classification fixed effects model) partition and F-test.

Table 1.8

ANOVA Comparing All Groups - NEG, SNM,SEN,POS.

Anova: Single Factor						
SUMMARY						
Groups	*Count*	*Sum*	*Average*	*Variance*		
negative control	6	0.015	0.0025	0		
snm	6	0.002408	0.000401	1.78E-07		
sen	6	0.002578	0.00043	2E-07		
pos	6	0.000293	4.88E-05	5.72E-10		
ANOVA						
Var. Source	*SS*	*df*	*MS*	*F*	*P-value*	*F crit*
Btw group	2.25E-05	3	7.48E-06	79.22174	2.83E-11	3.098393
W/in group	1.89E-06	20	9.45E-08			
Total	2.43E-05	23				

Anova: Single Factor						
SUMMARY						
Groups	*Count*	*Sum*	*Average*	*Variance*		
snm	6	0.002408	0.000401	1.78E-07		
sen	6	0.002578	0.00043	2E-07		
pos	6	0.000293	4.88E-05	5.72E-10		
ANOVA						
Var. Source	*SS*	*df*	*MS*	*F*	*P-value*	*F crit*
Btw Group	5.4E-07	2	2.7E-07	2.144802	0.151621	3.682317
W/in Group	1.89E-06	15	1.26E-07			
Total	2.43E-06	17				

Two Way ANOVA - Negative Controls and SNM Rats

Anova: Single Factor						
SUMMARY						
Groups	*Count*	*Sum*	*Average*	*Variance*		
negative control	6	0.015	0.0025	0		
snm	6	0.002408	0.000401	1.78E-07		
ANOVA						
Var. Source	*SS*	*df*	*MS*	*F*	*P-value*	*F crit*
Btw Group	1.32E-05	1	1.32E-05	148.6724	2.51E-07	4.964591
W/in Group	8.89E-07	10	8.89E-08			
Total	1.41E-05	11				

Two Way ANOVA - Negative Control and SWM Rats

Anova: Single Factor						
SUMMARY						
Groups	*Count*	*Sum*	*Average*	*Variance*		
negative control	6	0.015	0.0025	0		
sen	6	0.002578	0.00043	2E-07		
ANOVA						
Var. Source	*SS*	*df*	*MS*	*F*	*P-value*	*F crit*
Btw.Groups	1.29E-05	1	1.29E-05	128.8532	4.92E-07	4.964591
W/in Groups	9.98E-07	10	9.98E-08			
Total	1.39E-05	11				

Two Way ANOVA - Negative Control and POS Rats

Anova: Single Factor						
SUMMARY						
Groups	*Count*	*Sum*	*Average*	*Variance*		
negative control	6	0.015	0.0025	0		
pos	6	0.000293	4.88E-05	5.72E-10		
ANOVA						
Var. Source	*SS*	*df*	*MS*	*F*	*P-value*	*F crit*
Btw.Groups	1.8E-05	1	1.8E-05	63001	2.48E-20	4.964591
Wlin Groups	2.86E-09	10	2.86E-10			
Total	1.8E-05	11				

6. Appendix 2.1

Photolithography *(25)*

Physical tools are inadequate for making structures with dimensions on the order of micrometers. However, UV light provides the resolution necessary. Photolithography refers to the process that uses electromagnetic radiation in conjunction with an optical image on a mask, and a photosensitive film to produce a pattern on a substrate. Figure 2.25 Shows the photolithographic process sequence.

Figure 2.25

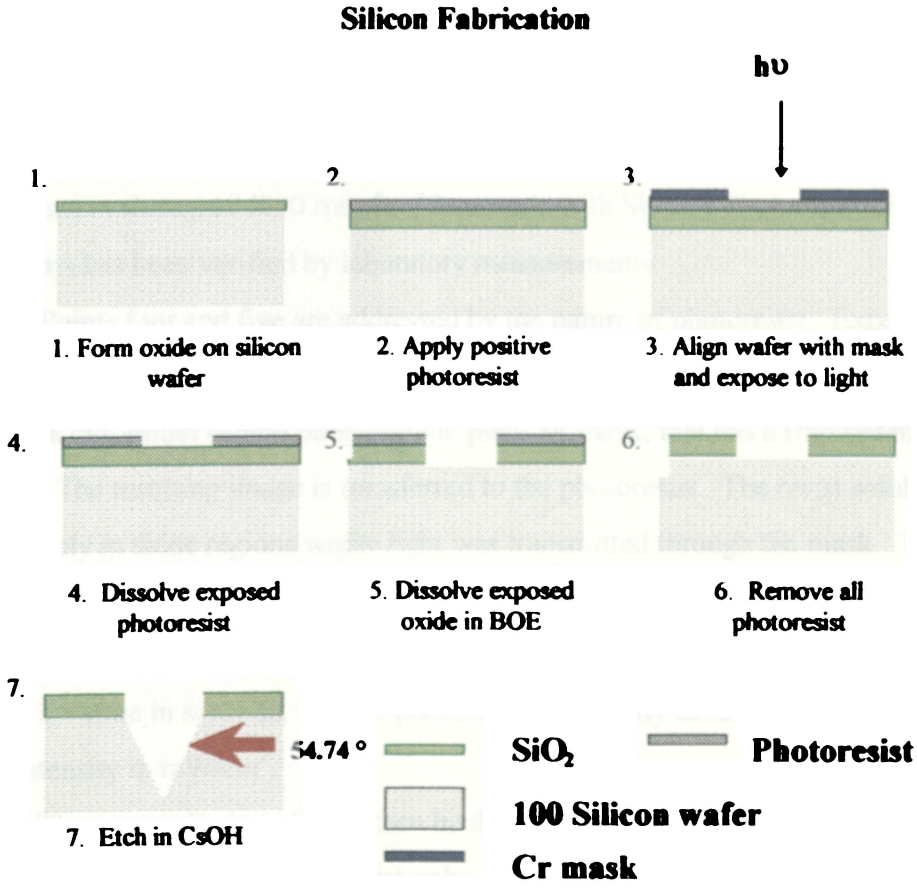

The photosensitive film, photoresist, must meet four requirements. They are as follows: 1. Good adhesion to the substrate surface 2. Uniform thickness 3. Reproducible thickness 4. Light sensitive 5. Resistance to etchant.

To achieve points one through three, photoresist is applied using centrifugal force. The substrate is held by a vacuum chuck, then the photoresist is added. The spindle upon which the chuck rests rotates at several thousand revolutions per minute (rpm) for tens of seconds. The formula used to relate spin speed to final thickness is as follows:

$$Z=kP^2/\sqrt{\omega} \qquad (2.9)$$

Where z is the final thickness (cm), P is the percentage of solids in the resist, and ω is the rotational velocity (radians/cm^2), and k is a constant. The thickness obtained using a spin velocity of 4000 rpm for 30 seconds with Shipley Photoresist 1818 is 1.8 μm. This has been verified by laboratory measurements.

Points four and five are addressed by the nature of photoresist. Exposure to UV radiation will cause a change in solubility of the photoresist. Radiation is applied through a chromium coated photographic plate, or mask, that has a transparent pattern. The resulting image is transferred to the photoresist. The resist solubility is altered only in those regions where light was transmitted through the mask. This step is termed exposure. The exposure time is determined using the following equation:

$$T=S/I \qquad (2.10)$$

Where T = time in seconds, S is the photoresist sensitivity in mJ/cm^2, and I is the lamp intensity in mW/cm^2.

The exposed substrate can then be developed by adding a solution that will dissolve the more soluble photoresist only. If the photoresist that was exposed is more soluble, the image in the photoresist is identical to the image on the mask. This is termed positive photoresist. If the exposure decreases the solubility, the resist is

negative. The photoresist remaining is then strengthened by baking for several minutes. This prevents the photoresist from dissolving in the etchant.

Now the substrate bearing the patterned photoresist is exposed to an etchant. The etchant removes only those portions of the substrate unprotected by the resist leaving the covered areas unetched. Thus, the pattern from the photoresist is transferred to the substrate. Once this is done, the photoresist can be stripped in organic solvents.

Anisotropic Etching ***(25,26)***

Once the mask pattern has been transferred to the substrate, the method for machining that pattern onto the solid substrate cannot used conventional tools. The pattern is machined using etching. Discussed here will be wet chemical etchants. Other methods, such as reactive ions in the gas phase, ion beams, and sputtering, may be used.

Isotropic etchants remove the substrate at a constant rate independent of the direction in the crystal. Anisotropic etchants, however, etch the different crystal planes at different rates. Because the etch rate is different in different planes, the geometry of the resulting feature depends on the crystal planes. The case discussed here will be silicon only.

Etchants such as potassium hydroxide and cesium hydroxide etch the <100> of silicon at least two orders of magnitude faster that in the <111> direction. The resulting depth and geometry of the feature is dependent on the width of the feature, the etch time, and the crystal plane. This relationship is illustrated in Figure 2.26.

Figure 2.26

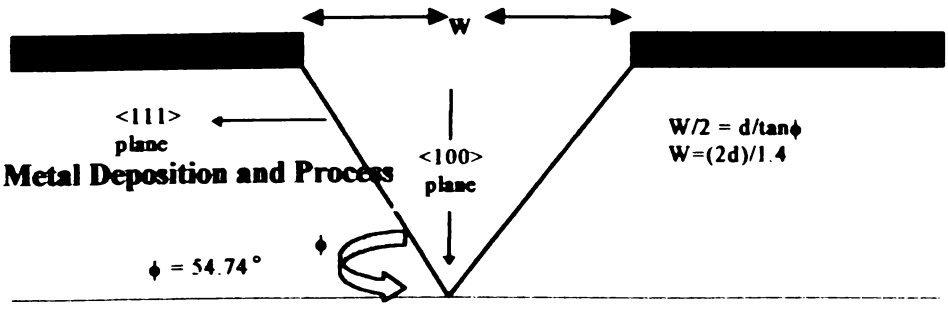

Metal Deposition and Process

Evaporation. A metal placed in a vacuum chamber and heated either resistively or by an ion source will begin to boil. The atoms in the gas phase travel by line of sight from the source to the substrate (silicon, glass or other wafers). This method works well if two situations are met. The first is that the metals have moderate boiling points (1000 °C). Additionally, evaporation is a useful method where poor wall coverage, that is the coverage of a vertical plane such as a channel wall, is desired or not a problem. A process where this is an advantage is metal lift-off, which will be discussed later in this section.

A quartz crystal that vibrates at a characteristic frequency is used to monitor the deposition rate and thickness. As the evaporated metal builds up on the crystal, its mass is increased by Δm, and thus the oscillation frequency is decreased according to the following relationship:

$$\Delta f = (1/\rho k)\, f_0^2\, (\Delta m/A)$$

where f_0 is the frequency, ρ is the density of the evaporated metal, A is the area of the crystal, and K is a constant. The film thickness, Δx, is calculated from :

$$t = k(\Delta f / f_0^2)$$

For a detailed discussion of different metal deposition methods, the reader is referred to *Thin Film Processes* edited by Vossen and Kern *(27)*.

Metal Lift-Off. Metals can be etched in patterns like silicon or glass, but the etching requires a negative resist or a negative mask. Negative resist does not survive many etch conditions, including aqua regia, the etching reagent for platinum. However, a process that does not require etching, lift-off, is suitable.

In this process the substrate is patterned using positive photoresist for photolithography. The patterned wafer is not etched, however. It is placed in an evaporator where an adhesion layer and metal layer are deposited. On glass, most metal layers adhere poorly, so chromium or titanium can be used to enhance adhesion. The entire wafer is covered with the metal film, but only in the areas where there is no photoresist is the metal truly deposited on the substrate. The

substrate is then placed in a solvent such as acetone to dissolve the photoresist. For this reason, poor step coverage is required. With poor step coverage the photoresist is more accessible to the solvent, and the metal deposited on the photoresist can be removed as the photoresist is dissolved. The result is the metal pattern from the mask on the substrate. A schematic of this process is found in Figure 2.27.

Figure 2.27

Lift-Off Metal Deposition

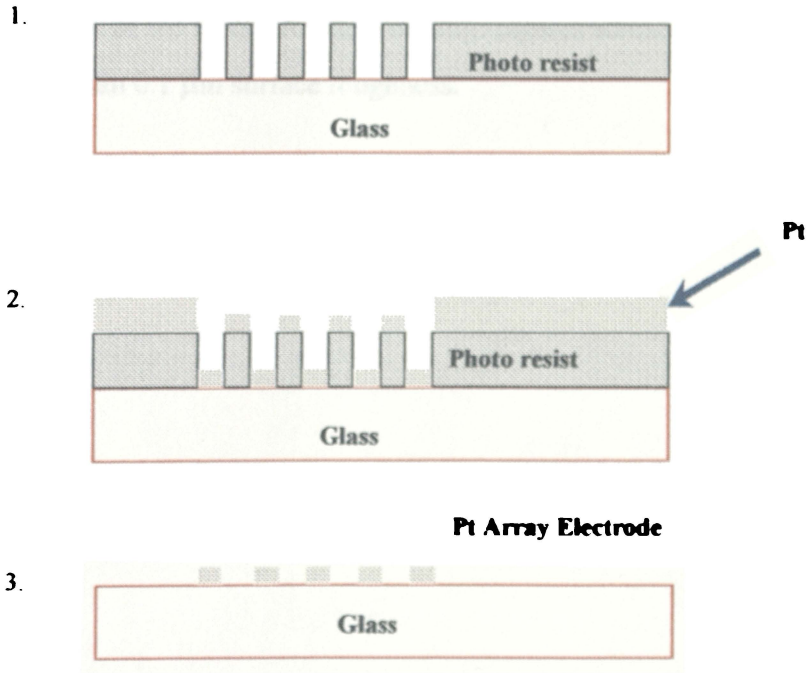

1. Result of photolithography of photoresist
2. Result of platinum evaporation on top of photoresist
3. Result of metal lift-off - the patterned metal

Anodic Bonding ***(25,26)***

Because the structures that are microfabricated are small, it is very difficult to couple two planar structures with epoxy or adhesives to form a permanent seal without damaging the features. However, the properties of silicon and glass allow bonding between these two substrates to occur by an ionic process. Figure 2.28 shows a

schematic of anodic bonding .At temperatures greater than 375 °C Na^+ ions in Pyrex glass become mobile. The negative terminus attracts the sodium ions, producing a depletion region at the silicon glass interface. A very high electric field across the depletion layer pulls the two surfaces into intimate contact. A fusion bond is formed between the silicon oxide at the surface and the glass. The bond strength is typically 2-3 MPa. This can be done between silicon dioxide and glass provided the silicon dioxide insulating layer is thin enough that the voltage applied exceeds the breakdown voltage of the layer. Anodic bonding requires an exceptionally clean surface and less than 0.1 μm surface roughness.

Figure 2.28

Anodic Bonding Principle

Principle:

Sodium ions in glass have increased mobility

Move to surface

Resulting E field pulls Si and glass surfaces into contact

Irreversible